

Anion-templated silver nanoclusters: precise synthesis and geometric structure

Yusuke Horita^a, Mai Ishimi^a and Yuichi Negishi^{a,b}

^aDepartment of Applied Chemistry, Faculty of Science, Tokyo University of Science, Shinjuku-ku, Japan;

^bResearch Institute for Science & Technology, Tokyo University of Science, Shinjuku-ku, Japan

ABSTRACT

Metal nanoclusters (NCs) are gaining much attention in nanoscale materials research because they exhibit size-specific physicochemical properties that are not observed in the corresponding bulk metals. Among them, silver (Ag) NCs can be precisely synthesized not only as pure Ag NCs but also as anion-templated Ag NCs. For anion-templated Ag NCs, we can expect the following capabilities: 1) size and shape control by regulating the central anion (anion template); 2) stabilization by adjusting the charge interaction between the central anion and surrounding Ag atoms; and 3) functionalization by selecting the type of central anion. In this review, we summarize the synthesis methods and influences of the central anion on the geometric structure of anion-templated Ag NCs, which include halide ions, chalcogenide ions, oxoanions, polyoxometalates, or hydride/deuteride as the central anion. This summary provides a reference for the current state of anion-templated Ag NCs, which may promote the development of anion-templated Ag NCs with novel geometric structures and physicochemical properties.

ARTICLE HISTORY

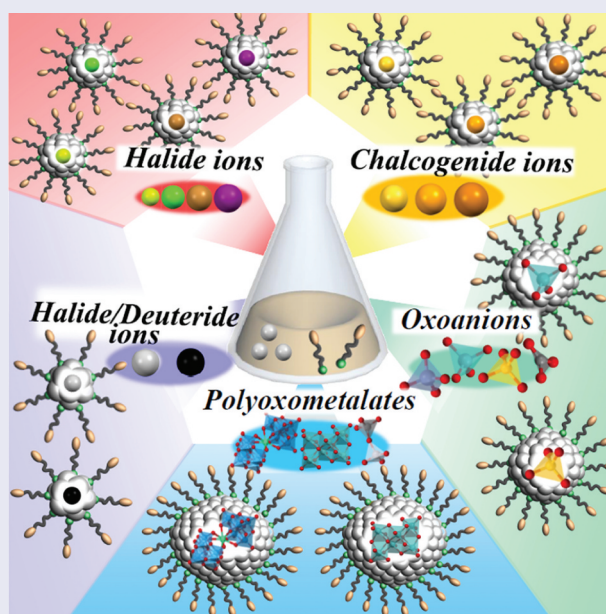
Received 28 February 2023

Revised 28 March 2023

Accepted 12 April 2023

KEYWORDS

Metal cluster; silver cluster; anion-templated cluster; geometric structure; synthesis method





1. Introduction

Aggregates of a few to several hundred metal atoms are called metal nanoclusters (NCs). Metal NCs are very small, with a particle size of 1–2 nm, which can give rise to novel geometric structures and discretization of electronic levels [1–13]. Related to these factors, size-specific physicochemical properties can emerge in metal NCs that are not observed in the

corresponding bulk metals [14–17]. Accordingly, metal NCs have attracted much attention in academic fields and industries related to materials chemistry [18–22].

Among the metal NCs, those composed of coinage metals, such as gold (Au) [23–85], silver (Ag) [86–103], and copper (Cu) [104–107], are particularly promising as novel functional materials because of their

CONTACT Yuichi Negishi  negishi@rs.tus.ac.jp  Department of Applied Chemistry, Faculty of Science, Tokyo University of Science, Kagurazaka, Shinjuku-ku, Tokyo 162-8601, Japan; Research Institute for Science & Technology, Tokyo University of Science, Shinjuku-ku, Tokyo 162-8601, Japan
© 2023 The Author(s). Published by National Institute for Materials Science in partnership with Taylor & Francis Group.

This is an Open Access article distributed under the terms of the Creative Commons Attribution License (<http://creativecommons.org/licenses/by/4.0/>), which permits unrestricted use, distribution, and reproduction in any medium, provided the original work is properly cited. The terms on which this article has been published allow the posting of the Accepted Manuscript in a repository by the author(s) or with their consent.

high stability. In particular, Ag NCs have been increasingly studied in recent years because of their luminescence with high quantum yield [108] and the specific catalytic ability for carbon dioxide (CO₂) reduction [109]. These Ag NCs can be synthesized with atomical precision using ligands, such as thiolate (SR) [110–115], phosphine (PR₃) [116–118], and acetylide (C≡CR) [119,120]. For ligand-protected Ag NCs containing anions at the central position (hereafter, anion-templated Ag NCs), synthesis of new NCs has been continuously reported since 1996.

The anion-templated metal NCs were discovered in the synthesis of Cu NCs. In 1976, Freeman et al. [121] and Schugar et al. [122] both synthesized Cl@Cu₁₄Cl (SC(CH₃)₂CH₂NH₂)₁₂, where SC(CH₃)₂CH₂NH₂ is penicillamine, and the element or compound before '@' is the central anion. In this case, chloride ions (Cl[−]), which were included in the reagents, served as the template anion. In 1993, Tang and colleagues reported on S@Cu₁₄(SPh)₁₂(PPh₃)₆ (S = sulfide ion, SPh = benzenethiolate, PPh₃ = triphenylphosphine, Table 1) [123], where carbon disulfide (CS₂) was used as the source of a template anion (S^{2−}), and thus, anion-templated Cu NCs were strategically synthesized. Later, they successfully determined the geometric structure of S@Ag₁₄(SPh)₁₂(PPh₃)₈·4MeOH·13H₂O (MeOH = methanol, H₂O = water) [124], which is the first report on anion-templated Ag NCs. In 2009, Wang and colleagues reported the synthesis of [CO₃@Ag₁₇(C≡C^tBu)₁₄]⁺ (CO₃ = carbonate ion, C≡C^tBu = *tert*-butylacetylene, Table 1) [125], which demonstrated that oxoanions (Ox) can also function as a template. Recently, Ag NCs encapsulating polyoxometalate (POM), which is formed by the condensation of Ox, hydride (H), or deuteride (D), have also been reported, and the types of anion species in anion-templated Ag NCs are diversifying (Figure 1).

In the synthesis of Ag NCs, the anion-template method is effective for generating new structures and new functions. Specifically, 1) the size and shape of Ag NCs can be controlled, 2) the charge interactions within Ag NCs can be well stabilized, and 3) novel functions can be added to Ag NCs, all depending on the selection of the central anion. Notably, several reviews have focused on anion-templated Ag NCs [126–130], but these reviews are limited and do not comprehensively summarize the synthesis methods and geometric structures obtained using all of the aforementioned anions (halide (X), chalcogenide (X'), Ox, POM, and H/D).

In this review, we categorize anions into five types, namely X, X', Ox, POM, and H/D, and describe the synthesis and geometric structures of anion-templated Ag NCs encapsulating these anions. The paper discusses the influences of central anions on the geometric structure of anion-templated Ag NCs by comparing representative

Table 1. The abbreviations for functional group names and compound names.

Abbreviation	Full name	Chemical formula
Ar	4-Anisyl group	−C ₆ H ₄ OCH ₃
ⁱ Bu	<i>sec</i> -Butyl group	−CH(CH ₃)CH ₂ CH ₃
^t Bu	<i>tert</i> -Butyl group	−C(CH ₃) ₃
Bz	Benzyl group	−CH ₂ C ₆ H ₅
Cy	Cyclohexyl group	−C ₆ H ₁₁
Et	Ethyl group	−CH ₂ CH ₃
Fc	Ferrocenyl group	C ₅ H ₅ FeC ₅ H ₄ −
Me	Methyl group	−CH ₃
Nap	Naphthalene group	−C ₁₀ H ₇
Ph	Phenyl group	−C ₆ H ₅
	Phenylene group	−C ₆ H ₄ −
Pr	Propyl group	−CH ₂ CH ₂ CH ₃
ⁱ Pr	<i>iso</i> -Propyl group	−CH(CH ₃)CH ₃
<i>p</i> -tol	<i>p</i> -Tolyl group	−C ₆ H ₄ CH ₃
<i>p</i> -tos	Tosyl group	−SO ₂ C ₆ H ₄ CH ₃
OAc	Acetate	CH ₃ CO ₂
S-Adm	1-Adamantanethioate	SC ₁₀ H ₁₆
Ala	Alanine	CH ₃ CH(NH ₂)CO ₂ H
BMIIm	1-Butyl-3-methylimidazolium	CH ₃ (CH ₂) ₃ NC ₃ H ₃ NCH ₃
4Cp	4-Cyanopyridine	NC ₅ H ₄ CN
Cys	Cysteine	HSCH ₂ CH(NH ₂)CO ₂ H
DCM	Dichloromethane	CH ₂ Cl ₂
DEF	Diethyl formamide	(C ₂ H ₅) ₂ NCHO
DMF	<i>N,N</i> -Dimethylformamide	(CH ₃) ₂ NCHO
DMAc	Dimethylacetamide	CH ₃ C(O)N(CH ₃) ₂
dppb	1,4-Bis(diphenylphosphino) butane	(C ₆ H ₅) ₂ PC ₄ H ₈ P(C ₆ H ₅) ₂
dppe	1,2-Bis(diphenylphosphino) ethane	(C ₆ H ₅) ₂ PC ₂ H ₄ P(C ₆ H ₅) ₂
dppf	1,1'-Bis(diphenylphosphino) ferrocene	(C ₆ H ₅) ₂ P[Fe(C ₅ H ₄) ₂]P(C ₆ H ₅) ₂
dppm	Bis(diphenylphosphino) methane	(C ₆ H ₅) ₂ PCH ₂ P(C ₆ H ₅) ₂
dppp	1,3-Bis(diphenylphosphino) propane	(C ₆ H ₅) ₂ PC ₃ H ₆ P(C ₆ H ₅) ₂
hfac	Hexafluoroacetylacetone	CF ₃ C(O)CC(O)CF ₃
OTf	(Trifluoromethyl)sulfonate	CF ₃ SO ₃
tfa	Trifluoroacetate	CF ₃ CO ₂
THF	Tetrahydrofuran	C ₄ H ₈ O
TMEDA	<i>N,N,N',N'</i> -Tetramethylethylenediamine	(CH ₃) ₂ NC ₂ H ₄ N(CH ₃) ₂
H ₂ PTA	Phthalic acid	C ₆ H ₄ (CO ₂ H) ₂
Pro	Proline	C ₄ H ₇ NHCO ₂ H
Py	Pyridine	C ₅ H ₅ N
Val	Valine	(CH ₃) ₂ CHCH(NH ₂)CO ₂ H

anion-templated Ag NCs. Owing to space limitations, all the chemical compositions of the reported anion-templated Ag NCs that are not described in detail are summarized in Tables 2–6. This summary aims to provide readers with the latest knowledge on anion-templated Ag NCs, serving as design guidelines for the creation of novel structures.

In Section 2, we describe the synthesis methods for anion-templated Ag NCs. In Section 3, we describe the results of the synthesis and geometric structures of the anion-templated Ag NCs while categorizing them by anion species. After a short conclusion in Section 4, the challenges and future avenues for the development of anion-templated Ag NCs are described in Section 5.

2. Synthesis methods

Anion-templated Ag NCs are generally synthesized by mixing Ag salts and ligand compounds in solution and adding a reducing agent or other agents to the solution.

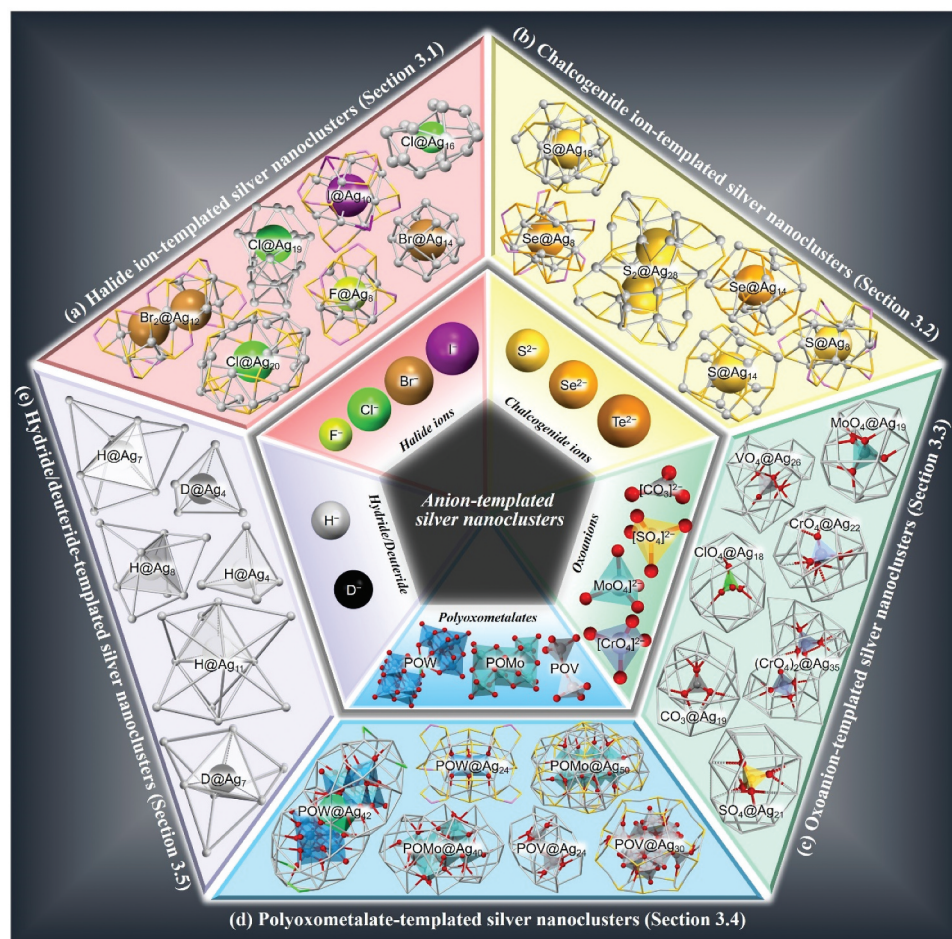


Figure 1. Diversification of anion-templated Ag NCs. (a) X-templated Ag NCs (X@Ag NCs; Section 3.1), (b) X'-templated Ag NCs (X'@Ag NCs; Section 3.2), (c) Ox-templated Ag NCs (Ox@Ag NCs; Section 3.3), (d) POM-templated Ag NCs (Pom@Ag NCs; Section 3.4), and (e) H/D-templated Ag NCs (H/D@Ag NCs; Section 3.5).

The addition of a reducing agent is not essential, and in some cases, anions can be formed without a reducing agent [131]. SR, PR₃, and C≡CR are frequently used as ligands because of their high affinity to Ag. During synthesis, a precursor, which induces the formation of a template anion, is generally added. However, the addition of precursors is also not essential, and in some cases, anions can be formed without adding precursors, as in the case of Cl@Cu₁₄(SC(CH₃)₂CH₂NH₂)₁₂

described in Section 1. In both cases, anion-templated Ag NCs cannot form unless the conditions are conducive to the generation of a central anion. In most cases, anions are formed by stirring the mixture to induce a chemical reaction (stirring method, Figure 2(a)). The solvothermal (Figure 2(b)) and ultrasonication methods (Figure 2(c)) are also often used.

The stirring method is the most frequently used, and the majority of anion-templated Ag NCs are synthesized

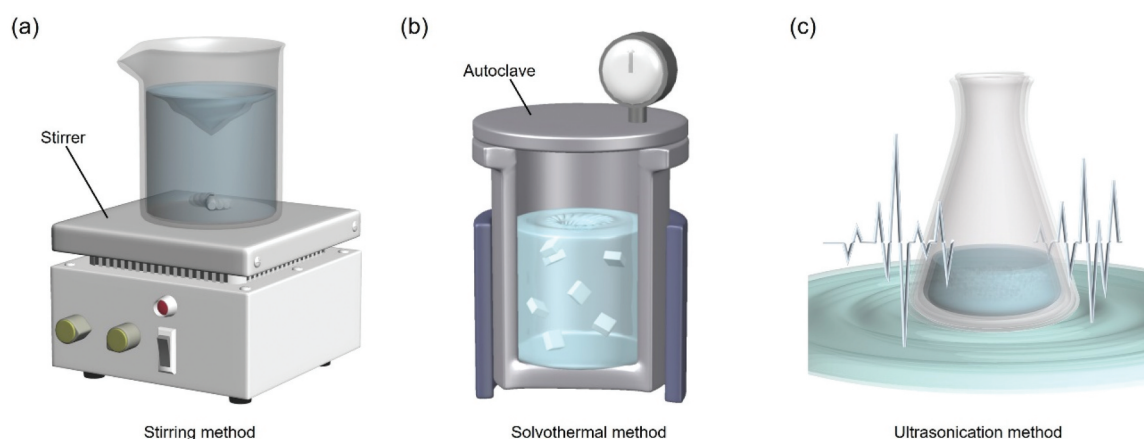


Figure 2. Three representative methods in the synthesis of anion-templated Ag NCs. (a) Stirring method, (b) solvothermal method, and (c) ultrasonication method.

by this method. In this method, specific central anions are produced by simple stirring and the addition of reaction accelerators. Stirring is generally performed at temperatures from -20 to $25\text{ }^{\circ}\text{C}$ [131–134]. When CO_3^{2-} is used as a template source, atmospheric CO_2 can also be used, where CO_2 is converted to CO_3^{2-} by adding N,N,N',N' -tetramethylethylenediamine (TMEDA, Table 1) to the reaction system: in this reaction, the basicity of the solvent is important to produce CO_3^{2-} from H_2CO_3 formed by hydration of CO_2 [125]. Solvothermal methods are also frequently used in the synthesis of anion-templated Ag NCs [135–140]. In these methods, the chemical species in the reaction system are thermally decomposed to produce central anions. Typically, the heating is conducted at lower temperatures (60 – $80\text{ }^{\circ}\text{C}$) than those used for the synthesis of metal nanoparticles. The reason is that high temperatures might result in the decomposition of Ox and POM.

In the ultrasonication method, a chemical source of the template anion is dissolved in a solvent, which is then sonicated to induce the formation of anions.

Using the ultrasonication method, the reaction solution can be heated and cooled more rapidly compared with the solvothermal method, allowing different reactions to proceed [141–144].

3. Examples of anion-templated Ag NCs

In the following sections, we describe the syntheses and geometric structures of anion-templated Ag NCs containing X (X@Ag_n NCs, Section 3.1, Figure 1(a)), X' ($\text{X}'\text{@Ag}_n$ NCs, Section 3.2, Figure 1(b)), Ox (Ox@Ag_n NCs, Section 3.3, Figure 1(c)), POM (POM@Ag_n NCs, Section 3.4, Figure 1(d)), and H/D (H/D@Ag_n NCs, Section 3.5, Figure 1(e)). The abbreviations for the ligands, functional groups, and solvents used in this review are summarized in Table 1.

3.1. Halide ion-templated Ag NCs

Table 2 summarizes the reported X@Ag_n NCs and includes their abbreviations [131–133,145–163]. In

Table 2. Representative X-templated Ag NCs.

No.	Chemical formula	Abbreviation	Center anion	z^a	Synthesis method	Year	Ref.
1	$[\text{Br@Ag}_7(\text{dppe})_3(\text{SeC}_2\text{H}_4\text{O}(\text{O})\text{CFC}_6)_6]^0$	Br@Ag7	Br^-	0	Stirring	2011	[156]
2	$[\text{F@Ag}_8(\text{S}_2\text{P}(\text{OEt})_2)_6][\text{PF}_6]$	F@Ag8a	F^-	+1	Stirring	2010	[132]
3	$[\text{F@Ag}_8(\text{S}_2\text{P}(\text{OPr})_2)_6][\text{PF}_6]$	F@Ag8b	F^-	+1	Stirring	2014	[133]
4	$[\text{Cl@Ag}_8(\text{Se}_2\text{P}(\text{OEt})_2)_6][\text{PF}_6]$	Cl@Ag8a	Cl^-	+1	Stirring	2004	[131]
5	$[\text{Cl@Ag}_8(\text{Se}_2\text{P}(\text{OPr})_2)_6][\text{PF}_6]$	Cl@Ag8b	Cl^-	+1	Stirring	2004	[131]
6	$[\text{Cl@Ag}_8(\text{Se}_2\text{P}(\text{O}^i\text{Pr})_2)_6][\text{PF}_6]$	Cl@Ag8c	Cl^-	+1	Stirring	2004	[131]
7	$[\text{Cl@Ag}_8(\text{S}_2\text{P}(\text{OEt})_2)_6][\text{PF}_6]$	Cl@Ag8d	Cl^-	+1	Stirring	2010	[132]
8	$[\text{Cl@Ag}_8(\text{S}_2\text{P}(\text{O}^i\text{Pr})_2)_6][\text{PF}_6]$	Cl@Ag8e	Cl^-	+1	Stirring	2014	[133]
9	$[\text{Br@Ag}_8(\text{Se}_2\text{P}(\text{OEt})_2)_6][\text{PF}_6]$	Br@Ag8a	Br^-	+1	Stirring	2004	[131]
10	$[\text{Br@Ag}_8(\text{Se}_2\text{P}(\text{OPr})_2)_6][\text{PF}_6]$	Br@Ag8b	Br^-	+1	Stirring	2004	[131]
11	$[\text{Br@Ag}_8(\text{Se}_2\text{P}(\text{O}^i\text{Pr})_2)_6][\text{PF}_6]$	Br@Ag8c	Br^-	+1	Stirring	2004	[131]
12	$[\text{Br@Ag}_8(\text{S}_2\text{P}(\text{O}^i\text{Pr})_2)_6][\text{PF}_6]$	Br@Ag8d	Br^-	+1	Stirring	2014	[133]
13	$[\text{I@Ag}_{10}(\text{S}_2\text{P}(\text{OPr})_2)_6]^0$	I@Ag10	I^-	0	Stirring	2014	[133]
14	$[\text{I@Ag}_{11}(\text{S}_2\text{P}(\text{O}^i\text{Pr})_2)_6][\text{PF}_6]$	I@Ag11a	I^-	+1	Stirring	2012	[157]
15	$[\text{I@Ag}_{11}(\text{Se}_2\text{P}(\text{O}^i\text{Pr})_2)_6][\text{PF}_6]$	I@Ag11b	I^-	+1	Stirring	2012	[157]
16	$[\text{Br}_2\text{@Ag}_{12}(\text{S}_2\text{P}(\text{OEt})_2)_6]^0$	Br2@Ag12	Br^-	0	Stirring	2013	[146]
17	$[\text{I@Ag}_{12}(\text{S}_2\text{P}(\text{C}_2\text{H}_4\text{Ph})_2)_6][\text{I}]$	I@Ag12	I^-	+1	Stirring	2014	[145]
18	$[\text{I}_2\text{@Ag}_{12}(\text{S}_2\text{P}(\text{OEt})_2)_6]^0$	I2@Ag12a	I^-	0	Stirring	2013	[146]
19	$[\text{I}_2\text{@Ag}_{12}(\text{Se}_2\text{P}(\text{OEt})_2)_6]^0$	I2@Ag12b	I^-	0	Stirring	2013	[146]
20	$[\text{F@Ag}_{14}(\text{C}\equiv\text{C}^i\text{Bu})_{12}][\text{BF}_4]$	F@Ag14	F^-	+1	Stirring	2002	[148]
21	$[\text{Cl@Ag}_{14}(\text{C}\equiv\text{C}^i\text{Bu})_{12}][\text{OH}]$	Cl@Ag14a	Cl^-	+1	Treating ^b	2001	[147]
22	$[\text{Cl@Ag}_{14}(\text{C}\equiv\text{C}^i\text{Bu})_{12}][\text{BF}_4]$	Cl@Ag14b	Cl^-	+1	Stirring	2001	[147]
23	$[\text{Br@Ag}_{14}(\text{C}\equiv\text{C}^i\text{Bu})_{12}][\text{BF}_4]$	Br@Ag14	Br^-	+1	Stirring	2001	[147]
24	$[\text{Cl@Ag}_8\text{Ni}_6(\text{SCMe}_2\text{CH}(\text{NH}_2)\text{CO}_2)_{12}]_3$ [Co(NH ₃) ₆] ₅ ~197 H ₂ O	Cl@Ag8Ni6	Cl^-	-5	Crystallization ^b	1981	[160]
25	$[\text{Cl@Ag}_8\text{Cu}_6(\text{C}\equiv\text{C}^i\text{Bu})_{12}][\text{BF}_4]$	Cl@Ag8Cu6	Cl^-	+1	Stirring	2013	[161]
26	$[\text{Br@Ag}_8\text{Cu}_6(\text{C}\equiv\text{C}^i\text{Bu})_{12}][\text{BF}_4]$	Br@Ag8Cu6	Br^-	+1	Stirring	2013	[161]
27	$[\text{Cl@Ag}_{16}(\text{C}\equiv\text{C}^i\text{Bu})_9(\text{hfac})(\text{OAc})]$ [Yb ₃ OH ₄ (^t BuPO ₃) ₃ (hfac) ₃ (MeOH) ₃] ⁰ ·4MeOH·H ₂ O	Cl@Ag16a	Cl^-	0	Stirring	2018	[158]
28	$[\text{Cl@Ag}_{16}(\text{C}\equiv\text{C}^i\text{Bu})_7(\text{hfac})_2(\text{BuPO}_3)(\text{MeOH})_2][\text{Yb}_6(\text{OH})_2\text{O}_6(\text{BuPO}_3)_6(\text{H}_2\text{O})_6(\text{MeOH})_6]^0$	Cl@Ag16b	Cl^-	0	Stirring	2018	[158]
29	$[\text{Cl@Ag}_{16}(\text{C}\equiv\text{C}^i\text{Bu})_{11}(\text{hfac})_3(\text{tfa})]^0$	Cl@Ag16c	Cl^-	0	Ultrasonication	2018	[159]
30	$[\text{Cl@Ag}_{16}(\text{S}^i\text{Bu})_8(\text{tfa})_7(\text{DMF})_4(\text{H}_2\text{O})]^0$ ·1.5DMF	Cl@Ag16d	Cl^-	0	Stirring	2019	[162]
31	$[\text{Cl@Ag}_{16}(\text{S}^i\text{Adm})_8(\text{tfa})_5(\text{DMF})_3(\text{H}_2\text{O})_2]^0$ ·DMF	Cl@Ag16e	Cl^-	0	Stirring	2022	[163]
32	$[\text{Cl@Ag}_{12}(\text{C}\equiv\text{CPh})_{14}(\text{AgPPh}_3)_6][\text{SbF}_6][\text{CH}_2\text{CINeEt}_3]$	Cl@Ag18a	Cl^-	+3	Stirring	2017	[149]
33	$[\text{Cl@Ag}_{12}(\text{C}\equiv\text{CPh})_{14}(\text{AgP}(p\text{-tol})_3)_6][\text{SbF}_6]$	Cl@Ag18b	Cl^-	+3	Stirring	2017	[149]
34	$[\text{Cl@Ag}_{19}(\text{C}\equiv\text{C}^i\text{Bu})_{11}(\text{tfa})_7]^0$	Cl@Ag19	Cl^-	0	Stirring	2008	[150]
35	$[\text{Cl@Ag}_{20}(\text{S}^i\text{Bu})_{10}(\text{tfa})_2][\text{tfa}]_7$ ·5MeOH	Cl@Ag20	Cl^-	+7	Stirring	2013	[151]
36	$[\text{Cl}_2\text{@Ag}_{21}(\text{C}\equiv\text{C}^i\text{Bu})_9(\text{BuPO}_3)_3\text{V}_3\text{O}_6(\text{OH})_2(\text{BuPO}_3)\text{VO}_2(\text{OH})](\text{MeOH})_2(\text{H}_2\text{O})_2]^0$ ·2MeOH·2H ₂ O	Cl2@Ag21	Cl^-	0	Stirring	2012	[152]
37	$[\text{Br@Ag}_{36}(\text{SPh}^i\text{Bu})_{36}][\text{Et}_3\text{NH}]$	Br@Ag36	Br^-	-1	Solvothermal	2010	[153]
38	$[\text{Cl@Ag}_{12}(\text{Ag}_{48}(\text{dppm})_{12})]^0$	Cl@Ag60	Cl^-	0	Crystallization ^b	2019	[154]
39	$[\text{Cl@Ag}_{216}\text{S}_{56}\text{Cl}_6(\text{C}\equiv\text{CPh})_{98}(\text{H}_2\text{O})_{12}]$ [Ag ₃ (C ₃ H ₄ N ₂)(H ₂ O) ₄][SbF ₆] ₂	Cl@Ag216	Cl^-	+1	Stirring	2017	[155]

^aCharge state of Ag NC. ^bSee references for details of the synthesis method.

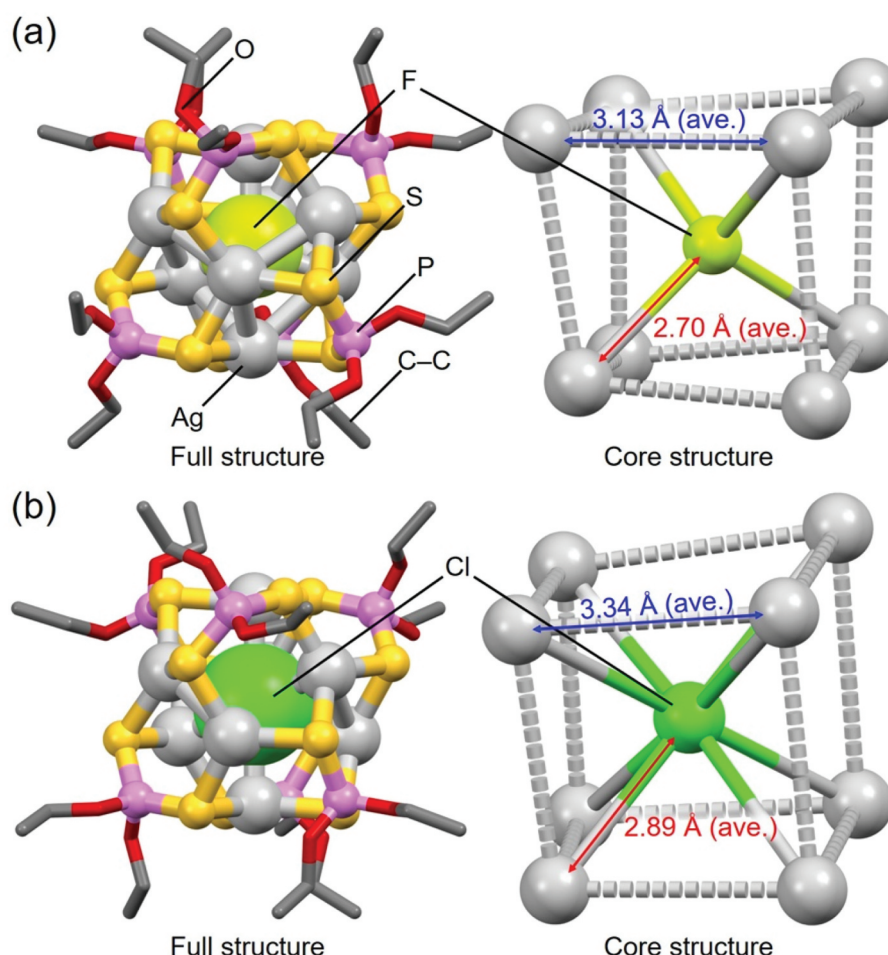


Figure 3. Full (left) and core (right) structures of (a) **2 (F@Ag8a)** and (b) **7 (Cl@Ag8d)**. Data are taken from ref [132].

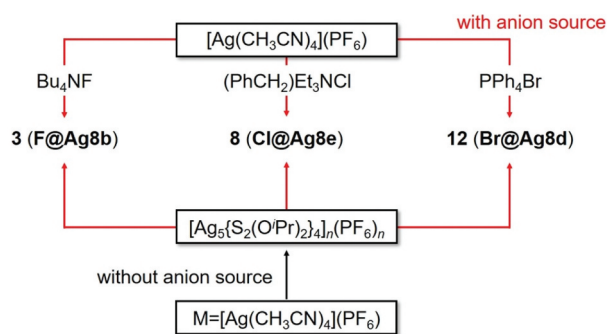


Figure 4. Two synthesis methods for **3 (F@Ag8b)**, **8 (Cl@Ag8e)**, and **12 (Br@Ag8d)**. Red lines are methods using anion sources. Black ones are methods without any anion sources. Data are taken from ref [133]. Reprinted with permission from [133], copyright (2014, the Royal Society of Chemistry).

the following section, we describe their syntheses and the effects of the different X species on the geometric structures of Ag NCs.

3.1.1. X@Ag₈NCs

There are numerous reports on X@Ag₈ NCs with a diverse range of central anions, including fluoride ions (F[−]), Cl[−], and bromide ions (Br[−]). All these X@Ag₈ NCs have been synthesized by Liu and colleagues. They reported the syntheses of **2 (F@Ag8a)**, **3**

(F@Ag8b), **4 (Cl@Ag8a)**, **5 (Cl@Ag8b)**, **6 (Cl@Ag8c)**, **7 (Cl@Ag8d)**, **8 (Cl@Ag8e)**, **9 (Br@Ag8a)**, **10 (Br@Ag8b)**, **11 (Br@Ag8c)**, and **12 (Br@Ag8d)** from 2004 to 2014 [131–133]. All of these X@Ag₈ NCs were synthesized using the stirring method. For the precursors of each X, tetrabutylammonium fluoride (Bu₄NF), tetrabutylammonium chloride (Bu₄NCl), tetrabutylammonium bromide (Bu₄NBr), benzyltriethylammonium chloride ((PhCH₂)Et₃NCl), or tetraphenylphosphonium bromide (PPh₄Br) were used, and the central X anion is formed by their dissociation in the reaction process.

These eleven X@Ag₈ NCs all contain the same number of Ag atoms, and their geometric structures are similar; they all have a distorted cubic framework composed of eight Ag atoms, with X located at the central position (Figure 3). However, the X–Ag distance differs slightly depending on the central X anion. For example, in **2 (F@Ag8a)**, the average X–Ag distance from the central X anion to the surrounding core Ag is 2.70 Å, whereas the distance is 2.89 Å in **7 (Cl@Ag8d)**. There is also a difference in the average Ag–Ag distance within the Ag₈ core between **2** and **7**; it is 3.13 Å for **2 (F@Ag8a)** and 3.34 Å for **7 (Cl@Ag8d)**. These results indicate that a smaller central X anion

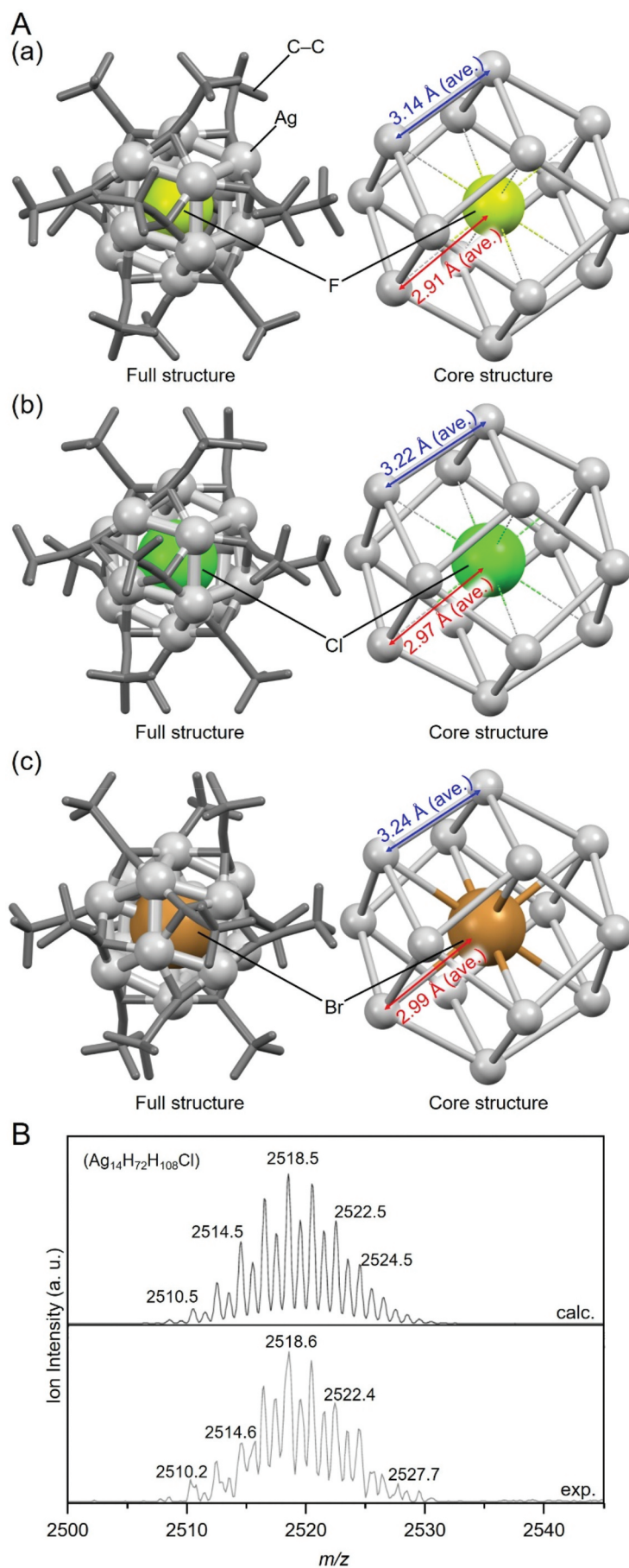


Figure 5. (A) Full (left) and core (right) structures of (a) 20 (**F@Ag14**), (b) 21 (**Cl@Ag14a**), and (c) 23 (**Br@Ag14**). (B) the observed and simulated ESI-MS pattern for 21 (**Cl@Ag14a**). Data are taken from refs [147,148]. Reprinted with permission from [147], copyright (2001, WILEY-VCH Verlag GmbH, Weinheim, Fed. Rep. of Germany).

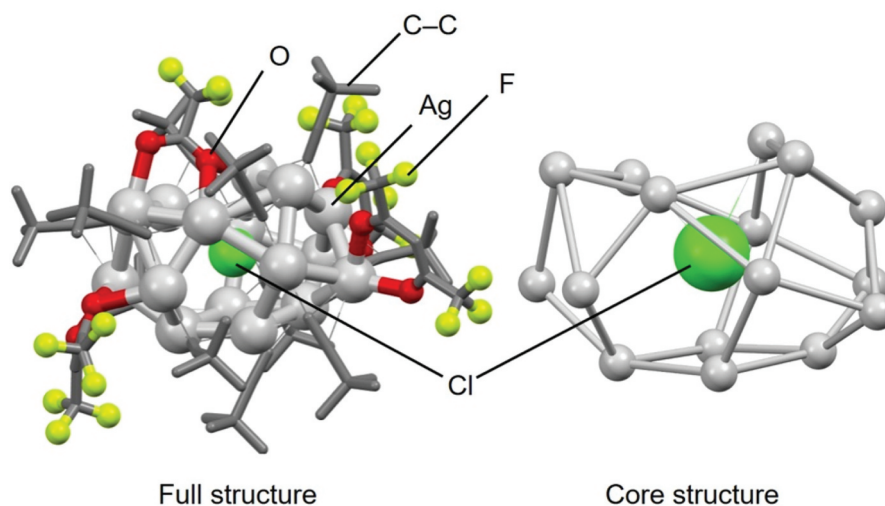


Figure 6. Full (left) and core (right) structures of 29 (**Cl@Ag16c**). Data are taken from ref [159].

results in a more contracted $X@Ag_8$ NCs framework. Furthermore, only four Ag atoms form bonds with the central F^- in **2** (**F@Ag8a**), whereas eight Ag atoms bond to the central Cl^- in **7** (**Cl@Ag8d**). Thus, a different type of central X anion induces a slight difference in the size of the $X@Ag_8$ NC framework and the number of bonds within the framework.

Moreover, in the synthesis performed by Liu and colleagues, under conditions without an anion source, one-dimensional structures of $[Ag_5(S_2P(O^iPr)_2)_4]_n(PF_6)_n$ were formed instead of $X@Ag_8$ NCs. However, it has been shown that the addition of an anion source to the resulting $[Ag_5(S_2P(O^iPr)_2)_4]_n(PF_6)_n$ leads to the formation of **3** (**F@Ag8b**), **8** (**Cl@Ag8e**), and **12** (**Br@Ag8d**) (Figure 4).

3.1.2. $X@Ag_{14}$ NCs

The synthesis of $X@Ag_{14}$ NC was reported by Rais and colleagues in 2001 [147] and 2002 [148]. These $X@Ag_{14}$ NCs are pioneering examples of Ag NCs containing X. In Table 2, **20** (**F@Ag14**), **21** (**Cl@Ag14a**), **22** (**Cl@Ag14b**), and **23** (**Br@Ag14**) correspond to these $X@Ag_{14}$ NCs, most of which were synthesized by the stirring method. In the synthesis of **21** (**Cl@Ag14a**), Ag-containing polymer compound $[Ag(C\equiv C^tBu)]_n$ was used as an Ag precursor, whereas silver tetrafluoroborate ($AgBF_4$) was used as an Ag precursor in the synthesis of **20** (**F@Ag14**), **22** (**Cl@Ag14b**), and **23** (**Br@Ag14**). The F^- in **20** (**F@Ag14**) was generated by the hydrolysis reaction [164,165] of the Ag precursor ($AgBF_4$). For **21** (**Cl@Ag14a**) and **22** (**Cl@Ag14b**), the Cl^- was generated by the dissociation of the chloroform (the reaction solvent) and Bu_4NCl added as the Cl^- source, respectively. In the synthesis of **23** (**Br@Ag14**), Bu_4NBr was added as the Br^- source.

Figure 5A shows the geometric structures of **20** (**F@Ag14**, Figure 5A(a)), **21** (**Cl@Ag14a**, Figure 5A(b)), and **23** (**Br@Ag14**, Figure 5A(c)), as determined by single-crystal X-ray diffraction (SC-XRD). All of the

$X@Ag_{14}$ NCs have a cubic framework consisting of eight Ag atoms, with an additional Ag atom on each of the six faces of the cube. This results in the construction of a rhombic dodecahedral Ag framework. Similar to $X@Ag_8$ NCs, the size of the Ag framework in $X@Ag_{14}$ NCs varies depending on the X at the central position. For example, for **20** (**F@Ag14**), **21** (**Cl@Ag14a**), and **23** (**Br@Ag14**), the average X–Ag distances are 2.91, 2.97, and 2.99 Å, respectively, and the average Ag–Ag distances are 3.14, 3.22, and 3.24 Å, respectively. The X–Ag distances in these $X@Ag_{14}$ NCs (X = F, Cl, and Br) are longer than those in the AgF (2.46 Å) [166], $AgCl$ (2.77 Å) [167], and $AgBr$ (2.89 Å) salts [167], indicating that the free volume exists in the Ag_{14} cage. The free volume decreases with the increasing ionic radius of X.

For **20** (**F@Ag14**), **22** (**Cl@Ag14b**), and **23** (**Br@Ag14**), electrospray ionization mass spectrometry (ESI-MS) has been performed, in addition to SC-XRD. Characteristic peaks appear in the spectra of **22** (**Cl@Ag14b**) and **23** (**Br@Ag14**) (Figure 5B), which means that these NCs can maintain their chemical composition in solution. In contrast, no peak has been observed at the position that can be attributed to **20** (**F@Ag14**), implying that **20** (**F@Ag14**) degrades in solution.

3.1.3. $X@Ag_{16}$ NCs

The synthesis of $X@Ag_{16}$ NC was also often reported. In Table 2, **27** (**Cl@Ag16a**), **28** (**Cl@Ag16b**), **29** (**Cl@Ag16c**), **30** (**Cl@Ag16d**), and **31** (**Cl@Ag16e**) correspond to these $X@Ag_{16}$ NCs. Among them, **27**, **28**, **30**, and **31** were prepared by the stirring method, whereas **29** was prepared by the ultrasonication method. Figure 6 shows the geometrical structure of **29** (**Cl@Ag16c**). This NC encapsulates a template chloride anion, with argentophilic $Ag\cdots Ag$ bond distances in the range of 2.703–3.286 Å. The chloride ion coordinates to three silver atoms in this structure. The $X@Ag_{16}$ core has ellipsoid structure. These structures are largely different from the

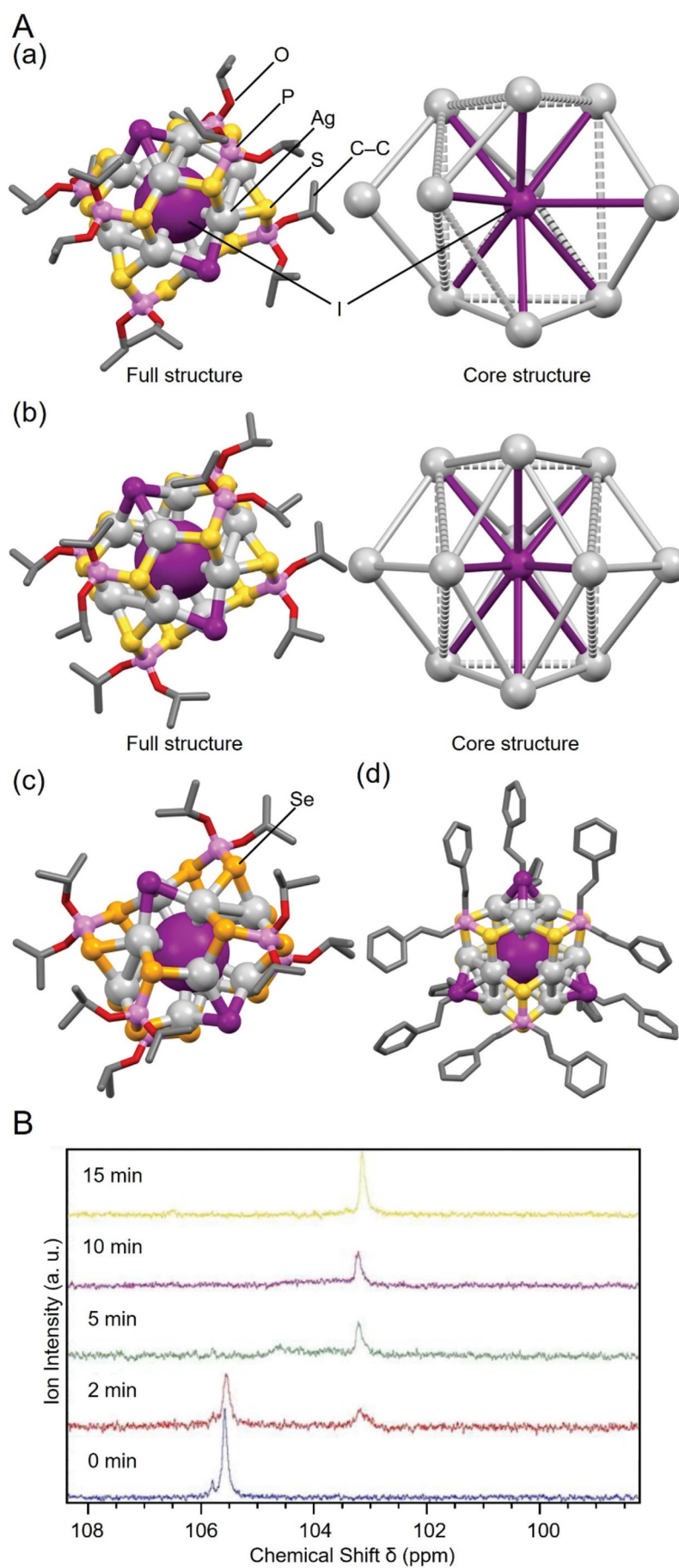


Figure 7. (A) Full (left) and core (right) structures of (a) 13 (**I@Ag10**), (b) 14 (**I@Ag11a**), (c) 15 (**I@Ag11b**), and (d) 17 (**I@Ag12**). (B) the $^{31}\text{P}\{^1\text{H}\}$ NMR spectra of monitoring the conversion within 15 minutes from 13 (**I@Ag10**) to 14 (**I@Ag11a**) by adding one equivalent of $[\text{Ag}(\text{CH}_3\text{CN})_4][\text{PF}_6]$ relative to the case of the synthesis of 13 (**I@Ag10**). Data are taken from refs [133,145,157]. Reprinted with permission from [133], copyright (2014, the Royal Society of Chemistry).

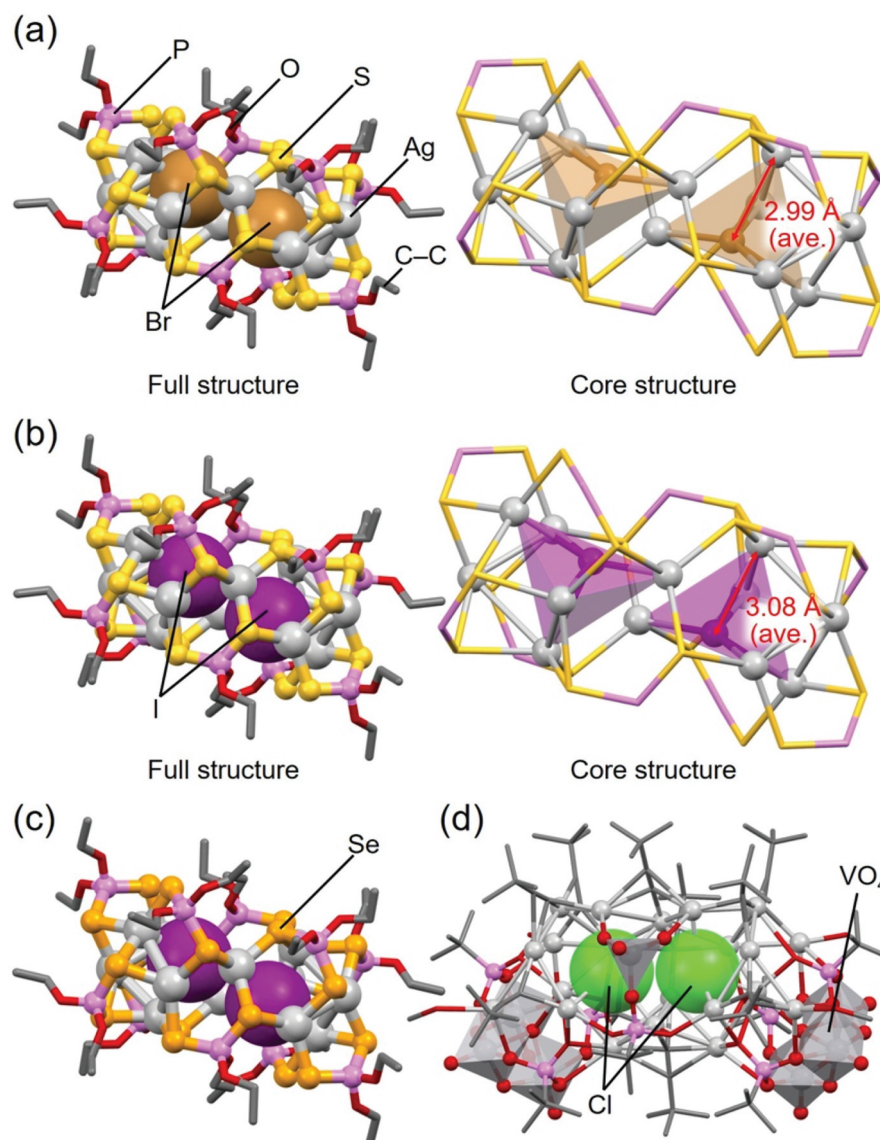


Figure 8. Full (left) and core (right) structures of (a) 16 ($\text{Br}_2\text{@Ag}_{12}$) and (b) 18 ($\text{I}_2\text{@Ag}_{12a}$). Full structures of (c) 19 ($\text{I}_2\text{@Ag}_{12b}$) and (d) 36 ($\text{Cl}_2\text{@Ag}_{21}$). Data are taken from refs [146,152].

above-described X@Ag_8 and X@Ag_{14} NCs. Thus, the structure of X@Ag_n core strongly changes depending on the number of Ag atoms.

3.1.4. Other X@Ag_n NCs

At the end of this section, we introduce the syntheses of X@Ag_n NCs that are different from the Ag NCs described in Sections 3.1.1 and 3.1.2.

The first example is the I@Ag_n NC, containing an iodide ion (I^-). Representative examples of I@Ag_n NCs include 13 (I@Ag_{10}) [133], 14 (I@Ag_{11a}), 15 (I@Ag_{11b}) [157], and 17 (I@Ag_{12}) [145] (Figure 7A). All of these I@Ag_n NCs have been synthesized by Liu and colleagues. They used tetrabutylammonium iodide (Bu_4NI) as the I^- precursor and the stirring method for synthesis. In the syntheses of 13 (I@Ag_{10}) and 14 (I@Ag_{11a}), although the same ligands were used, an excess of one equivalent of the Ag precursor was added in the synthesis of 14 (I@Ag_{11a}) over the case of 13

(I@Ag_{10}). They tracked the effect of this excess Ag precursor on the chemical composition of the product by multinuclear (^1H and ^{31}P) magnetic resonance spectroscopy (^{31}P $\{^1\text{H}\}$ NMR). The results demonstrated that 14 (I@Ag_{11a}) begins to form approximately 5 minutes after initiation of the reaction (Figure 7B). Comparing the geometric structures, 13 (I@Ag_{10}) has a cage structure with one Ag atom missing from the Ag_{11} cage of 14 (I@Ag_{11a}). The addition of an extra Ag precursor caused the addition of an Ag atom to the missing site, resulting in the conversion of 13 (I@Ag_{10}) to 14 (I@Ag_{11a}). From this observation, they suggested that NCs with one Au atom added to 13 (I@Ag_{10}) could be obtained by adding the compound that would serve as an Au precursor to the solution of 13 (I@Ag_{10}).

The second example is the $\text{X}_2\text{@Ag}_n$ NC, in which two X anions are encapsulated within one Ag framework. Liu and colleagues reported the

syntheses of **16** (**Br₂@Ag₁₂**), **18** (**I₂@Ag_{12a}**), and **19** (**I₂@Ag_{12b}**) [146] in 2013, and Xie and Mak reported the synthesis of **36** (**Cl₂@Ag₂₁**) [152] in 2012 (Table 2). These X₂@Ag_n NCs are generally similar in shape, and all of them have peanut- or butterfly-shaped frameworks composed of Ag and S atoms (Figure 8). The average X–Ag distance in **16** (**Br₂@Ag₁₂**) is 2.80 Å, which is longer than the average X–Ag distance (2.98 Å) in **18** (**I₂@Ag_{12a}**), protected by the same ligand. This indicates that the X–Ag distance also varies with the size of the central X anion in the case of X₂@Ag_n NCs, similar to X@Ag₈ and X@Ag₁₄ NCs.

3.2. Chalcogenide ion-templated Ag NCs

In this section, we describe the X'@Ag_n NCs that encapsulate X' at the central position. Table 3 summarizes the representative X'@Ag_n NCs [124,133–135,137,143,144,168–182]. Again, to discuss the effects of the central X' species on the geometric structure of the X'@Ag_n NCs, we limit the examples to the X'@Ag₉ NCs and X'@Ag₁₄ NCs.

3.2.1. X'@Ag₉ NCs

For X'@Ag₉ NCs, the synthesis of **42** (**S@Ag₉**) and **43** (**Se@Ag₉**) with S^{2−} or selenide ion (Se^{2−}) at the central position has been reported by Liu and colleagues in 2017 [134] (Table 3). Both X'@Ag₉ NCs were synthesized by mixing the Ag precursor, tetrakis(acetonitrile) copper(I) hexafluorophosphate (Ag(MeCN)₄PF₆), and the ligand precursor, chalcogen-containing ammonium salt (NH₄X'₂P(OEt)₂, X' = S or Se), in acetone, followed by the addition of NaX'H (X' = S or Se), which was then stirred at a low temperature (−20 or 0 °C). For the synthesis of **42** (**S@Ag₉**), a polymer compound ([Ag₅(S₂P(OEt)₂)₄(PF₆)_n) can be used as a precursor, instead of the ligand precursor.

Figure 9A shows the geometric structures of **42** (**S@Ag₉**) and **43** (**Se@Ag₉**), as determined by SC-XRD [134]. Both X'@Ag₉ NCs have a geometric structure with three Ag atoms surrounding an hourglass-shaped Ag₆ core. However, there are also differences between them. For example, focusing on the hourglass-shaped Ag₆ core, the average Ag–Ag distance is slightly shorter in **42** (**S@Ag₉**) than in **43** (**Se@Ag₉**), with 3.40 and 3.66 Å, respectively. The average X'–Ag distance is also slightly shorter for **42** (**S@Ag₉**)

Table 3. Representative X'-templated Ag NCs.

No.	Chemical formula	Abbreviation	Center anion	z	Synthesis method	Year	Ref.
40	[S@Ag ₈ (S ₂ P(O'Pr) ₂) ₆] ⁰	S@Ag8	S ^{2−}	0	Stirring	2014	[133]
41	[Se@Ag ₈ (Se ₂ P(O'Pr) ₂) ₆] ⁰	Se@Ag8	Se ^{2−}	0	Stirring	1999	[179]
42	[S@Ag ₉ (S ₂ P(OEt) ₂) ₈][Na]	S@Ag9	S ^{2−}	−1	Stirring	2017	[134]
43	[Se@Ag ₉ (Se ₂ P(OEt) ₂) ₈][Na]	Se@Ag9	Se ^{2−}	−1	Stirring	2017	[134]
44	[S@Ag ₁₀ (S ₂ P(OEt) ₂) ₈] ⁰	S@Ag10	S ^{2−}	0	Stirring	2004	[169]
45	[Se@Ag ₁₀ (Se ₂ P(OEt) ₂) ₈] ⁰	Se@Ag10a	Se ^{2−}	0	Stirring	2002	[168]
46	[Se@Ag ₁₀ (Se ₂ P(O'Pr) ₂) ₈] ⁰	Se@Ag10b	Se ^{2−}	0	Stirring	2002	[168]
47	[S@Ag ₁₁ (S ₂ P(OEt) ₂) ₈][PF ₆]	S@Ag11a	S ^{2−}	+1	Stirring	2011	[170]
48	[S@Ag ₁₁ (S ₂ P(OPr) ₂) ₈][PF ₆]	S@Ag11b	S ^{2−}	+1	Stirring	2011	[170]
49	[S@Ag ₁₁ (S ₂ P(O'Pr) ₂) ₈][PF ₆]	S@Ag11c	S ^{2−}	+1	Stirring	2011	[170]
50	[S@Ag ₁₁ (C≡C'Bu) ₂ (S ₂ P(OEt) ₂) ₇] ⁰	S@Ag11d	S ^{2−}	0	Stirring	2018	[177]
51	[Se@Ag ₁₁ (S ₂ P(OEt) ₂) ₆] ⁰	Se@Ag11a	Se ^{2−}	0	Stirring	2006	[178]
52	[Se@Ag ₁₁ (S ₂ P(O'Pr) ₂) ₆] ⁰	Se@Ag11b	Se ^{2−}	0	Stirring	2006	[178]
53	[Se@Ag ₁₁ (S ₂ P(O'Bu) ₂) ₆] ⁰	Se@Ag11c	Se ^{2−}	0	Stirring	2006	[178]
54	[S@Ag ₁₄ (SPh) ₁₂ (PPh ₃) ₈] ⁰ ·4MeOH·13H ₂ O	S@Ag14a	S ^{2−}	0	Stirring	1996	[124]
55	[S@Ag ₁₄ (SPhCN) ₁₂ (PPh ₃) ₈][FeCl ₂ (THF) ₄] ₃	S@Ag14b	S ^{2−}	0	Stirring	2011	[174]
56	[S@Ag ₁₄ (SPhCNS) ₁₂ (PPh ₃) ₈] ⁰	S@Ag14c	S ^{2−}	0	Treating ^a	2011	[174]
57	[S@Ag ₁₄ (PPh ₃) ₆ (SC ₂ H ₄ O)(CFC) ₁₂] ⁰	S@Ag14d	S ^{2−}	0	Stirring	2011	[156]
58	[S@Ag ₁₄ (C≡CPh) ₈ (S ₂ P(OEt) ₂) ₄ (TMEDA) ₂] ⁰ ·5MeOH	S@Ag14e	S ^{2−}	0	Stirring	2018	[177]
59	[S@Ag ₁₄ (C≡CPh) ₈ (S ₂ P(O'Pr) ₂) ₄ (TMEDA) ₂] ⁰ ·7MeOH	S@Ag14f	S ^{2−}	0	Stirring	2018	[177]
60	[Se@Ag ₆ (AgPPh ₃) ₈ (SePh) ₁₂] ⁰ ·11THF	Se@Ag14	Se ^{2−}	0	Treating ^a	2010	[175]
61	[Se _{0.5} @Ag ₆ (AgPPh ₃) ₈ (SePh) ₁₂][Ph ₃ SnCl ₂] ₆ ·THF	Se_{0.5}@Ag14a	Se ^{2−}	+1	Treating ^a	2010	[175]
62	[Se _{0.5} @Ag ₆ (AgPPh ₃) ₈ (SePh) ₁₂][Cy ₃ SnCl ₂] ₆ ·THF	Se_{0.5}@Ag14b	Se ^{2−}	+1	Treating ^a	2010	[175]
63	[S@Ag ₁₅ (S ^t Bu) ₁₂ (dppb) ₃][OTf]·H ₂ O	S@Ag15	S ^{2−}	+1	Solvothermal	2021	[180]
64	[S@Ag ₁₇ (SPhCO ₂ H) ₁₆][NH ₄] ₁₇ ·22H ₂ O	S@Ag17	S ^{2−}	−17	Ultrasonication	2011	[144]
65	[S@Ag ₁₈ (SPh ^t Bu) ₁₆ (dppp) ₄] ⁰ ·DMF·5MeCN·3MeOH	S@Ag18a	S ^{2−}	0	Solvothermal	2017	[135]
66	[S@Ag ₁₈ (SCH ₂ Ph ^t Bu) ₁₆ (PPh ₃) ₈] ⁰	S@Ag18b	S ^{2−}	0	Stirring	2020	[171]
67	[S@Ag ₂₀ (S ^t Bu) ₁₀ (tfa) ₈ (MeCN) ₄] ⁰ ·EtOH	S@Ag20	S ^{2−}	0	Treating ^a	2022	[181]
68	[S ₂ @Ag ₂₃ (SPhOSiMe ₃) ₁₅ (SPhOH) ₃ (PPh ₃) ₈] ⁰	S₂@Ag23	S ^{2−}	0	Stirring	2011	[174]
69	[S ₂ @Ag ₂₈ (ArP(O)S ₂) ₁₂ (PPh ₃) ₁₂] ⁰	S₂@Ag28	S ^{2−}	0	Stirring	2005	[176]
70	[S@Ag ₁₂ @(C ^t BuPO ₃) ₉ @Ag ₃₆ (S ^t Bu) ₂₃ (CH ₃ O) ₂ (NO ₃) ₃] ⁰ ·2MeOH] _n	[S@Ag48]_n	S ^{2−}	0	Stirring	2015	[172]
71	[S@Ag ₅₀ S ₁₂ (S ^t Bu) ₂₀][tfa] ₄	S@Ag50	S ^{2−}	+4	Crystallization	2022	[182]
72	[S@Ag ₁₁ @(C ^t BuPO ₃) ₇ (MoO ₄) ₂ @Ag ₄₀ (S ^t Bu) ₂₇ (CH ₃ O) ₂ (NO ₃) ₂ (H ₂ O) ₂] ⁰ ·8MeOH·1.5H ₂ O] _n	[S@Ag51]_n	S ^{2−}	0	Stirring	2015	[172]
73	[S@Ag ₅₆ S ₁₂ (S ^t Bu) ₂₀ ·100Ac·6DMF·MeOH	S@Ag56	S ^{2−}	+10	Ultrasonication	2013	[143]
74	[S@Ag ₆₀ S ₁₄ (S ^t Pr) ₂₄ (OTf) ₁₄ (MeOH)(DMF) ₂ ·2DCM] ⁰ ·8H ₂ O	S@Ag60	S ^{2−}	0	Solvothermal	2018	[137]
75	[S@Ag ₆₂ S ₁₂ (S ^t Bu) ₃₂][BF ₄] ₄	S@Ag62	S ^{2−}	+4	Solvothermal	2010	[173]

^aSee citation for detailed synthesis method.

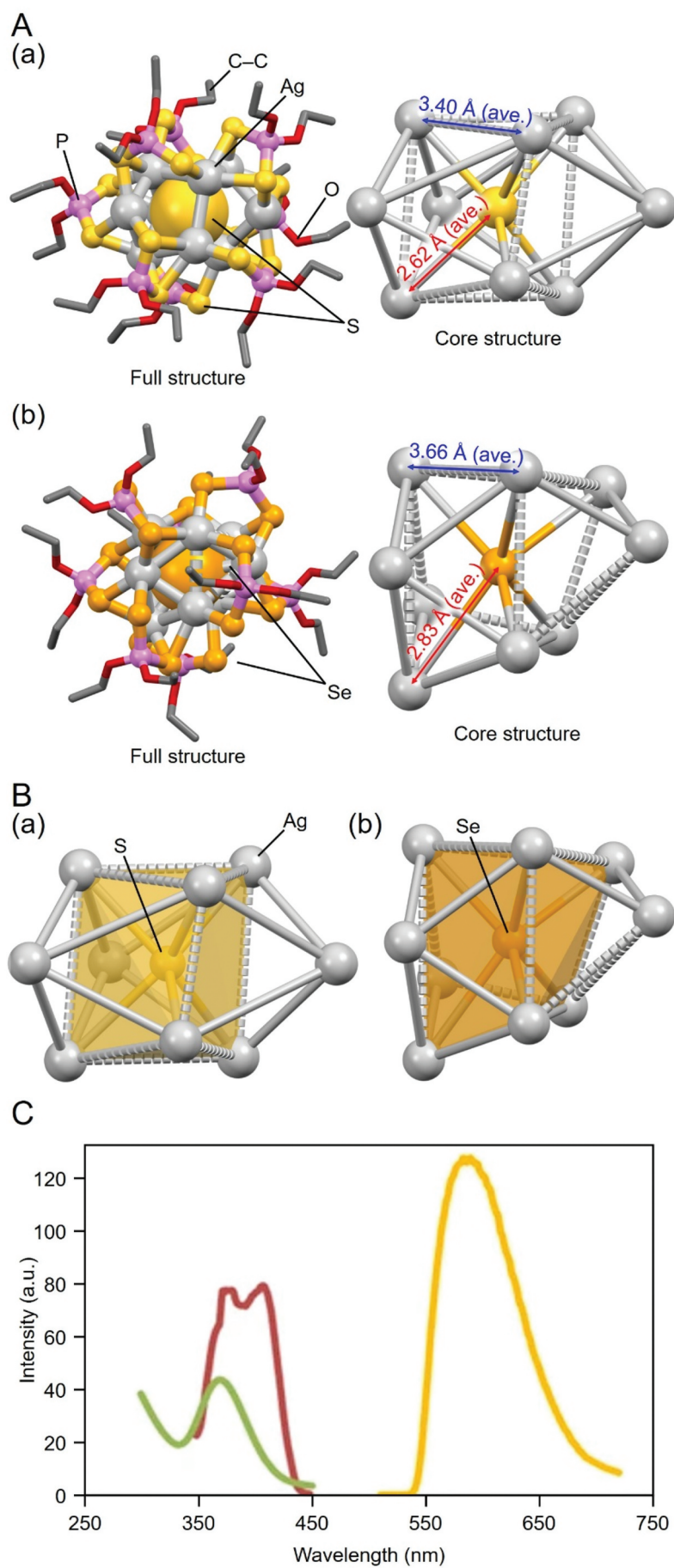


Figure 9. (A) Full (left) and core (right) structures of (a) 42 (**S@Ag9**) and (b) 43 (**Se@Ag9**). (B) Illustration on the differences in distortion in the a and B core structures. (C) Absorption (green, $\epsilon = 8760 \text{ (M}^{-1} \text{ cm}^{-1})$) and photoluminescence spectra (excitation, red; emission, orange) of 42 (**S@Ag9**) at 77 K. Data are taken from ref [134]. Reprinted with permission from [123], copyright (2016, Springer Science Business Media New York).

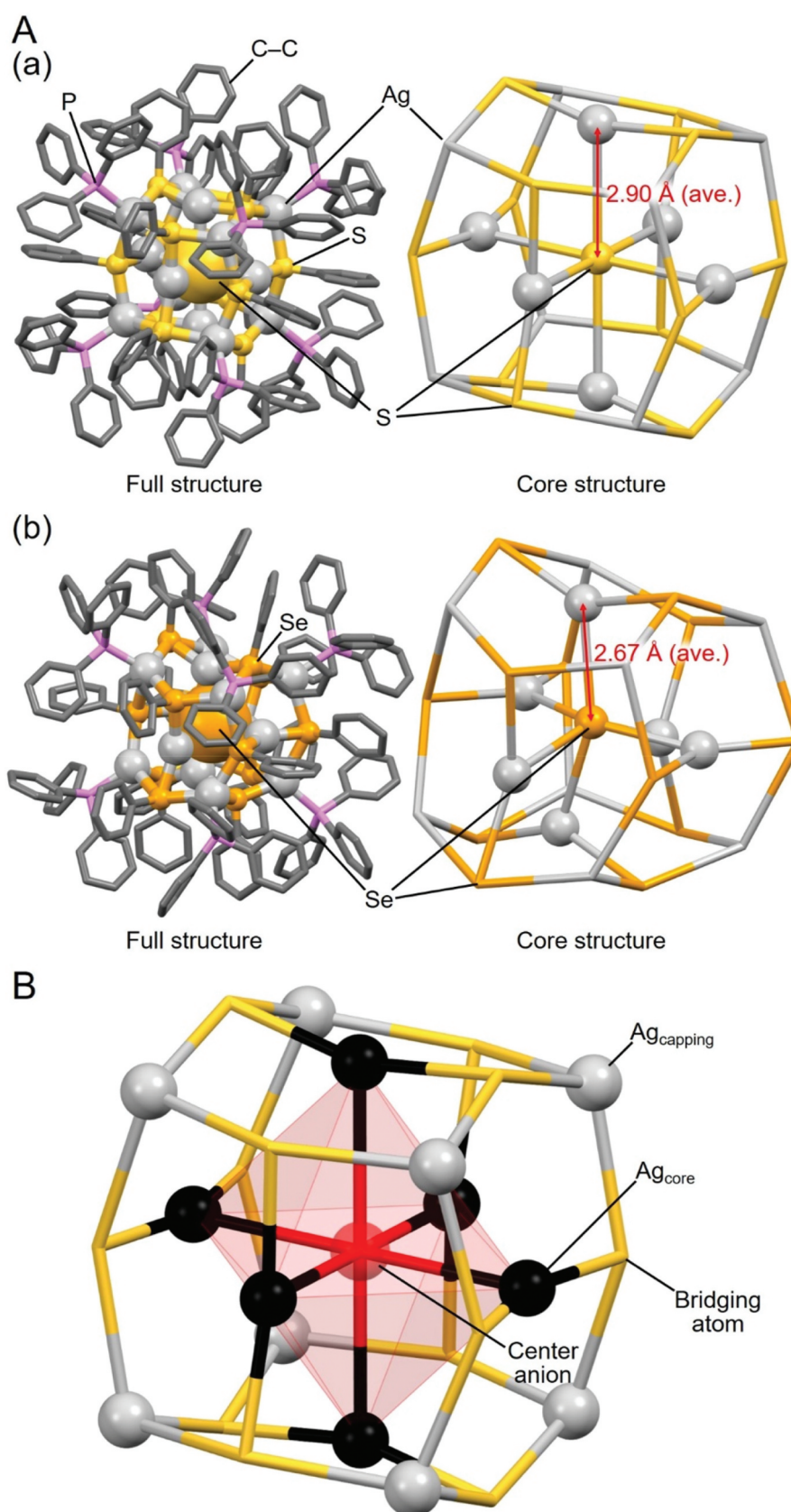


Figure 10. (A) Full (left) and core (right) structures of (a) 54 ($\text{S@Ag}_{14}\text{a}$) and (b) 60 (Se@Ag_{14}). (B) Schematic illustration of the geometric structure in the $\text{X}'\text{@Ag}_{14}$ NCs model. Data are taken from refs [124,175].

compared with 43 (Se@Ag_9), exhibiting 2.62 and 2.83 Å, respectively. These factors lead to a slightly different distortion of the Ag_9 framework (Figure 9B)

The different central X' anions also affect the electronic structures of Ag NCs [134]. As shown in Figure 9C, a peak is observed at 370 nm in the optical absorption spectrum of 42 (S@Ag_9), whereas peaks

appear around 400 and 450 nm in the optical absorption spectrum of **43** (Se@Ag₉) (Figure 9C) [134]. These differences are due to the varying degrees of charge transfer between the central X' anion and the Ag framework.

3.2.2. X'@Ag₁₄ NCs

For X'@Ag₁₄ NCs, **54** (S@Ag_{14a}), **55** (S@Ag_{14b}), **56** (S@Ag_{14c}), **57** (S@Ag_{14d}), and **60** (Se@Ag₁₄) have been reported (Table 3). The former examples, **54** (S@Ag_{14a}), **55** (S@Ag_{14b}), and **56** (S@Ag_{14c}) and **57** (S@Ag_{14d}), which encapsulate S²⁻, were reported by Jin and colleagues [124], Fuhr and colleagues [174], and Corrigan and colleagues [156], respectively, and **60** (Se@Ag₁₄), which encapsulates Se²⁻, was synthesized by Dehnen and colleagues [175]. Notably, **54** (S@Ag_{14a}) and **60** (Se@Ag₁₄) are protected by the same ligand, and both have been synthesized using Ag(I)-PR₃ compounds as an Ag precursor. In the case of **54** (S@Ag_{14a}), it was synthesized simply by dissolving the Ag precursor ((PPh₃)₂Ag(S₂CSPH)) in DCM, whereas **60** (Se@Ag₁₄) was synthesized by slowly dropping the Se²⁻ precursor (PhSeSiMe₃) into a THF solution containing the Ag precursor ((PPh₃)₃AgNO₃) and 1,4-bis(trichlorostannyl)butane (Cl₃Sn(CH₂)₄SnCl₃). Based on these results, it can be inferred that the synthesis of Se@Ag_n NCs requires more complex steps than that of S@Ag_n NCs.

Figure 10A shows the geometric structures of **54** (S@Ag_{14a}) and **60** (Se@Ag₁₄). Both frameworks have a geometric structure with one Ag atom on each facet of a four-sided bipyramidal core formed by the bonding of the central X' anion with six Ag atoms (Figure 10B). In these cage structures, consisting of fourteen Ag atoms, chalcogen atoms are bridging the Ag atoms. Thus, these cage structures are different from those of **20** (F@Ag₁₄), **21** (Cl@Ag_{14a}), **22** (Cl@Ag_{14b}), and **23** (Br@Ag₁₄), described in Section 3.1.2 (Figure 5). The average X'-Ag distance in **54** (S@Ag_{14a}) is 2.91 Å, and that in **60** (Se@Ag₁₄) is 2.67 Å. Accordingly, **54** (S@Ag_{14a}) has a larger free volume in the cage structure. The longer average X'-Ag bond length in **54** (S@Ag_{14a}) indicates that the smaller ionic radii of the central S²⁻ anion (1.91 ± 0.07 Å) [183] is responsible, compared with the larger ionic radii of Se²⁻ (2.09 ± 0.04 Å) [183], which is unlike the X@Ag_n and X'@Ag₉ NCs. This probably occurs because the Ag-X' bond is relatively strong and X'@Ag₁₄ NCs cannot easily change their cage structure with the changing ionic radius of the central anion. This also appears to be the reason why the average X'-Ag length in **54** (S@Ag_{14a}) is relatively long.

3.3. Oxoanion-templated Ag NCs

In the following section, we describe the Ox@Ag_n NCs that encapsulate Ox ions at the central position. The representative Ox@Ag_n NCs are summarized in Table 4 [125,135–137,141–143,158,159,172,177,181,184–206]. Among them, we first describe the syntheses and geometric structures of Ag NCs that encapsulate metallic oxide ions (MOx) (Section 3.3.1) or nonmetallic oxide ions (NMOx) (Section 3.3.2). Then, we discuss how the differences in the central anions affect the geometric structures of Ox@Ag_n NCs (Section 3.3.3).

3.3.1. MOx@Ag_n NCs

Typical examples of central MOx anions are chromate (CrO₄²⁻), molybdate (MoO₄²⁻), and vanadate (VO₄³⁻) (Table 4).

Pioneering examples for CrO₄@Ag_n NCs are **118** (CrO₄@Ag₂₂, Figure 11(a)) and **139** ((CrO₄)₂@Ag₃₅, Figure 11(b)), reported by Wang and colleagues in 2009 [187]. The former, **118** (CrO₄@Ag₂₂), was synthesized by adding TMEDA to a methanol solution containing [AgC≡C^tBu]_n and AgBF₄ and then adding potassium dichromate (K₂Cr₂O₇). The latter, **139** ((CrO₄)₂@Ag₃₅, Figure 11(b)), was synthesized using [AgC≡CPh]_n instead of [AgC≡C^tBu]_n. In addition to these reports, K₂Cr₂O₇ has often been used as a precursor for CrO₄²⁻ [136,185,187]. Notably, for **118** (CrO₄@Ag₂₂), the products did not contain TMEDA. However, even these NCs cannot be synthesized without the addition of TMEDA during synthesis. On the contrary, **139** ((CrO₄)₂@Ag₃₅) has a geometric structure in which TMEDA is chelated to Ag. Unlike the former, the latter forms a giant peanut-like structure because of the inclusion of two CrO₄²⁻ anions. Because AgC≡CPh is less bulky than AgC≡C^tBu, large NCs can form in the synthesis of the latter. These observations agree with those for SR-protected Au_n NCs [207].

Regarding MoO₄@Ag_n NCs, **108** (MoO₄@Ag₂₀, Figure 12) [186] was synthesized by adding the POM complex [Mo₆O₁₉](ⁿBu₄N)₂, the precursor of MoO₄²⁻, and tetraethylammonium hydroxide (Et₄NOH) to a methanol solution containing AgC≡C^tBu and AgCF₃CO₂ (pH = 6.7, stirring method). For MoO₄@Ag_n NCs, unlike the case of CrO₄@Ag_n NCs, (NH₄)₆Mo₇O₂₄·4 H₂O, MoO₂(acac)₂ (acac = acetylacetonate), and Na₂MoO₄ can also be used as precursors of the central anion (MoO₄²⁻) [135,172,191]. When trifluoroacetic acid (CF₃CO₂H) was used instead of AgCF₃CO₂ to increase the acidity of the solution (pH = 3.5), Ag NCs encapsulating Mo₆O₁₉ (POM) were synthesized instead of MoO₄²⁻ (MOx). These results indicate that controlling the solution pH is required for synthesizing the MoO₄@Ag_n NCs using POM as a precursor [208].

Regarding VO₄@Ag_n NCs, **132** (VO₄@Ag₂₆, Figure 13) was synthesized by adding ammonium

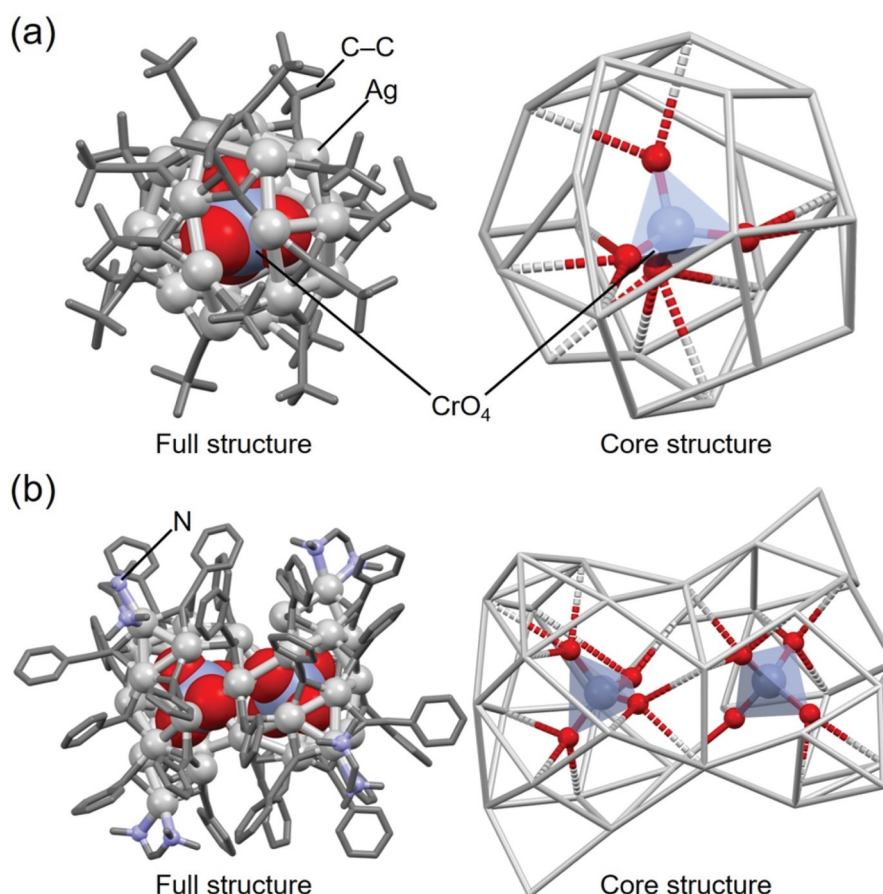
Table 4. Representative Ox-templated Ag NCs.

No.	Chemical formula	Abbreviation	Center anion	z	Synthesis method	Year	Ref.
76	[CO ₃ @Ag ₁₂ (C≡C ^t Bu) ₄ (S ₂ P(OEt) ₂) ₆] ⁰ ·0.5H ₂ O	CO₃@Ag12	[CO ₃] ²⁻	0	Stirring	2018	[177]
77	[NO ₃ @Ag ₁₅ (o-FPhC≡C) ₁₀][NO ₃] ₄	NO₃@Ag15	[NO ₃] ⁻	+4	Stirring	2014	[185]
78	[(NO ₃) ₂ @Ag ₁₆ (C≡CPh) ₄ [(^t BuPO ₃) ₄ V ₄ O ₈] ₂ (DMF) ₆ (NO ₃) ₂] ⁰ ·DMF·H ₂ O	(NO₃)₂@Ag16a	[NO ₃] ⁻	0	Stirring	2011	[184]
79	[(NO ₃) ₂ @Ag ₁₆ (C≡CPh) ₄ [(^t BuPO ₃) ₄ V ₄ O ₈] ₂ (DEF) ₆ (NO ₃) ₂] ⁰	(NO₃)₂@Ag16b	[NO ₃] ⁻	0	Stirring	2012	[198]
80	[(NO ₃) ₂ @Ag ₁₆ (C≡C ^t Bu) ₄ [(^t BuPO ₃) ₄ V ₄ O ₈] ₂ (DMF) ₆ (NO ₃) ₂] ⁰ ·DMF·2H ₂ O	(NO₃)₂@Ag16c	[NO ₃] ⁻	0	Stirring	2012	[198]
81	[(NO ₃) ₂ @Ag ₁₆ (C≡C ^t Bu) ₄ [(^t BuPO ₃) ₄ V ₄ O ₈] ₂ (DMF) ₆ (NO ₃) ₂]-[(NO ₃) ₂ @Ag ₁₆ (C≡C ^t Bu) ₄ [(^t BuPO ₃) ₄ V ₄ O ₈] ₂ (DMF) ₄ (Py) ₂ (NO ₃) ₂]-DMF·5H ₂ O	[(NO₃)₂@Ag16]₂	[NO ₃] ⁻	0	Stirring	2012	[198]
82	[SO ₃ @Ag ₁₆ (S ₂ P(OEt) ₂) ₁₂] ₂ [PF ₆] ₄	[SO₃@Ag16]₂	[SO ₃] ²⁻	+4	Stirring	2014	[192]
83	[SeO ₃ @Ag ₁₆ (S ₂ P(OEt) ₂) ₁₂] ₂ [PF ₆] ₄	[SeO₃@Ag16]₂	[SeO ₃] ²⁻	+4	Stirring	2014	[192]
84	[TeO ₃ @Ag ₁₆ (S ₂ P(OEt) ₂) ₁₂] ₂ [PF ₆] ₄	[TeO₃@Ag16]₂	[TeO ₃] ²⁻	+4	Stirring	2014	[192]
85	[C ₂ O ₄ @Ag ₁₆ (S ₂ P(OEt) ₂) ₁₂] ₂ [PF ₆] ₄	[C₂O₄@Ag16]₂	[C ₂ O ₄] ²⁻	+4	Stirring	2022	[201]
86	[C ₄ O ₄ @Ag ₁₆ (S ₂ P(OEt) ₂) ₁₂] ₂ [PF ₆] ₄	[C₄O₄@Ag16]₂	[C ₄ O ₄] ²⁻	+4	Stirring	2022	[201]
87	[SO ₄ @Ag ₁₆ (S ₂ P(OEt) ₂) ₁₂] ₂ [PF ₆] ₄	[SO₄@Ag16]₂	[SO ₄] ²⁻	+4	Stirring	2011	[191]
88	[SeO ₄ @Ag ₁₆ (S ₂ P(OEt) ₂) ₁₂] ₂ [PF ₆] ₄	[SeO₄@Ag16]₂	[SeO ₄] ²⁻	+4	Stirring	2011	[191]
89	[CrO ₄ @Ag ₁₆ (S ₂ P(OEt) ₂) ₁₂] ₂ [PF ₆] ₄	[CrO₄@Ag16]₂	[CrO ₄] ²⁻	+4	Stirring	2011	[191]
90	[MoO ₄ @Ag ₁₆ (S ₂ P(OEt) ₂) ₁₂] ₂ [PF ₆] ₄	[MoO₄@Ag16]₂	[MoO ₄] ²⁻	+4	Stirring	2011	[191]
91	[CO ₃ @Ag ₁₇ (C≡C ^t Bu) ₁₄][OTf]	CO₃@Ag17	[CO ₃] ²⁻	+1	Stirring	2009	[125]
92	[ClO ₄ @Ag ₁₈ (C≡C ^t Pr) ₁₂][ClO ₄] ₅	ClO₄@Ag18	[ClO ₄] ⁻	+5	Stirring	2014	[185]
93	[CrO ₄ @Ag ₁₈ (C≡C ^t Pr) ₁₂][ClO ₄] ₄	CrO₄@Ag18	[CrO ₄] ²⁻	+4	Stirring	2014	[185]
94	[CO ₃ @Ag ₁₉ (C≡C ^t Bu) ₁₆][BF ₄]-MeOH	CO₃@Ag19	[CO ₃] ²⁻	+1	Stirring	2009	[125]
95	[NO ₃ @Ag ₁₉ (S ^t Bu) ₁₀ (tfa) ₈ (4Cp)] ⁰ ·2H ₂ O	NO₃@Ag19	[NO ₃] ⁻	0	Ultrasonication	2022	[204]
96	[SO ₄ @Ag ₁₉ (C≡C ^t Bu) ₈ (Ph ₂ PO ₂) ₆ (tfa) ₃ (MeOH)] ⁰	SO₄@Ag19	[SO ₄] ²⁻	0	Solvothermal	2022	[203]
97	[CrO ₄ @Ag ₁₉ (C≡C ^t Bu) ₈ (Ph ₂ PO ₂) ₆ (tfa) ₃ (MeOH)] ⁰	CrO₄@Ag19	[CrO ₄] ²⁻	0	Solvothermal	2022	[203]
98	[MoO ₄ @Ag ₁₉ (C≡C ^t Bu) ₁₂ (hfac) ₂ (tfa) ₃] ⁰	MoO₄@Ag19	[MoO ₄] ²⁻	0	Ultrasonication	2018	[159]
99	[CO ₃ @Ag ₂₀ (S ^t Bu) ₁₀ (DMF) ₆ (NO ₃) ₈] ⁰	CO₃@Ag20a	[CO ₃] ²⁻	0	Ultrasonication	2013	[141]
100	[CO ₃ @Ag ₂₀ (S ^t Bu) ₁₀ (OAc) ₈ (DMF) ₄] ⁰ ·DMF·MeOH	CO₃@Ag20b	[CO ₃] ²⁻	0	Ultrasonication	2013	[143]
101	[CO ₃ @Ag ₂₀ (S ^t Bu) ₁₀ (NO ₃) ₈ (DMAC) ₄] ⁰	CO₃@Ag20c	[CO ₃] ²⁻	0	Ultrasonication	2018	[206]
102	[CO ₃ @Ag ₂₀ (S ^t Bu) ₁₀ (PhCO ₂) ₈ (DMAC) ₂] ⁰ ·2MeCN	CO₃@Ag20d	[CO ₃] ²⁻	0	Stirring	2018	[206]
103	[CO ₃ @Ag ₂₀ (S ^t Bu) ₁₀ (C ₁₂ H ₆ O ₂ NCH ₂ CO ₂) ₈ (MeCN) ₂] ⁰ ·2MeCN	CO₃@Ag20e	[CO ₃] ²⁻	0	Stirring	2018	[206]
104	[CO ₃ @Ag ₂₀ (S ^t Bu) ₁₀ (FCCO ₂) ₈ (MeCN) ₄] ⁰ ·MeCN·2H ₂ O	CO₃@Ag20f	[CO ₃] ²⁻	0	Stirring	2018	[206]
105	[CO ₃ @Ag ₂₀ (S ^t Bu) ₁₀ (tfa) ₈ (MeCN) ₄] ⁰	CO₃@Ag20g	[CO ₃] ²⁻	0	Ultrasonication	2022	[204]
106	[CO ₃ @Ag ₂₀ (S ^t Bu) ₁₀ (tfa) ₈ (DMF) ₃ (H ₂ O)] ⁰ ·DMF	CO₃@Ag20h	[CO ₃] ²⁻	0	Treating ^a	2022	[181]
107	[AsO ₄ @Ag ₂₀ (C≡C ^t Bu) ₈ (Ph ₂ PO ₂) ₇ (tfa) ₂ (MeCN)] ⁰ ·4MeCN·2H ₂ O	AsO₄@Ag20	[AsO ₄] ³⁻	0	Solvothermal	2020	[200]
108	[MoO ₄ @Ag ₂₀ (C≡C ^t Bu) ₁₃ (tfa) ₅] ⁰	MoO₄@Ag20	[MoO ₄] ²⁻	0	Stirring	2009	[186]
109	[CO ₃ @Ag ₂₀ (S ^t Bu) ₁₀ (OAc) ₈ (DMF) ₂ ·2H ₂ O] _n	[CO₃@Ag20a]_n	[CO ₃] ²⁻	0	Stirring	2014	[197]
110	[CO ₃ @Ag ₂₀ (PrS) ₁₀ (NO ₃) ₈ (DMF) ₂] _n	[CO₃@Ag20b]_n	[CO ₃] ²⁻	0	Solvothermal	2016	[196]
111	[SO ₄ @Ag ₂₀ (S ^t Bu) ₁₀ (PhSO ₃) ₈ (H ₂ O) ₄] ⁰ ·2H ₂ O] _n	[SO₄@Ag20a]_n	[SO ₄] ²⁻	0	Solvothermal	2018	[137]
112	[SO ₄ @Ag ₂₀ (S ^t Pr) ₁₀ (PTA) ₃ (HPTA) ₂] _n	[SO₄@Ag20b]_n	[SO ₄] ²⁻	0	Solvothermal	2022	[202]
113	[SO ₄ @Ag ₂₁ (C≡C ^t Bu) ₁₈][BF ₄]	SO₄@Ag21	[SO ₄] ²⁻	+1	Stirring	2009	[187]
114	[CO ₂ @Ag ₂₀ Cu ₂ S ₂ (S ^t Bu) ₁₀ (tfa) ₈ (DMAC) ₄] ⁰ ·DMAC	CO₂@Ag20Cu2	[CO ₂] ⁰	0	Stirring	2022	[181]
115	[CO ₃ @Ag ₂₂ (S ^t Bu) ₁₀ (L-Ala) ₄ (NO ₃) ₆ (MeCN) ₂ ·H ₂ O	CO₃@Ag22a	[CO ₃] ²⁻	0	Stirring	2018	[206]
116	[CO ₃ @Ag ₂₂ (S ^t Bu) ₁₀ (D-Ala) ₄ (NO ₃) ₆ (MeCN) ₂ ·H ₂ O	CO₃@Ag22b	[CO ₃] ²⁻	0	Stirring	2018	[206]
117	[NO ₃ @Ag ₂₂ (C≡C ^t Bu) ₁₄ (^t BuPO ₃) ₂ (hfac)(tfa)(OH)] ⁰ ·MeCN	NO₃@Ag22	[NO ₃] ⁻	0	Stirring	2018	[159]
118	[CrO ₄ @Ag ₂₂ (C≡C ^t Bu) ₁₈][BF ₄] ₂	CrO₄@Ag22	[CrO ₄] ²⁻	+2	Stirring	2009	[187]
119	[AsO ₄ @Ag ₂₂ (Ph ₂ PO ₂) ₇ (C≡C ^t Bu) ₁₀ (MeOH)(H ₂ O)] ₂ [PF ₆] ₂	AsO₄@Ag22	[AsO ₄] ³⁻	0	Solvothermal	2020	[200]
120	[SO ₄ @Ag ₂₂ (S ^t Pr) ₁₂ (NO ₃) ₆][NO ₃] ₂] _n	[SO₄@Ag22]_n	[SO ₄] ²⁻	+2	Solvothermal	2016	[196]
121	[CrO ₄ @Ag ₂₂ (C≡CPh) ₁₆ (OTf) ₄] _n	[CrO₄@Ag22]_n	[CrO ₄] ²⁻	0	Solvothermal	2017	[136]
122	[CO ₃ @Ag ₂₃ (S ^t Bu) ₁₀ (L-Val) ₆ (NO ₃) ₄ (MeCN)][OH]	CO₃Ag23a	[CO ₃] ²⁻	+1	Stirring	2018	[206]
123	[CO ₃ @Ag ₂₃ (S ^t Bu) ₁₀ (D-Val) ₆ (NO ₃) ₄ (MeCN)][OH]	CO₃Ag23b	[CO ₃] ²⁻	+1	Stirring	2018	[206]
124	[CO ₃ @Ag ₂₄ (S ^t Bu) ₁₀ (L-Pro) ₈ (NO ₃) ₄ (H ₂ O)] ⁰ ·4MeCN·3H ₂ O	CO₃Ag24a	[CO ₃] ²⁻	0	Stirring	2018	[206]
125	[CO ₃ @Ag ₂₄ (S ^t Bu) ₁₀ (D-Pro) ₈ (NO ₃) ₄ (H ₂ O)] ⁰ ·4MeCN·3H ₂ O	CO₃Ag24b	[CO ₃] ²⁻	0	Stirring	2018	[206]
126	[(C ₄ O ₄) ₂ @Ag ₂₄ (tfa) ₄ (C≡C ^t Bu) ₁₆]-2MeCN	C₄O₄Ag24	[C ₄ O ₄] ²⁻	0	Solvothermal	2015	[205]
127	[MoO ₄ @Ag ₂₄ (SPhMe) ₁₂ (dppm) ₆ (MoO ₄) ₄] ⁰ ·2BF ₄ ·C ₂ H ₅ NO	MoO₄@Ag24a	[MoO ₄] ²⁻	0	Solvothermal	2017	[135]
128	[MoO ₄ @Ag ₂₄ (SPhMe) ₁₂ (dppm) ₆ (MoO ₄) ₄] ⁰ ·2OTf	MoO₄@Ag24b	[MoO ₄] ²⁻	0	Solvothermal	2017	[135]
129	[MoO ₄ @Ag ₂₄ (SPhMe) ₁₂ (dppf) ₆ (MoO ₄) ₄] ⁰ ·2OTf	MoO₄@Ag24c	[MoO ₄] ²⁻	0	Solvothermal	2017	[135]
130	[MoO ₄ @Ag ₂₄ (SPhMe) ₁₂ (dppb) ₆ (MoO ₄) ₄] ⁰ ·2OTf	MoO₄@Ag24d	[MoO ₄] ²⁻	0	Solvothermal	2017	[135]
131	[(NO ₃) ₂ @Ag ₂₆ (o-MePhC≡C) ₁₆][NO ₃] ₈ ·5H ₂ O	(NO₃)₂@Ag26	[NO ₃] ⁻	+8	Stirring	2014	[185]
132	[VO ₄ @Ag ₂₆ (C≡C ^t Bu) ₁₃ (tfa) ₁₀ (MeCN) ₂ (MeOH) ₃] ⁰ ·MeOH	VO₄@Ag26	[VO ₄] ³⁻	0	Solvothermal	2019	[142]
133	[(CO ₃) ₂ @Ag ₂₆ (C≡C ^t Bu) ₁₆ (S ₂ P(OEt) ₂) ₄][OH] ₂ ·4MeOH·6H ₂ O	(CO₃)₂@Ag26	[CO ₃] ²⁻	+2	Stirring	2018	[177]
134	[(CrO ₄) ₂ @Ag ₃₀ (SCH ₂ Nap) ₁₈ (DMAC) ₂ (tfa) ₈]	(CrO₄)₂@Ag30	[CrO ₄] ²⁻	0	Stirring	2019	[195]

(Continued)

Table 4. (Continued).

No.	Chemical formula	Abbreviation	Center anion	z	Synthesis method	Year	Ref.
135	$[(\text{CrO}_4)_2@Ag_{31}(\text{C}\equiv\text{CPh})_{22}(\text{OTf})_4][\text{OTf}]\cdot 2\text{MeOH}\cdot\text{H}_2\text{O}]_n$	[CrO₄@Ag31]_n	$[\text{CrO}_4]^{2-}$	+1	Solvothermal	2017	[136]
136	$[(\text{C}_5\text{O}_5)_2@Ag_{32}\text{S}_2(\text{S}_2\text{P}(\text{OEt})_2)_{22}][\text{PF}_6]_2$	(C₅O₅)₂@Ag32	$[\text{C}_5\text{O}_5]^{2-}$	+2	Stirring	2022	[201]
137	$[\text{NO}_3@Ag_{33}\text{S}_3(\text{S}^t\text{Bu})_{16}(\text{tfa})_9(\text{MeCN})_2][\text{NO}_3]$	NO₃@Ag33	$[\text{NO}_3]^-$	+1	Stirring	2014	[190]
138	$[(\text{VO}_4)_2@Ag_{34}(\text{C}\equiv\text{C}^t\text{Bu})_{22}(\text{NO}_3)_6]\cdot 8\text{H}_2\text{O}$	(VO₄)₂@Ag34	$[\text{VO}_4]^{3-}$	0	Stirring	2012	[198]
139	$[(\text{CrO}_4)_2@Ag_{35}(\text{C}\equiv\text{CPh})_{28}(\text{TMEDA})_4][\text{BF}_4]_3$	(CrO₄)₂@Ag35	$[\text{CrO}_4]^{2-}$	+3	Stirring	2009	[187]
140	$[\text{TeO}_6@Ag_{36}(\text{C}\equiv\text{C}^t\text{Bu})_{18}(\text{tfa})_{12}]$	TeO₆@Ag36	$[\text{TeO}_6]^{6-}$	0	Solvothermal	2020	[193]
141	$[\text{SO}_4@Ag_{40}\text{S}_4(\text{S}_2\text{P}(\text{OEt})_2)_{24}][\text{PF}_6]_6$	SO₄@Ag40a	$[\text{SO}_4]^{2-}$	+6	Stirring	2020	[194]
142	$[\text{SO}_4@Ag_{40}\text{Se}_4(\text{S}_2\text{P}(\text{OEt})_2)_{24}][\text{PF}_6]_6$	SO₄@Ag40b	$[\text{SO}_4]^{2-}$	+6	Stirring	2020	[194]
143	$[(\text{CO}_3@Ag_{42}(\text{C}\equiv\text{C}^t\text{Bu})_{27}(\text{MeCN})_2)[\text{CoW}_{12}\text{O}_{40}]_2][\text{BF}_4]$	CO₃@Ag42a	$[\text{CO}_3]^{2-}$	+1	Crystallization ^a	2010	[188]
144	$[\text{CO}_3@Ag_{42}(\text{C}\equiv\text{C}^t\text{Bu})_{27}(\alpha\text{-A-SiW}_9\text{Nb}_3\text{O}_{40})_2][\text{Bu}_4\text{N}]$	CO₃@Ag42b	$[\text{CO}_3]^{2-}$	-1	Treating ^a	2015	[199]
145	$[\text{MoO}_4@Ag_{12}(\text{C}^t\text{BuPO}_3)_6\text{S}_6@Ag_{36}(\text{S}^t\text{Bu})_{24}][\text{MeOH}]_6$	MoO₄@Ag48	$[\text{MoO}_4]^{2-}$	-6	Stirring	2015	[172]
146	$[(\text{WO}_4)_2(\text{Ag}_{16}\text{S}_6)@Ag_{56}(\text{C}\equiv\text{C}^t\text{Bu})_{27}(\text{C}^t\text{BuPO}_3)_{12}(\text{OAc})(\text{MeCN})_2(\text{H}_2\text{O})][\text{H}_2\text{P}_2\text{W}_{18}\text{O}_{62}]^0$	WO₄@Ag72	$[\text{WO}_4]^{2-}$	0	Solvothermal	2018	[158]
147	$[\text{SO}_4@Ag_{78}\text{S}_{15}(\text{SC}_5\text{H}_9)_{27}(\text{tfa})_{12}][\text{tfa}]_7$	SO₄@Ag78	$[\text{SO}_4]^{2-}$	-7	Crystallization ^a	2018	[189]

^aSee citation for detailed synthesis method.Figure 11. Full (left) and core (right) structures of (a) 118 (**CrO₄@Ag22**) and (b) 139 (**(CrO₄)₂@Ag35**). Data are taken from ref [187].

metavanadate (NH_4VO_3) to a MeOH/MeCN mixture containing $[\text{AgC}\equiv\text{C}^t\text{Bu}]_n$ and AgCF_3CO_2 and heating the solution to 70 °C (solvothermal method). It has been experimentally shown that larger Ag NCs can be formed when trivalent VO_4^{3-} is used as a template source than when divalent CrO_4^{2-} and MoO_4^{2-} are used, although the reason remains unclear.

3.3.2. NMOx@Ag_n NCs

Anions in the form of NMOx include CO_3^{2-} , NO_3^- , $\text{X}'\text{O}_3^{2-}$, $\text{X}'\text{O}_4^{2-}$ ($\text{X}' = \text{S}, \text{Se}, \text{Te}$), and ClO_4^- . Representative NMOx@Ag_n NCs are described in Table 4. Salts containing the respective oxides are generally used as precursors for the central NMOx anion. However, there are exceptions. For example, in the synthesis of **91** (**CO₃@Ag17**) and **94**

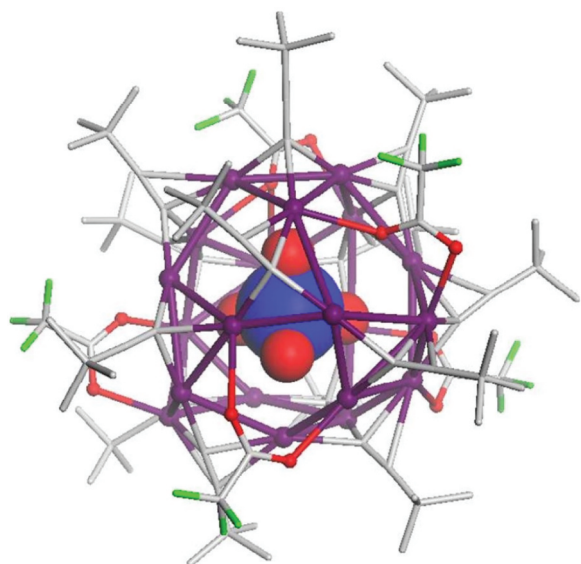


Figure 12. The full geometric structure of 108 ($\text{MoO}_4\text{@Ag}_{20}$). Reprinted with permission from [186], copyright (2009, American Chemical Society).

($\text{CO}_3\text{@Ag}_{19}$) [125], the central anion was produced by the conversion of atmospheric CO_2 to CO_3^{2-} by TMEDA. The use of atmospheric CO_2 was also adapted in the synthesis of **99** ($\text{CO}_3\text{@Ag}_{20a}$) and **100** ($\text{CO}_3\text{@Ag}_{20b}$).

The geometric structures of **94** ($\text{CO}_3\text{@Ag}_{19}$) [125] and **113** ($\text{SO}_4\text{@Ag}_{21}$) [187], protected by the same ligand, are shown in Figure 14. Both NMOx@Ag_n NCs were reported by Wang and colleagues in 2009 and were synthesized using similar compounds and methods, except for the central anion precursor. Despite the similarities in their syntheses, these NMOx@Ag_n NCs differ in the number of constituent Ag atoms, with **113** ($\text{SO}_4\text{@Ag}_{21}$) exhibiting a larger Ag cage structure than **94** ($\text{CO}_3\text{@Ag}_{19}$). The NMOx anions encapsulated in **94** ($\text{CO}_3\text{@Ag}_{19}$) and **113** ($\text{SO}_4\text{@Ag}_{21}$) contain three and four O atoms, respectively. Because Ag atoms form bonds with O atoms when NMOx acts as a central anion, SO_4^{2-} can form bonds with a larger

number of Ag atoms than CO_3^{2-} . The SO_4^{2-} also requires a larger ionic volume than CO_3^{2-} . These factors contribute to the formation of Ag cage structures that are larger in $\text{SO}_4\text{@Ag}_n$ NCs than in $\text{CO}_3\text{@Ag}_n$ NCs.

3.3.3. Comparison between Ox@Ag_n NCs

In 2014, Liu and colleagues reported the synthesis of **87** ($[\text{SO}_4\text{@Ag}_{16}]_2$), **88** ($[\text{SeO}_4\text{@Ag}_{16}]_2$), **89** ($[\text{CrO}_4\text{@Ag}_{16}]_2$), and **90** ($[\text{MoO}_4\text{@Ag}_{16}]_2$). Although these Ox@Ag_n NCs include the same ligand, they have different central Ox anions.

Figure 15 shows the geometric structures of **87** ($[\text{SO}_4\text{@Ag}_{16}]_2$), **88** ($[\text{SeO}_4\text{@Ag}_{16}]_2$), **89** ($[\text{CrO}_4\text{@Ag}_{16}]_2$), and **90** ($[\text{MoO}_4\text{@Ag}_{16}]_2$) [191]. These Ox@Ag_n NCs have similar Ag cage structures, and Ox is surrounded by sixteen Ag atoms in all of them, which consists of an icosahedral Ag₁₂ framework with four surrounding Ag atoms. The structures of these Ox@Ag_n NCs are dimerized via S and Ag bonding.

However, several differences also exist in the coordination mode between the central Ox anion and Ag atoms, and in the degree of distortion in the Ag cage structures (Figure 15). Specifically, differences occur in the Ag–O coordination mode, with $\mu_4; \eta^2, \eta^1, \eta^1$ for **87** ($[\text{SO}_4\text{@Ag}_{16}]_2$), $\mu_6; \eta^2, \eta^2, \eta^1, \eta^1$ for **88** ($[\text{SeO}_4\text{@Ag}_{16}]_2$), $\mu_6; \eta^2, \eta^2, \eta^2$ for **89** ($[\text{CrO}_4\text{@Ag}_{16}]_2$), and $\mu_8; \eta^3, \eta^3, \eta^2$ for **90** ($[\text{MoO}_4\text{@Ag}_{16}]_2$). In addition, **87** ($[\text{SO}_4\text{@Ag}_{16}]_2$), **88** ($[\text{SeO}_4\text{@Ag}_{16}]_2$), and **89** ($[\text{CrO}_4\text{@Ag}_{16}]_2$) have a uniform orientation of tetrahedral Ox against the Ag framework, whereas the orientation of tetrahedral Ox in **90** ($[\text{MoO}_4\text{@Ag}_{16}]_2$) is different (Figure 15).

The sizes of the central anions also differ slightly among **87** ($[\text{SO}_4\text{@Ag}_{16}]_2$), **88** ($[\text{SeO}_4\text{@Ag}_{16}]_2$), and **89** ($[\text{CrO}_4\text{@Ag}_{16}]_2$), which affects their overall structure. For example, the average Ag–Ag distances in the icosahedral Ag₁₂ framework surrounding the central anion Ox are estimated to be 4.016 Å, 4.051 Å, and

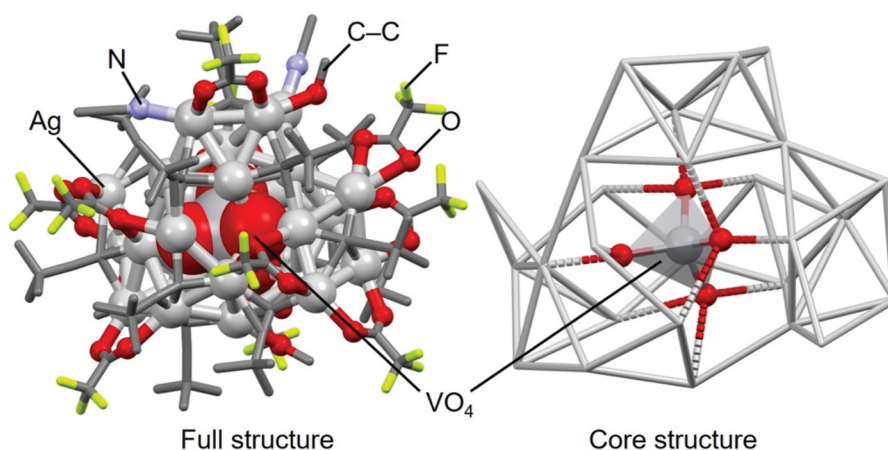


Figure 13. Full (left) and core (right) structures of 132 ($\text{VO}_4\text{@Ag}_{26}$). Data are taken from ref [142].

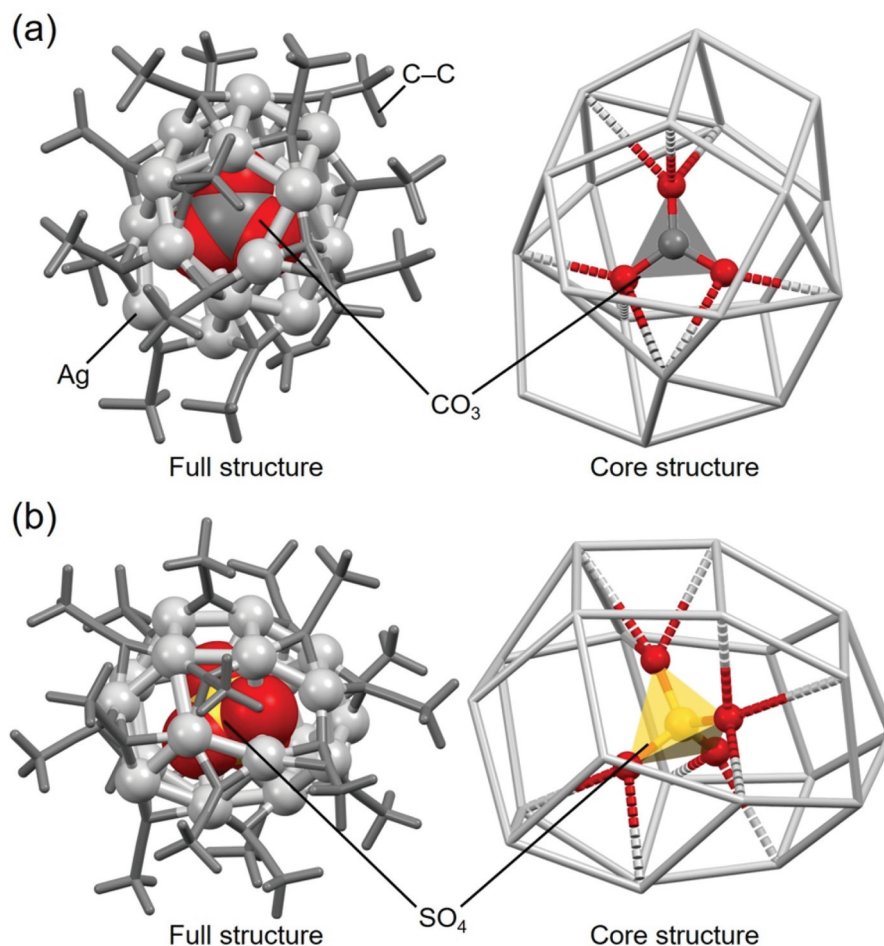


Figure 14. Full (left) and core (right) structures of (a) 94 ($\text{CO}_3@\text{Ag}_{19}$) and (b) 113 ($\text{SO}_4@\text{Ag}_{21}$). Data are taken from refs [125,187].

4.033 Å, respectively. The order of the average Ag–Ag distances is consistent with that of the average central atom–O distances in the central Ox anion (SO_4^{2-} , 1.464 Å; SeO_4^{2-} , 1.632 Å; CrO_4^{2-} , 1.628 Å). Thus, the size of the Ag framework in $\text{Ox}@\text{Ag}_n$ NCs depends on the size of the central Ox anion.

For **90** ($[\text{MoO}_4@\text{Ag}_{16}]_2$), the average Mo–O distance for the central MoO_4^{2-} anion is 1.721 Å, which is longer than the central atom–O distance in the other Ox systems. This may be the reason why **90** ($[\text{MoO}_4@\text{Ag}_{16}]_2$) encapsulates the central MoO_4^{2-} anion in a different orientation compared with the other $\text{Ox}@\text{Ag}_n$ NCs. The average Ag–Ag distance (4.052 Å) in the icosahedral Ag_{12} framework is also longer in **90** ($[\text{MoO}_4@\text{Ag}_{16}]_2$) than in **87** ($[\text{SO}_4@\text{Ag}_{16}]_2$), **88** ($[\text{SeO}_4@\text{Ag}_{16}]_2$), and **89** ($[\text{CrO}_4@\text{Ag}_{16}]_2$). However, the degree of extension in the icosahedral Ag_{12} framework in **90** ($[\text{MoO}_4@\text{Ag}_{16}]_2$) is not significant (0.001 Å) when accounting for the difference in size between SeO_4^{2-} and MoO_4^{2-} anions (0.089 Å). In **90** ($[\text{MoO}_4@\text{Ag}_{16}]_2$), the central MoO_4^{2-} anion is encapsulated in a different orientation compared with the others, which appears to induce a relaxation of the extension in the icosahedral Ag_{12} framework.

In addition, **82** ($[\text{SO}_3@\text{Ag}_{16}]_2$), **83** ($[\text{SeO}_3@\text{Ag}_{16}]_2$), and **84** ($[\text{TeO}_3@\text{Ag}_{16}]_2$) were reported by Liu and

colleagues in 2015 (Table 4) [192]. The geometric structures of these $\text{Ox}@\text{Ag}_n$ NCs (Figure 16) are similar to **87** ($[\text{SO}_4@\text{Ag}_{16}]_2$) and **88** ($[\text{SeO}_4@\text{Ag}_{16}]_2$) (Figure 15). In Section 3.3.2, we explained that the central Ox anion can induce different geometric structures (e.g. planar triangular or tetrahedral) depending on the number of O atoms, and $\text{Ox}@\text{Ag}_n$ NCs with different numbers of Ag atoms can be formed depending on the central Ox anion. However, **82** ($[\text{SO}_3@\text{Ag}_{16}]_2$), **83** ($[\text{SeO}_3@\text{Ag}_{16}]_2$), and **84** ($[\text{TeO}_3@\text{Ag}_{16}]_2$) have the same number of Ag atoms and the same shape, despite having a different number of O atoms in the central Ox anion compared with **87** ($[\text{SO}_4@\text{Ag}_{16}]_2$) and **88** ($[\text{SeO}_4@\text{Ag}_{16}]_2$). This is likely because the central $\text{X}'\text{O}_3^{2-}$ anion ($\text{X}' = \text{S}, \text{Se}, \text{or Te}$) has a triangular pyramidal shape, instead of a triangular shape (Figure 16). In **82** ($[\text{SO}_3@\text{Ag}_{16}]_2$), **83** ($[\text{SeO}_3@\text{Ag}_{16}]_2$), and **84** ($[\text{TeO}_3@\text{Ag}_{16}]_2$), there are only three O atoms bonded to the triangular pyramid, but there are lone pairs at the apex (X') of the pyramid, which maintains the surrounding icosahedral Ag_{12} framework. These results indicate that the geometric structure of $\text{Ox}@\text{Ag}_n$ NCs is greatly affected not only by the number of O atoms in the Ox anion but also by the shape of the Ox anion.

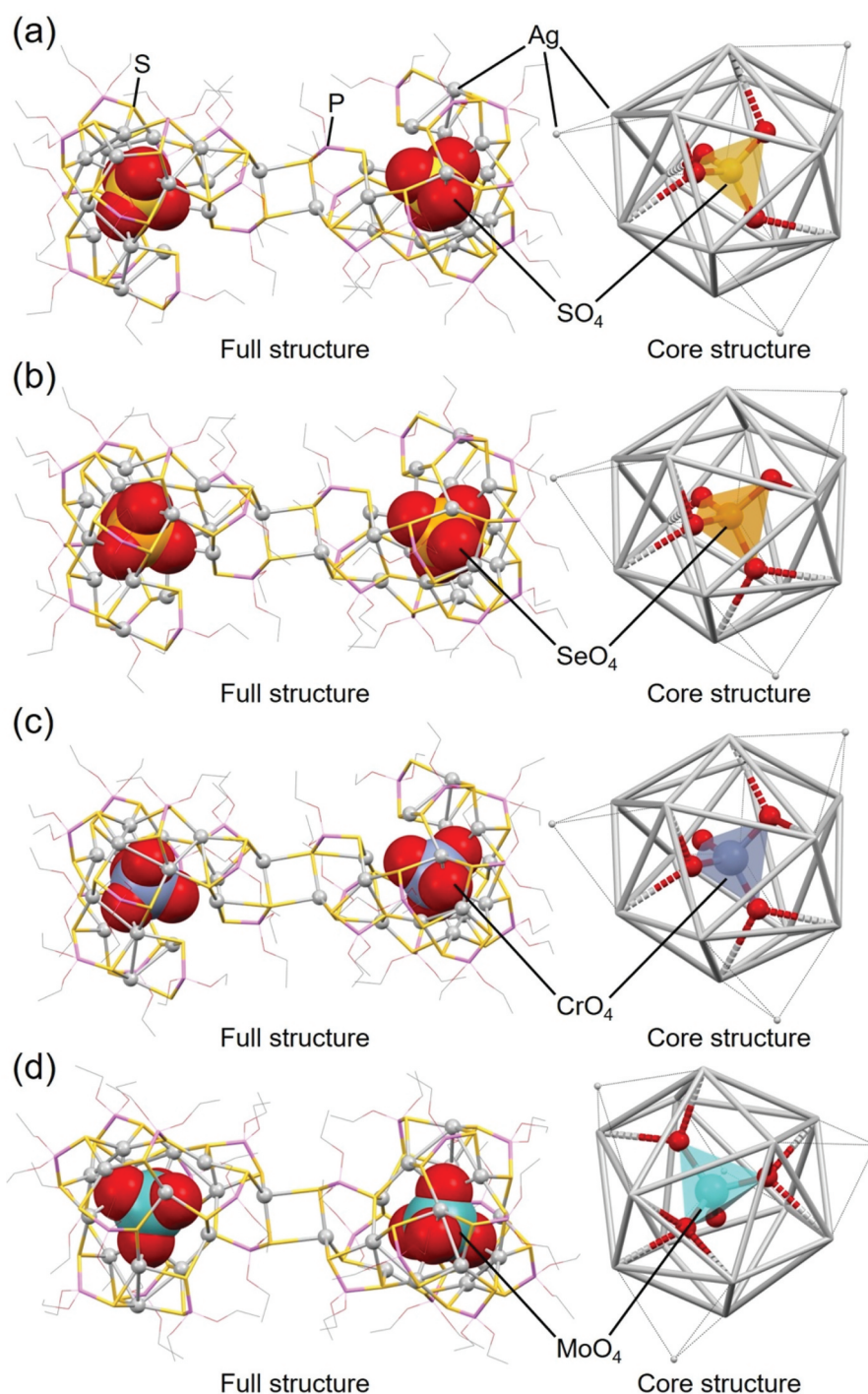


Figure 15. Full (left) and core (right) structures of (a) 87 ($[\text{SO}_4@Ag_{16}]_2$), (b) 88 ($[\text{SeO}_4@Ag_{16}]_2$), (c) 89 ($[\text{CrO}_4@Ag_{16}]_2$), and (d) 90 ($[\text{MoO}_4@Ag_{16}]_2$). Data are taken from ref [191].

3.4. Polyoxometalate-templated Ag NCs

Table 5 summarizes the representative $\text{POM}@Ag_n$ NCs [135,137–140,152,158,159,184,186,202,204,209–228]. Many of them contain polyoxovanadate ($\text{POV}@Ag_n$ NCs), polyoxomolybdate ($\text{POMo}@Ag_n$ NCs), and polyoxotungstate ($\text{POW}@Ag_n$ NCs), and the number of reported examples decreases in the order of $\text{POMo}@Ag_n$ NCs > $\text{POV}@Ag_n$ NCs > $\text{POW}@Ag_n$ NCs. More than half of the $\text{POM}@Ag_n$ NCs were reported after 2018, demonstrating that these anion-templated Ag_n NCs have been receiving attention more recently.

The $\text{POM}@Ag_n$ NCs are characterized by a higher number of constituent Ag atoms than other anion-templated Ag_n NCs, such as $X@Ag_n$ NCs, $X'@Ag_n$ NCs, and $\text{Ox}@Ag_n$ NCs. This is because the encapsulated POMs are generally larger than X, X', and Ox. The smallest $\text{POM}@Ag_n$ NC reported is **148** ($\text{POV}@Ag_{22}$) [204], which encapsulates $[\text{V}_2\text{O}_7]^{4-}$ and was found in 2022 by Jin and colleagues. Despite having the smallest size, **148** ($\text{POV}@Ag_{22}$) is larger than most Ag NCs that encapsulate X or X'. Therefore, POM is effective in synthesizing Ag NCs with

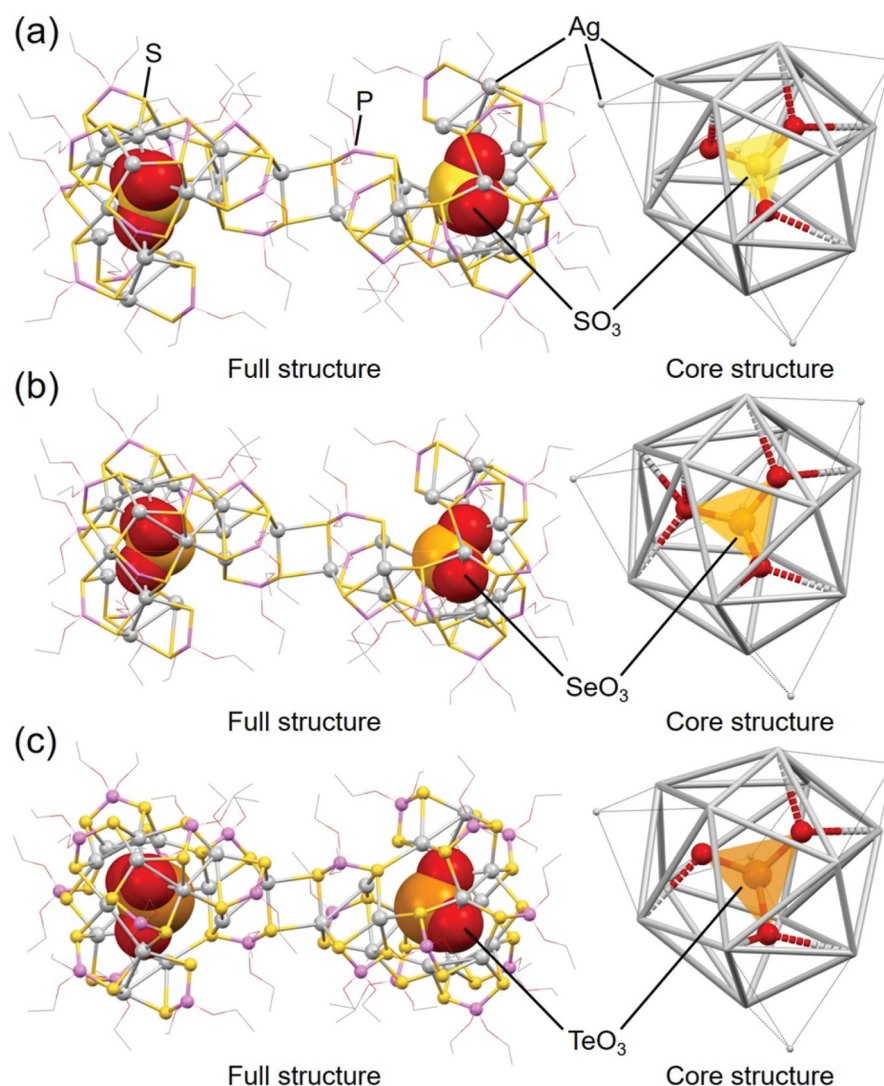


Figure 16. Full (left) structures and core (right) structures of (a) 82 ($[\text{SO}_3@Ag16]_2$), (b) 83 ($[\text{SeO}_3@Ag16]_2$), and (c) 84 ($[\text{TeO}_3@Ag16]_2$). Data are taken from ref [192].

somewhat larger frameworks. The history of research on $\text{POM}@Ag_n$ NCs is short, and currently, the largest anion-templated Ag NCs are **39** ($\text{Cl}@Ag216$) [155] and **147** ($\text{SO}_4@Ag78$) [189]. However, it is expected that larger anion-templated Ag NCs will be created in the future using POM as an anion template.

Mak and colleagues first reported on **149** ($\text{POV}@Ag24a$), **165** ($\text{POV}@Ag40a$), and **167** ($\text{POMo}@Ag40$) in 2009 [186]. POM had already attracted attention as a functional material at that time, and because the O atom of POM has a high affinity for Ag(I) ions, there had been several reports on the synthesis of POM–Ag(I) complexes before then [229–234]. However, there were no reported examples of compounds that encapsulate POM in the Ag framework until the report of Mak and colleagues.

In that report, they also found that the chemical compositions of the products vary depending on the presence or absence of stabilizers in the organic

solvent during the reaction. Specifically, they compared the chemical composition of the products when $\text{CF}_3\text{CO}_2\text{H}$ was added as a stabilizer for POM to make the solution acidic and when AgCF_3CO_2 was added as a stabilizer for POM to make the solution neutral. In the former experimental condition, **165** ($\text{POV}@Ag40a$) or **167** ($\text{POMo}@Ag40$) was formed, encapsulating $[\text{V}_{10}\text{O}_{28}]^{6-}$ or $[\text{Mo}_6\text{O}_{22}]^{8-}$, whereas in the latter experimental condition, **149** ($\text{POV}@Ag24a$) or **108** ($\text{MoO}_4@Ag20$) was formed, encapsulating smaller POMs such as $[\text{V}_2\text{O}_7]^{4-}$ or Ox, $[\text{MoO}_4]^{2-}$ (Table 4). Regarding **165** ($\text{POV}@Ag40a$) and **167** ($\text{POMo}@Ag40$), although they contain the same number of Ag atoms, there is a large difference in the edge-to-edge Ag–Ag distances between them (17.665 Å for **165** ($\text{POV}@Ag40a$) vs. 14.309 Å for **167** ($\text{POMo}@Ag40$), Figure 17). This is because the Ag framework in **167** ($\text{POMo}@Ag40$) is regularly and compactly surrounding the central

Table 5. Representative POM-templated Ag NCs.

No.	Chemical formula	Abbreviation	Center anion	z	Synthesis method	Year	Ref.
148	[V ₂ O ₇ @Ag ₂₂ (S ^t Bu) ₈ (S ₂ P(OEt) ₂) ₉][OH]·H ₂ O	POV@Ag22	[V ₂ O ₇] ⁴⁻	+1	Stirring	2022	[204]
149	[V ₂ O ₇ @Ag ₂₄ (C≡C ^t Bu) ₁₄ (tfa) ₆] ⁰ ·2MeOH	POV@Ag24a	[V ₂ O ₇] ⁴⁻	0	Stirring	2009	[186]
150	[V ₂ O ₇ @Ag ₂₄ (C≡C ^t Bu) ₁₄ (hfac) ₆] ⁰	POV@Ag24b	[V ₂ O ₇] ⁴⁻	0	Ultrasonication	2018	[159]
151	[W ₂ O ₉ @Ag ₂₄ (S ^t Bu) ₁₄ (S ₂ P(O ^t Pr) ₂) ₉] ⁰ ·MeOH	POW@Ag24	[W ₂ O ₉] ⁴⁻	0	Stirring	2022	[204]
152	[P ₂ W ₁₅ Nb ₃ O ₆₂ @Ag ₂₅ (C≡C ^t Bu) ₁₆ (MeCN) ₄] ⁰ ·11MeCN	POW@Ag25	[P ₂ W ₁₅ Nb ₃ O ₆₂] ⁹⁻	0	Crystallization ^a	2015	[222]
153	[V ₁₀ V ₂ O ₃₄ @Ag ₃₀ (S ^t Bu) ₂₀] ⁰ ·10MeOH	POV@Ag30a	[V ₁₀ V ₂ O ₃₄] ¹⁰⁻	0	Solvothermal	2016	[225]
154	[V ₁₀ V ₂ O ₃₄ @Ag ₃₀ (S ^t Bu) ₂₀] ⁰ ·7MeOH	POV@Ag30b	[V ₁₀ V ₂ O ₃₄] ¹⁰⁻	0	Stirring	2016	[225]
155	[V ₁₀ V ₂ O ₃₄ @Ag ₃₀ (S ^t Bu) ₂₀] ⁰ ·8MeOH	POV@Ag30c	[V ₁₀ V ₂ O ₃₄] ¹⁰⁻	0	Stirring	2016	[225]
156	[Mo ₂ O ₈ @Ag ₃₀ (S ^t Bu) ₁₅ (PhSO ₃) ₁₁ (MeOH) ₂ (H ₂ O)·H ₂ O] ₂	[POMo@Ag30]₂	[Mo ₂ O ₈] ⁴⁻	0	Solvothermal	2018	[137]
157	[(W ₆ O ₂₁)@Ag ₃₄ (S ^t Bu) ₂₆ (tfa)] [tfa]·Et ₃ N·20MeOH	POW@Ag34	[W ₆ O ₂₁] ⁶⁻	+1	Stirring	2012	[209]
158	[SiW ₉ O ₃₄ @Ag ₃₄ Cu ₆ (C≡C ^t Bu) ₁₈ (^t BuPO ₃) ₉ (MeCN) ₂ (H ₂ O)] ⁰ ·2MeCN	POW@Ag34Cu6	[SiW ₉ O ₃₄] ¹⁰⁻	0	Solvothermal	2018	[158]
159	[((O ₂)V ₂ O ₆) ₂ @Ag ₃₆ (C≡C ^t Bu) ₁₂ ((^t BuPO ₃) ₃ V ₄ O ₈) ₂ (^t BuPO ₃) ₂ (NO ₃) ₇ (2-ClPy)(DMF))[Et ₄ N] ₃	POV@Ag36	[(O ₂)V ₂ O ₆] ⁴⁻	-3	Stirring	2012	[152]
160	[(α-Mo ₅ O ₁₈)@Ag ₃₆ (S ^t Pr) ₁₈ (PhSO ₃) ₁₂ (DMF) ₆] ⁰	POMo@Ag36a	[α-Mo ₅ O ₁₈] ⁶⁻	0	Solvothermal	2018	[137]
161	[(Mo ₅ O ₁₈)@Ag ₃₆ (S ^t Pr) ₁₈ (O ₃ SPHMe) _{13.5} (MeCN)· 1.5MeCN][^t Bu ₄ N] _{1.5}	POMo@Ag36b	[Mo ₅ O ₁₈] ⁶⁻	-1.5	Solvothermal	2018	[220]
162	[^t Bu ₄ NH][β-Mo ₅ O ₁₈] ₂ @Ag ₃₆ (S ^t Bu) ₁₈ (PhSO ₃) ₁₃ (MeOH)] ⁰ _n	[POMo@Ag36]_n	[β-Mo ₅ O ₁₈] ⁶⁻	0	Solvothermal	2018	[137]
163	[SiW ₉ O ₃₄ @Ag ₃₇ Cu ₆ (C≡C ^t Bu) ₁₈ (^t BuPO ₃) ₉ (MeCN) ₆] [SiW ₁₂ O ₄₀] _{0.5} [OH]	POW@Ag37Cu6	[SiW ₉ O ₃₄] ¹⁰⁻	+3	Solvothermal	2018	[158]
164	[α-Mo ₅ O ₁₈ @Ag ₃₈ (^t BuS) ₁₈ (PhCO ₂) ₁₄ ·2(DCM)] ⁰	POMo@Ag38	[α-Mo ₅ O ₁₈] ⁶⁻	0	Ultrasonication	2018	[219]
165	[V ₁₀ O ₂₈ @Ag ₄₀ (C≡C ^t Bu) ₂₂ (tfa) ₁₂] ⁰ ·4MeOH	POV@Ag40a	[V ₁₀ O ₂₈] ⁶⁻	0	Stirring	2009	[186]
166	[V ₂ O ₇ @Ag ₄₀ (C≡C ^t Bu) ₂₂ (^t BuPO ₃) ₄ (hfac) ₄ (tfa) ₂ (H ₂ O) ₂] ⁰	POV@Ag40b	[V ₂ O ₇] ⁴⁻	0	Ultrasonication	2018	[159]
167	[Mo ₆ O ₂₂ @Ag ₄₀ (C≡C ^t Bu) ₂₀ (tfa) ₁₂] ⁰ ·2MeOH	POMo@Ag40	[Mo ₆ O ₂₂] ⁸⁻	0	Stirring	2009	[186]
168	[α-SiW ₁₀ O ₃₇ @Ag ₄₁ (C≡C ^t Bu) ₂₇ (MeCN) ₃] [β-SiW ₁₂ O ₄₀] ₁ ·H ₂ O·4MeCN	POW@Ag41	[α-SiW ₁₀ O ₃₇] ¹⁰⁻	-4	Solvothermal	2016	[216]
169	[(Mo ₇ O ₂₄)@Ag ₄₁ (S ^t Pr) ₁₉ (p-tos) ₁₆ (MeOH) ₄ ·4MeOH] ⁰	POMo@Ag41	[Mo ₇ O ₂₄] ⁶⁻	0	Solvothermal	2018	[220]
170	[Ho(W ₅ O ₁₈) ₂ @Ag ₄₂ (C≡C ^t Bu) ₂₈ Cl ₄][OH]	POW@Ag42a	[Ho(W ₅ O ₁₈) ₂] ⁹⁻	+1	Solvothermal	2013	[210]
171	[EuW ₁₀ O ₃₆ @Ag ₄₂ (C≡C ^t Bu) ₂₈ (NO ₃) ₄ ·NO ₃]	POW@Ag42b	[EuW ₁₀ O ₃₆] ⁹⁻	0	Solvothermal	2018	[217]
172	[Eu(W ₅ O ₁₈) ₂ @Ag ₄₂ (C≡C ^t Bu) ₂₈ Cl ₄][OH]·H ₂ O	POW@Ag42	[Eu(W ₅ O ₁₈) ₂] ⁹⁻	+1	Solvothermal	2015	[221]
173	[((O ₂)V ₂ O ₆) ₃ Ag ₄₃ (C≡CPh) ₁₉ ((^t BuPO ₃) ₄ V ₄ O ₈) ₃ (DMF) ₆] ⁰ ·5DMF·2H ₂ O	POV@Ag43	[(O ₂)V ₂ O ₆] ⁴⁻	0	Stirring	2011	[184]
174	[K(H ₂ O)HP ₅ W ₃₀ O ₁₁₀ @Ag ₄₃ (C≡C ^t Bu) ₂₉ (CN)(MeCN) (H ₂ O)] ⁰ ·4MeCN	POW@Ag43	[K(H ₂ O)HP ₅ W ₃₀ O ₁₁₀] ¹³⁻	0	Solvothermal	2021	[227]
175	[(V ₂ O ₇) ₂ @Ag ₄₄ (C≡C ^t Bu) ₁₄ (V ₃ O ₉) ₆][BzEt ₃ N] ₈ [Et ₄ N] ₂	POV@Ag44	[V ₂ O ₇] ⁴⁻	-10	Stirring	2012	[224]
176	[V ₁₀ O ₂₈ @Ag ₄₄ (SET) ₂₀ (PhSO ₃) ₁₈ (H ₂ O) ₂] ⁰ _n	[POV@Ag44]_n	[V ₁₀ O ₂₈] ⁶⁻	0	Solvothermal	2019	[138]
177	[Mo ₆ O ₂₂ @Ag ₄₄ (S ^t Pr) ₂₀ (PhCO ₂) ₁₆ (MeCN) ₂] ⁰ · 2MeCN	POMo@Ag44	[Mo ₆ O ₂₂] ⁸⁻	0	Solvothermal	2018	[139]
178	[(Mo ₆ O ₁₉ @Ag ₄₄ (SET) ₂₄ (SCl ₄) ₃] ⁰ _n	[POMo@Ag44]_n	[Mo ₆ O ₁₉] ²⁻	0	Solvothermal	2019	[138]
179	[(V ₁₀ O ₂₈ @Ag ₄₆ (SET) ₂₃ (PhSO ₃) ₁₅ (CO ₃) ₃] ⁰ _n	[POV@Ag46]_n	[V ₁₀ O ₂₈] ⁶⁻	0	Solvothermal	2019	[138]
180	[V ₁₀ O ₂₈ @Ag ₄₆ (S ^t Pr) ₂₈ (tfa) ₁₂ (DMF) ₂] ⁰	POV@Ag46a	[V ₁₀ O ₂₈] ⁶⁻	0	Solvothermal	2022	[202]
181	[V ₁₀ O ₂₈ @Ag ₄₆ (S ^t Pr) ₃₀ (tfa) ₈ (PhCO ₂) ₂ (DMF) ₄] ⁰	POV@Ag46b	[V ₁₀ O ₂₈] ⁶⁻	0	Solvothermal	2022	[202]
182	[Mo ₆ O ₂₂ @Ag ₄₆ (SPH ^t Bu) ₃₂ (dppm) ₄ (MeCN) ₈][OTf] ₆	POMo@Ag46	[Mo ₆ O ₂₂] ⁸⁻	+6	Solvothermal	2017	[135]
183	[Mo ₈ O ₂₈ @Ag ₄₈ (p-MePhS) ₂₄ (tfa) ₁₄ (H ₂ O) ₄ (DMF) ₂][tfa] ₂	POMo@Ag48	[Mo ₈ O ₂₈] ⁸⁻	+2	Solvothermal	2019	[140]
184	[V ₁₀ O ₂₈ @Ag ₅₀ (SPH ^t Bu) ₃₂ (tfa) ₈ (DMF) ₆ (H ₂ O) ₄][tfa] ₄ ·12DMF	POV@Ag50	[V ₁₀ O ₂₈] ⁶⁻	+4	Solvothermal	2022	[228]
185	[Mo ₈ O ₂₈ @Ag ₅₀ (S ^t Pr) ₂₄ (PhCO ₂) ₁₈ (MeCN) ₂] ⁰ · 4MeCN	POMo@Ag50a	[Mo ₈ O ₂₈] ⁸⁻	0	Solvothermal	2018	[139]
186	[Mo ₈ O ₂₈ @Ag ₅₀ (S ^t Pr) ₂₄ (4-MePhCO ₂) ₁₄ (PhCO ₂) ₄ (MeCN) ₄] ⁰	POMo@Ag50b	[Mo ₈ O ₂₈] ⁸⁻	0	Solvothermal	2018	[139]
187	[Mo ₈ O ₂₈ @Ag ₅₀ (S ^t Pr) ₂₄ (4-MePhCO ₂) _{16.5} (PhCO ₂) _{1.5}] ⁰	POMo@Ag50c	[Mo ₈ O ₂₈] ⁸⁻	0	Solvothermal	2018	[139]
188	[Mo ₈ O ₂₈ @Ag ₅₀ (S ^t Pr) ₂₄ (3-MePhCO ₂) ₁₈ (3-MePhCO ₂ H)(MeCN) ₂] ⁰	POMo@Ag50d	[Mo ₈ O ₂₈] ⁸⁻	0	Solvothermal	2018	[139]
189	[(WO ₆)(SiW ₉ O ₃₄)@Ag ₅₁ (C≡C ^t Bu) ₂₇ (^t BuPO ₃) ₃ (OAc) ₃ (MeCN) ₃] ₁ ·0.5 [H ₈ SiW ₁₂ O ₄₀][BF ₄]	POW@Ag51	[(WO ₆)(SiW ₉ O ₃₄)] ¹⁶⁻	+1	Solvothermal	2018	[158]
190	[Cr ^{III} ₄ Cr ^{VI} ₈ O ₃₆ @Ag ₅₆ (S ^t Pr) ₂₈ (tfa) ₁₂ (NapCO ₂) ₄ (MeCN) ₈] ⁰ ·2MeCN	POCr@Ag56	[Cr ^{III} ₄ Cr ^{VI} ₈ O ₃₆] ¹²⁻	0	Solvothermal	2020	[226]
191	[Mo ₆ O ₂₂ @Ag ₅₈ S ₂ (SPH ^t Bu) ₃₆ (tfa) ₁₀ (H ₂ O) ₈] ⁰	POMo@Ag58	[Mo ₆ O ₂₂] ⁸⁻	0	Solvothermal	2015	[214]
192	[(Mo ₆ O ₂₂) ₂ Ag ₆₀ (C≡C ^t Bu) ₃₈][OTf] ₆	POMo@Ag60	[Mo ₆ O ₂₂] ⁸⁻	+6	Solvothermal	2010	[211]
193	[Mo ₂₀ O ₆₆ @Ag ₆₂ (S ^t Bu) ₄₀ (Mo ₆ O ₁₉) ₃ (MeCN) ₂][OTf] ₄	POMo@Ag62	[Mo ₂₀ O ₆₆] ¹²⁻	+4	Stirring	2015	[215]
194	[(Mn ^{III} Mn ^{IV} ₂ Mo ₁₄ O ₅₆)@Ag ₆₄ (C≡C ^t Bu) ₃₈ (tfa) ₈][OH]·10MeCN·2H ₂ O	POMo@Ag64	[Mn ^{III} Mn ^{IV} ₂ Mo ₁₄ O ₅₆] ¹⁷⁻	+1	Solvothermal	2016	[212]
195	[(PW ₉ O ₃₄) ₂ @Ag ₆₇ (p-PPhS) ₃₆ (DMAC) ₂ (tfa) ₆][tfa] ₇ (DMAC) _x	POW@Ag67	[PW ₉ O ₃₄] ⁹⁻	+7	Stirring	2019	[223]
196	[(PW ₉ O ₃₄) ₂ @Ag ₇₀ (C≡C ^t Bu) ₄₄ (H ₂ O) ₂][BF ₄] ₈ ·2[BMIIm]BF ₄ ·3H ₂ O	POW@Ag70	[PW ₉ O ₃₄] ⁹⁻	+8	Solvothermal	2014	[213]
197	[(EuW ₁₀ O ₃₆) ₂ @Ag ₇₂ (C≡C ^t Bu) ₄₈ Cl ₂ ·4BF ₄]	POW@Ag72	[EuW ₁₀ O ₃₆] ⁹⁻	0	Solvothermal	2018	[217]
198	[(Mo ₆ O ₂₂) ₂ @Ag ₇₆ (SPHOMe) ₂₈ (dppm) ₈ (MoO ₄) ₁₆ (H ₂ O) ₈ ·8MeOH·4MeCN] ⁰	POMo@Ag76	[Mo ₆ O ₂₂] ⁸⁻	0	Ultrasonication	2018	[218]

^aSee citation for detailed synthesis method.

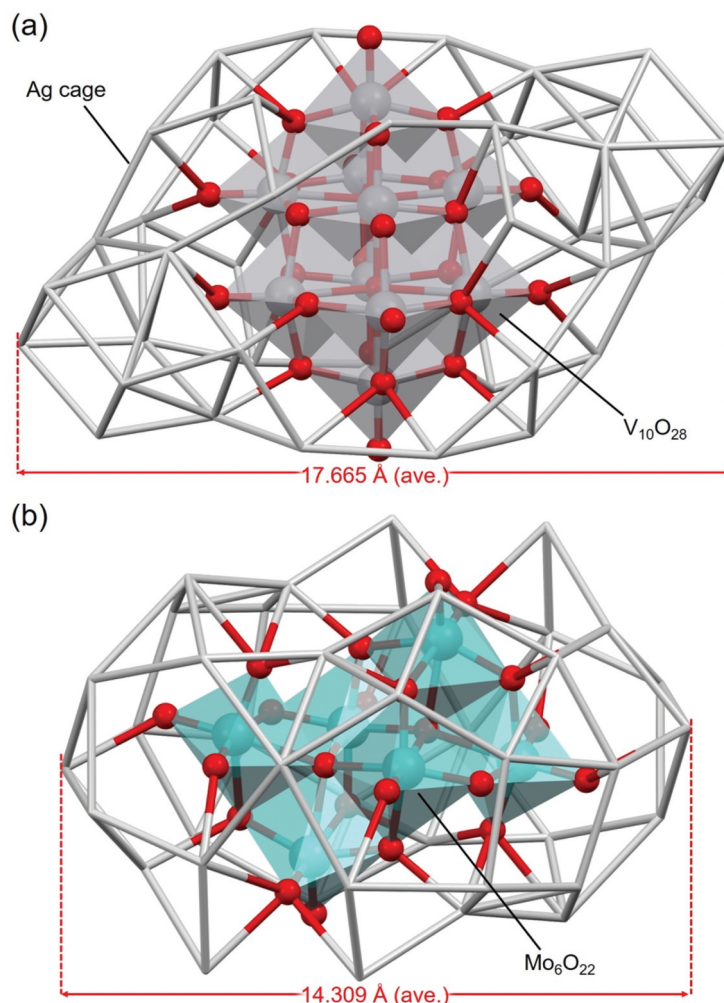


Figure 17. The full geometric structures of (a) 165 (**Pov@Ag40a**), and (b) 167 (**POMo@Ag40**). Data are taken from ref [186].

[Mo₆O₂₂]⁸⁻ anion, resulting in a more spherical shape compared with that of 165 (**POV@Ag40a**).

Many studies on the synthesis of novel POM@Ag_n NCs and their mechanisms have been reported since 2009. Reviews of these POM@Ag_n NCs have recently been reported by Li, Zheng, and colleagues [127], and Hu, Shi, Ji, and colleagues [129]. Therefore, we look at the differences between POM@Ag_n NCs and other anion-templated Ag NCs, which have not been described in previous reviews.

For example, 29 (**Cl@Ag16c**, Table 2, Figure 18 (a)), 98 (**MoO₄@Ag19**, Table 4, Figure 18(b)), and 150 (**POV@Ag24b**, Table 5, Figure 18(c)) have increasing numbers of Ag atoms in this order [159]. This result demonstrates the trend described at the beginning of this section (Section 3.4), stating that POM encapsulation tends to yield larger-sized Ag NCs. This trend is also observed in the Ag NCs linked by phosphonic acid in the Ag framework (117 (**NO₃@Ag22**, Figure 18(d)) and 166 (**POV@Ag40b**, figure 18(e))). In addition, Jin and colleagues reported the synthesis of Ag NCs (**Ag@Ag16**, Figure 18(f)) in which the central Cl⁻ anion in 29

(**Cl@Ag16c**) is replaced by an Ag atom [159]. **Ag@Ag16** has the same number of Ag atoms, but a different cage structure, compared with 29 (**Cl@Ag16c**). This result indicates that Ag NCs without the central anion can be synthesized by making slight modifications to the synthesis methods of anion-templated Ag NCs described in this review.

3.5. Hydride/deuteride-templated Ag NCs

Finally, we describe Ag NCs that contain H⁻ and D⁻ as central anions. Table 6 summarizes the representative H/D@Ag_n NCs [132,235–240]. The number of reports on H/D@Ag_n NCs is smaller than that on other anion-templated Ag NCs, and the first report of H/D@Ag_n NCs was in 2010. In H/D@Ag_n NCs, the Ag₁₁ framework has the highest number of constituent Ag atoms. Thus, H and D tend to yield smaller Ag NCs than those obtained with other anions.

The earliest H/D@Ag_n NCs were 207 (**H@Ag8a**), 208 (**H@Ag8b**), 209 (**H@Ag8c**), 212 (**D@Ag8a**), 213 (**D@Ag8b**), and 214 (**D@Ag8c**), all reported in 2010 by Liu and colleagues [132,236]. Although the

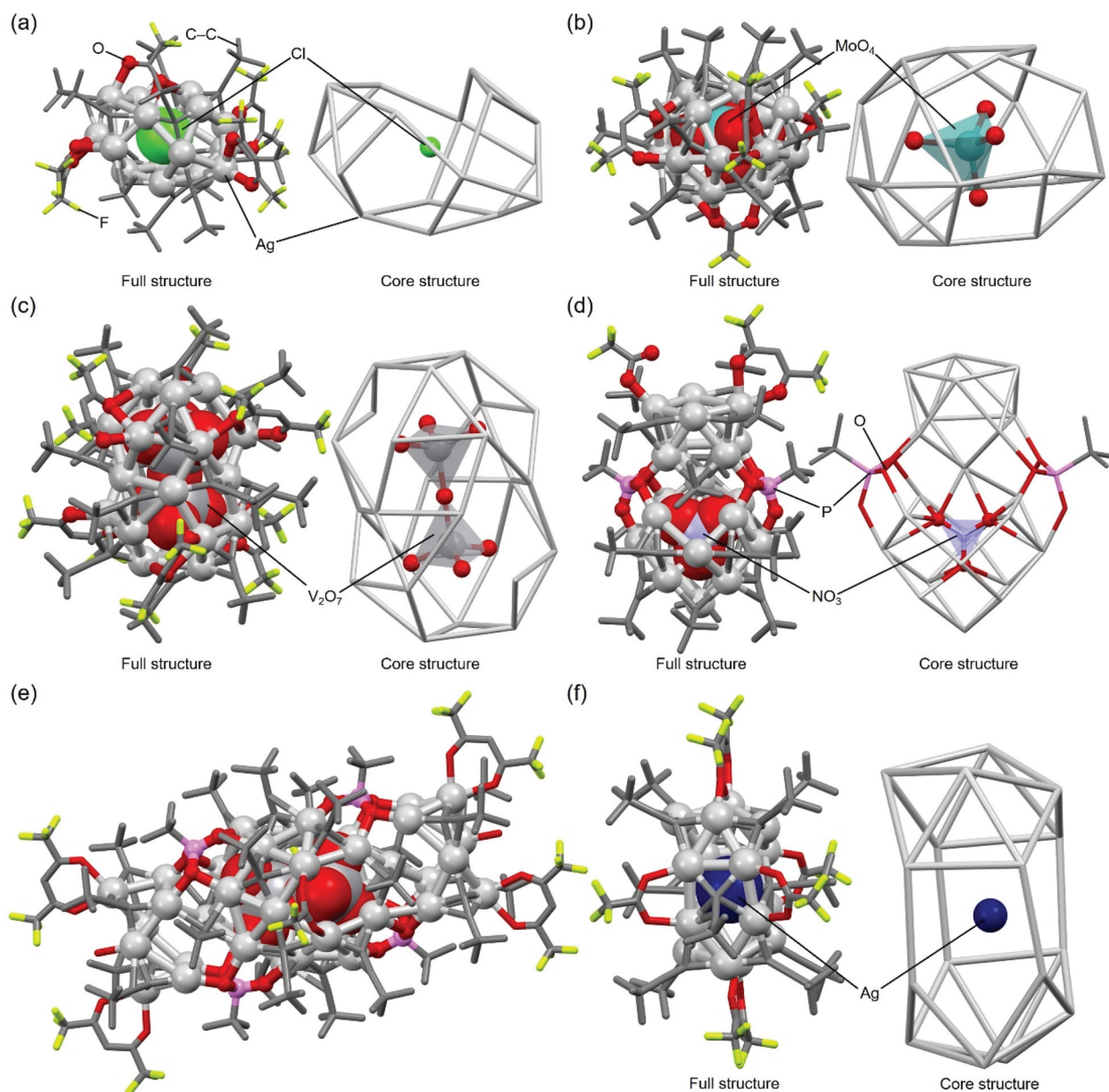


Figure 18. Full (left) and core (right) structures of (a) 29 (**Cl@Ag16c**), (b) 98 (**MoO₄@Ag19**), (c) 150 (**POV@Ag24b**), (d) 117 (**NO₃@Ag22**), (e) 166 (**POV@Ag40b**) and (f) **Ag@Ag16**. For (a)–(d) and (f), the core structure is shown to the right of the full structure, respectively. Data are taken from ref [159].

Table 6. Representative H/D-templated Ag NCs.

No.	Chemical formula	Abbreviation	Center anion	z	Synthesis method	Year	Ref.
199	(Δ) ₄ -[Na] ₉ [H@Ag ₄ {Rh(L-Cys) ₃] ₄].nH ₂ O	H@Ag4Rh4	H ⁻	-9	Stirring	2021	[240]
200	(Δ) ₄ -[Na] ₉ [D@Ag ₄ {Rh(L-Cys) ₃] ₄].nH ₂ O	D@Ag4Rh4	H ⁻	-9	Stirring	2021	[240]
201	[H@Ag ₇ {Se ₂ P(O ⁱ Pr) ₂ }] ₆ ⁰	H@Ag7a	H ⁻	0	Stirring	2013	[235]
202	[H@Ag ₇ {S ₂ P(OEt) ₂ }] ₆ ⁰	H@Ag7b	H ⁻	0	Stirring	2013	[235]
203	[H@Ag ₇ {S ₂ C≡C(CN) ₂ }] ₆ [Bu ₄ N] ₆	H@Ag7c	H ⁻	-6	Stirring	2019	[238]
204	[D@Ag ₇ {Se ₂ P(O ⁱ Pr) ₂ }] ₆ ⁰	D@Ag7a	H ⁻	0	Stirring	2013	[235]
205	[D@Ag ₇ {S ₂ P(OEt) ₂ }] ₆ ⁰	D@Ag7b	H ⁻	0	Stirring	2013	[235]
206	[D@Ag ₇ {S ₂ C≡C(CN) ₂ }] ₆ [Bu ₄ N] ₆	D@Ag7c	D ⁻	-6	Stirring	2019	[238]
207	[H@Ag ₈ {Se ₂ P(O ⁱ Pr) ₂ }] ₆ [PF ₆]	H@Ag8a	H ⁻	+1	Stirring	2010	[236]
208	[H@Ag ₈ {Se ₂ P(OEt) ₂ }] ₆ [PF ₆]	H@Ag8b	H ⁻	+1	Stirring	2010	[236]
209	[H@Ag ₈ {S ₂ P(OEt) ₂ }] ₆ [PF ₆]	H@Ag8c	H ⁻	+1	Stirring	2010	[132]
210	[H@Ag ₈ {S ₂ C≡C(CN) ₂ }] ₆ [Bu ₄ N] ₅	H@Ag8d	H ⁻	-5	Stirring	2011	[239]
211	[H@Ag ₈ {S ₂ P(O ⁱ Pr) ₂ }] ₆ [PF ₆]	H@Ag8e	H ⁻	+1	Stirring	2014	[133]
212	[D@Ag ₈ {Se ₂ P(O ⁱ Pr) ₂ }] ₆ [PF ₆]	D@Ag8a	D ⁻	+1	Stirring	2010	[236]
213	[D@Ag ₈ {Se ₂ P(OEt) ₂ }] ₆ [PF ₆]	D@Ag8b	D ⁻	+1	Stirring	2010	[236]
214	[D@Ag ₈ {S ₂ P(OEt) ₂ }] ₆ [PF ₆]	D@Ag8c	D ⁻	+1	Stirring	2010	[132]
215	[D@Ag ₈ {S ₂ C≡C(CN) ₂ }] ₆ [Bu ₄ N] ₅	D@Ag8d	D ⁻	-5	Stirring	2011	[239]
216	[H@Ag ₁₁ {S ₂ CNPr ₂ }] ₉ [NO ₃]	H@Ag11	H ⁻	+1	Stirring	2011	[237]
217	[D@Ag ₁₁ {S ₂ CNPr ₂ }] ₉ [NO ₃]	D@Ag11	D ⁻	+1	Stirring	2011	[237]

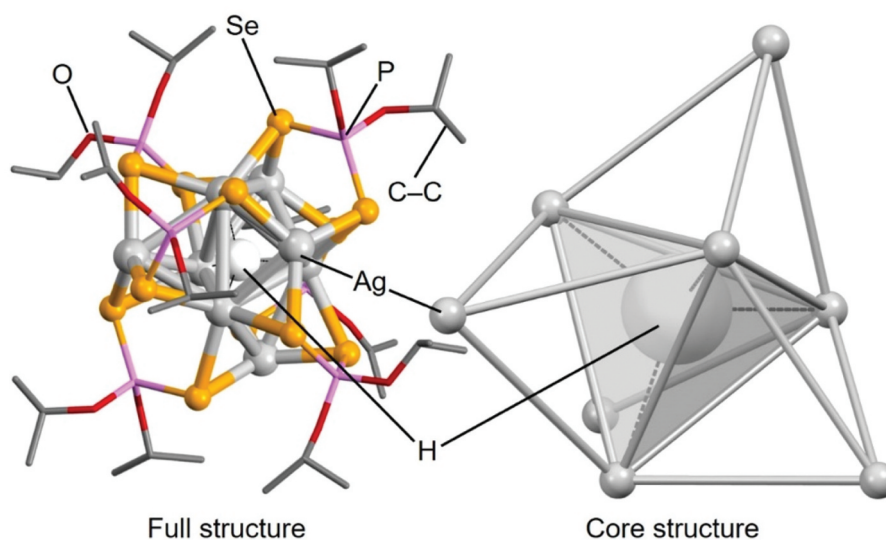


Figure 19. Full (left) and core (right) structures of 207 (**H@Ag8a**). Data are taken from ref [236].

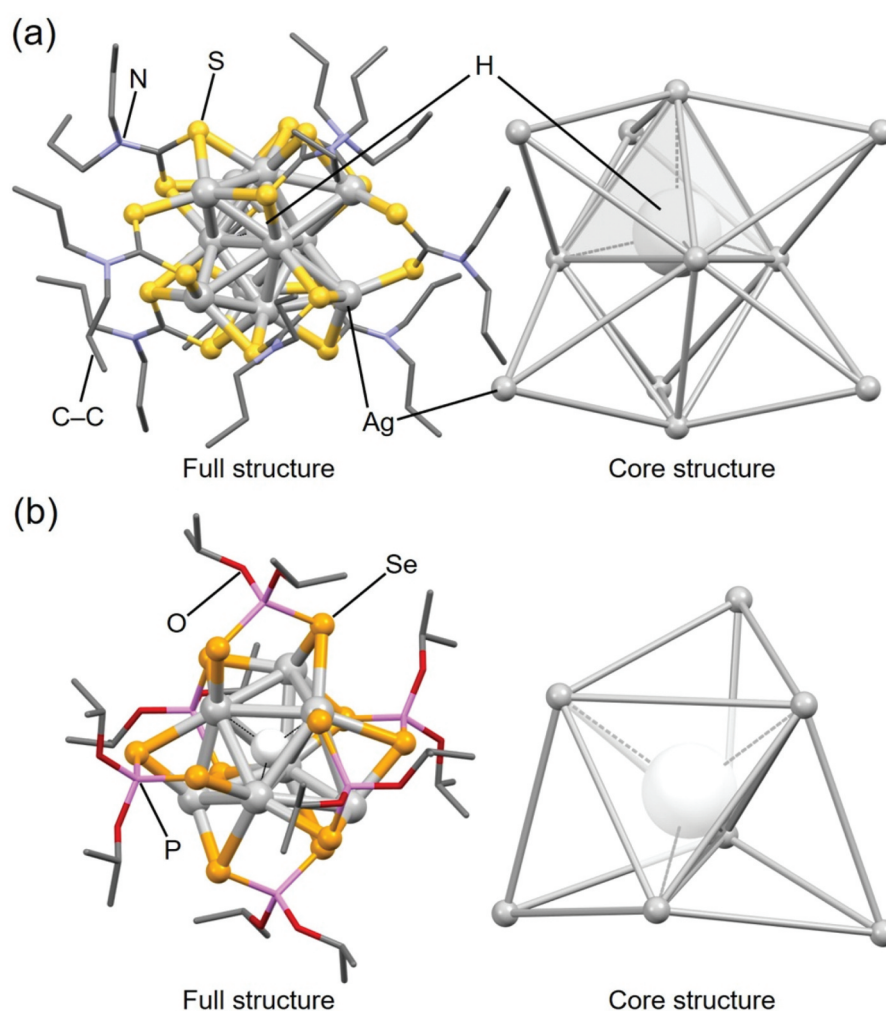


Figure 20. Full (left) and core (right) structures of (a) 216 (**H@Ag11**) and (b) 201 (**H@Ag7a**). Data are taken from refs [235,237].

formation of $[\text{Ag}_4\text{H}]^+$ complexes had been previously observed in the gas phase [241], the isolation of ligand-protected H/D@Ag_n NCs had not been reported. Regarding the syntheses, **207** (**H@Ag8a**) and **208** (**H@Ag8b**) were obtained by stirring Ag

$(\text{MeCN})_4\text{PF}_6$ and $\text{NH}_4\text{Se}_2\text{P}(\text{OR})_2$ ($R = i\text{Pr}$ or Et) in THF for 1 h, then cooling the resulting solution to -20°C , to which NaBH_4 was added. Similarly, **212** (**D@Ag8a**) and **213** (**D@Ag8b**) were obtained, but using NaBD_4 instead of NaBH_4 . The synthesis of **209**

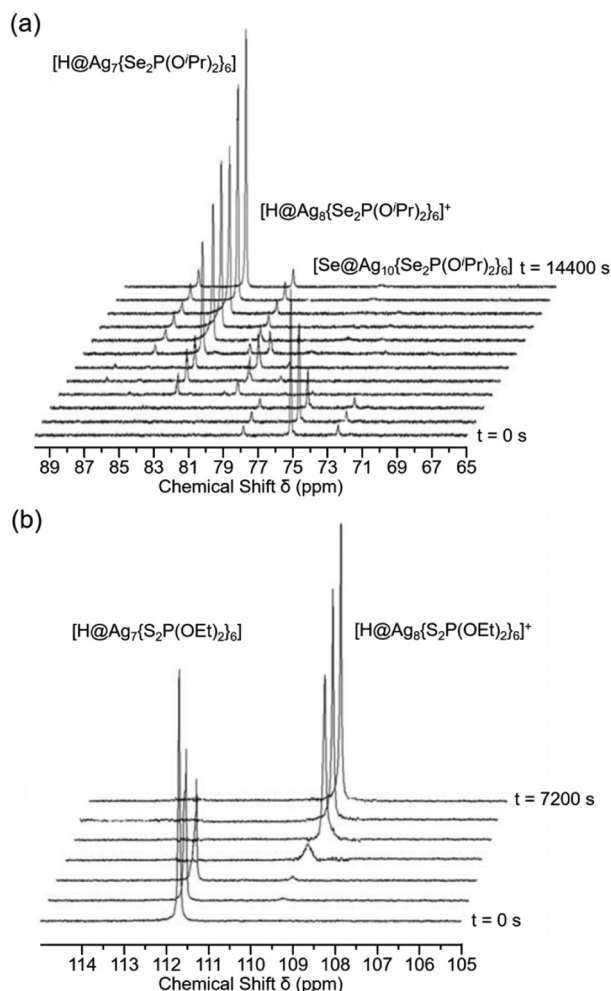


Figure 21. (A) the transformation of Se@Ag_{10} to H@Ag_8 and H@Ag_7 . (b) Silver uptake of $[\text{H@Ag}_7\{\text{S}_2\text{P}(\text{OEt})_2\}_6]$ to $[\text{H@Ag}_8\{\text{S}_2\text{P}(\text{OEt})_2\}_6]^+$ in the presence of one equivalent of $[\text{Ag}(\text{MeCN})_4][\text{PF}_6]$ (fig7, 21), monitored by ^{31}P NMR spectroscopy. Reprinted with permission from [235], copyright (2013, American Chemical Society).

(**H@Ag8c**) and **214** (**D@Ag8c**) was conducted in a similar manner. Interestingly, these synthesis methods are similar to those of H-protected Ag nanoclusters [242,243], but the products were different. This reason is expected to be clarified in the future work. In addition to such direct synthesis methods, they also added NaBH_4 to solutions of X@Ag_8 NCs (**2** (**F@Ag8a**) or **7** (**Cl@Ag8d**), table 2) and monitored the reaction process by ^{31}P NMR spectroscopy. In both cases, the central anion was replaced by H and D within a few minutes, inducing the formation of **209** (**H@Ag8c**) and **214** (**D@Ag8c**).

As an example of the H/D@ Ag_8 NCs, Figure 19 shows the geometric structure of **207** (**H@Ag8a**) [236]. The Ag atoms that form the Ag framework are classified into two categories: 1) Ag atoms that form a tetrahedron surrounding H^- and 2) Ag atoms that surround the tetrahedron. Thus, the Ag_8 framework is formed by four Ag atoms capping each triangular facet of a tetrahedron composed of four Ag, which is

different from the distorted cubic framework of X@Ag_8 NCs (Figure 3) [132].

Liu and colleagues also reported other H/D@ Ag_n NCs, including H/D@ Ag_7 NCs and H/D@ Ag_{11} NCs. For example, **216** (**H@Ag11**, Figure 20(a)) and **217** (**D@Ag11**) were reported in 2011 [237], and **201** (**H@Ag7a**, Figure 20(b)), **202** (**H@Ag7b**), **204** (**D@Ag7a**), and **205** (**D@Ag7b**) were reported in 2013 [235]. Overall, the synthetic methods are similar to those for H/D@ Ag_8 NCs. Specifically, for **216** (**H@Ag11**) and **217** (**D@Ag11**), AgNO_3 was used as the Ag salt and $\text{NaS}_2\text{CNPr}_2$ as the ligand precursor, which were mixed according to the stoichiometric ratio, and the resulting solutions were then reduced in the liquid phase at -20°C for 3 hours. For **201** (**H@Ag7a**), **202** (**H@Ag7b**), **204** (**D@Ag7a**), and **205** (**D@Ag7b**), $\text{Ag}(\text{CH}_3\text{CN})_4\text{PF}_6$ was used as the Ag salt and $\text{NH}_4\text{Se}_2\text{P}(\text{O}^i\text{Pr})_2$ or $\text{NH}_4\text{S}_2\text{P}(\text{OEt})_2$ as the ligand precursor. The resulting DCM solution was reduced with NaBH_4 or NaBD_4 at room temperature to obtain the H/D@ Ag_7 NCs. H@ Ag_7 NCs can also be synthesized by the reaction of $\text{X}'\text{@Ag}_{10}(\text{E}_2\text{P}(\text{OR})_2)_8$ ($\text{X}' = \text{Se}$, $R = ^i\text{Pr}$ or $\text{X}' = \text{S}$, $R = \text{Et}$) with two equivalent amounts of $[\text{BH}_4]^-$. Reaction tracking by ^{31}P NMR revealed that 1) H@ Ag_8 NCs, such as **207** (**H@Ag8a**), are formed as reaction intermediates in these reactions (Figure 21(a)), and 2) H@ Ag_8 NCs are obtained (regenerated) by the reaction of the obtained H@ Ag_7 NCs with an equal amount of Ag salt (Figure 21(b)).

Figure 20(a) shows the geometric structure of **216** (**H@Ag11**). The Ag_{11} framework is formed by capping six Ag atoms against the three-way bipyramidal Ag_5 structure, with the central H^- anion encapsulated in only one of the triangular pyramids. Because the H is difficult to observe by SC-XRD, the location of the H is concluded by predicting the geometric structure with the minimum energy using density functional theory calculations. This is the first example of such a three-way bipyramidal molecular structure capped by six Ag atoms [237].

In **201** (**H@Ag7a**, Figure 20(b)), H is encapsulated in the tetrahedral Ag_4 framework, and three of the four triangles in the tetrahedron are capped by Ag atoms to form the Ag_7 framework. The geometric structure of **201** (**H@Ag7a**) is the same as that of **207** (**H@Ag8a**), except one capped Ag atom is removed from the Ag_8 framework. The difference in the number of Ag atoms in both cases leads to a difference in the coordination between the Ag(I) and ligand. For example, in **207** (**H@Ag8a**), one coordination mode (μ_2, μ_2) occurs between Ag and the two Se atoms in $\text{Se}_2\text{P}(\text{O}^i\text{Pr})_2$, whereas in **201** (**H@Ag7a**), two coordination modes (μ_2, μ_2 and μ_2, μ_1) occur between Ag and the two Se atoms. Removing one capped Ag atom cleaves the three Ag–Se bonds. This

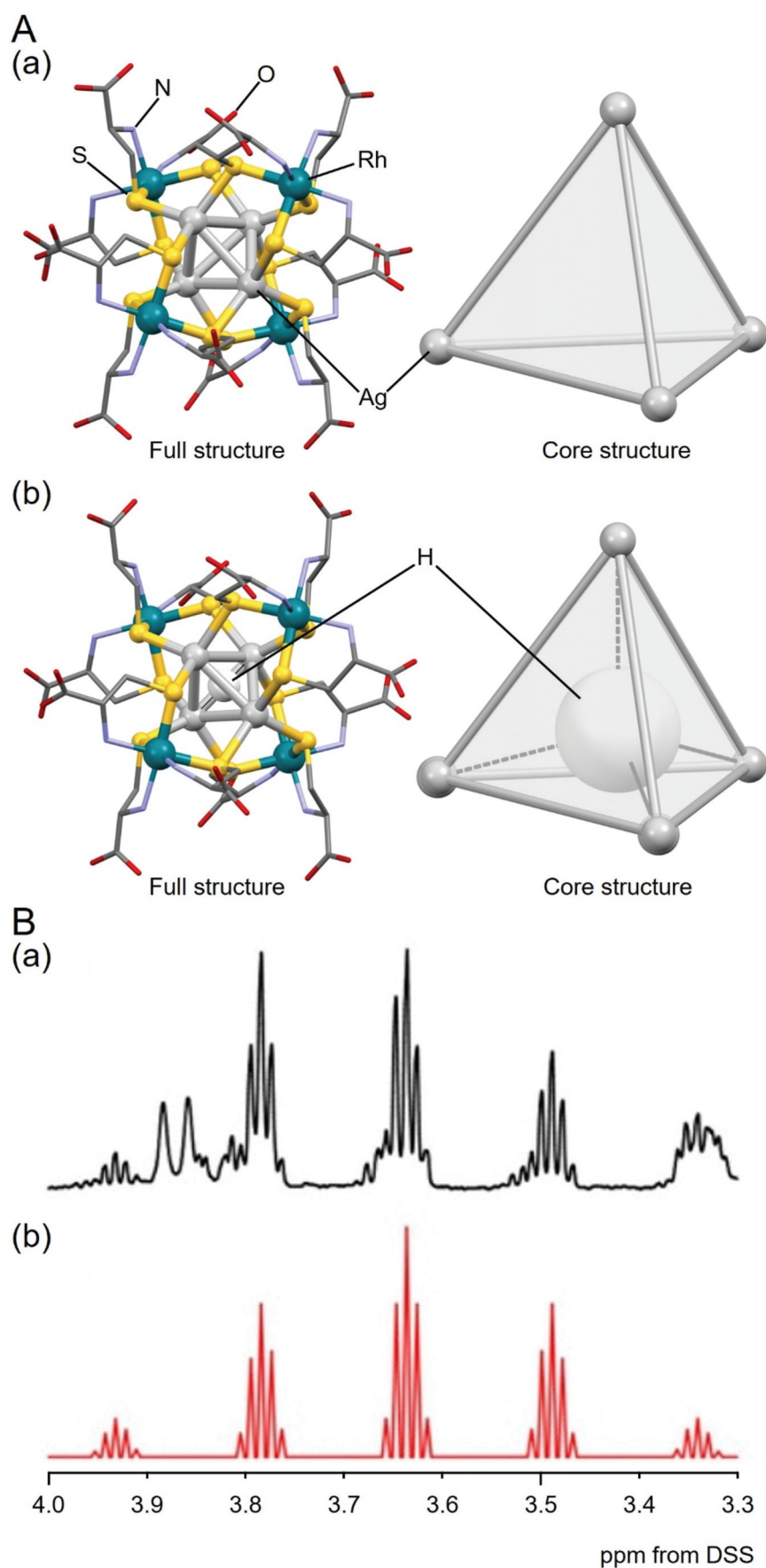


Figure 22. (A) Full (left) and core (right) structures of (a) Ag₄Rh₄ and (b) 199 (H@Ag₄Rh₄). (B) (a) Observed ¹H NMR spectrum of 199 (H@Ag₄Rh₄) in NaOH/D₂O and (b) simulated ¹H NMR spectrum for the [Ag₄H]³⁺ moiety. Sodium 4,4-dimethyl-4-silaphentane-1-sulfonate (DSS) was used as the internal reference. Data are taken from ref [240]. Reprinted with permission from [240], copyright (2021, American Chemical Society).

results in a new coordination mode (μ_2, μ_1) between the three Se and Ag atoms, changing the coordination pattern between the Ag(I) and ligand [235].

In the H/D@Ag_n NCs described above, the H/D@Ag₄ core structure is included. For a long time, there has been no report on the isolation of H/D@Ag₄ NCs without capping by Ag atoms. In 2021, Konno and colleagues succeeded in isolating two types of H/D@Ag₄ NCs, **199** (H@Ag₄Rh₄) and **200** (D@Ag₄Rh₄) [240]. Their synthesis methods differ significantly from the syntheses of H/D@Ag_n NCs described above. Specifically, **199** (H@Ag₄Rh₄) and **200** (D@Ag₄Rh₄) were formed by inserting H or D into [Ag₄{Rh(L-Cys)₃}]₄[Na]₈ (Ag₄Rh₄, Figure 22A(a)), which has an empty Ag framework. They reacted Ag₄Rh₄ with NaBH₄ or NaBD₄ in an aqueous NaOH solution, followed by the addition of an excess amount of ethanol to obtain powders of **199** (H@Ag₄Rh₄, Figure 22A(b)) or **200** (D@Ag₄Rh₄). They also examined the reaction mechanism for this reaction by X-ray absorption spectroscopy and magnetic measurements. The results suggested that this reaction did not cause the reduction of Ag(I) in [Ag(I)₄]⁴⁺ by NaBH₄ but caused the formation of [Ag(I)₄H]³⁺, in which H is included at the central position. Because it is difficult to definitively conclude the position of H in the product using SC-XRD, they confirmed the presence and position of the central H anion by ¹H NMR analysis (Figure 22B). The overall geometric structures of Ag₄Rh₄ and **199** (H@Ag₄Rh₄) are similar, both having a slightly distorted tetrahedral Ag₄ framework. These geometric structures are also similar to (Δ)4-[Zn₄O(Rh(L-Cys)₃)₄] [244–247]. However, closer inspection reveals that the structure is slightly more contracted in **199** (H@Ag₄Rh₄) than that in Ag₄Rh₄, which indicates that the insertion of H may contract the structure of the Ag NCs. The contraction of the framework is also observed in Cu₈ NCs with H[−] inclusion [247, 248].

For **199** (H@Ag₄Rh₄), $J_{H-107Ag} = 68.75$ Hz, $J_{H-108Ag} = 79.25$ Hz), it has also been shown that the coupling constant between the Ag atom and central H[−] anion is approximately twice as large as that of **207** (H@Ag₈a, $J_{Ag-H} = 33$ Hz). The higher coupling constant is explained by the average bond distance between the Ag atom and central H[−] anion, which is much shorter in **199** (H@Ag₄Rh₄) (1.86 Å) compared with that in **207** (H@Ag₈a) (2.50 Å).

4. Conclusion

This review summarizes the synthesis and geometric structure of a wide variety of anion-templated Ag NCs. Through this summary, the following points were discussed:

- (1) The current synthesis methods are broadly categorized into the stirring method, solvothermal method, and ultrasonication method, with the stirring method being the most widely used.
- (2) The reported central anion species are generally grouped into X (halide ion), X' (chalcogenide ion), Ox (oxoanion), POM (polyoxometalate), and H/D (hydride/deuteride).
- (3) The anion species affect the Ag NC volume, where POM is more effective for synthesizing larger anion-templated Ag NCs and H/D utilization is more effective for synthesizing smaller anion-templated Ag NCs.
- (4) When X is used as an anion species, it is possible to synthesize Ag NCs with the same number of Ag atoms but different central anions. In this case, the X–Ag and Ag–Ag distances tend to extend with the increasing size of the central X anion.
- (5) When X is used as the anion species, if X' is present in the system, the cage structure can contain both Ag and X'. Because these cage structures are tough, they can also contain large X' anions such as I[−]. Additionally, under these conditions, anion-templated Ag NCs can be synthesized in which two X anions are encapsulated within one Ag framework.
- (6) When X' is used as the anion species, the cage structure can be formed with Ag only if the number of Ag atoms is small. However, under these conditions, both Ag and X' are often included in the cage structure.
- (7) When Ox or POM is used as the anion species, the number of Ag atoms in the cage structure can easily be varied because of the diversity of these anions. The chemical composition and geometric structure of the resulting anion-templated Ag NCs vary depending on the number of O atoms in the central anions and the geometric structure of the central anions. Moreover, the chemical compositions of the central Ox and POM anions significantly depend on the synthesis conditions.
- (8) For Ag NCs using H/D as anion species, unlike other anion-templated Ag NCs, they can be synthesized not only by liquid-phase reduction but also by the reaction of X@Ag_n NCs with [BH₄][−], or by the insertion of H[−] or D[−] into empty Ag NCs.

Considering this breadth of knowledge, many anion-templated Ag NCs with novel geometric structures may be created in the future.

5. Outlook

As described in this review, a large number of anion-templated Ag NCs have been reported, which

indicates that the use of the anion-template method is quite effective in creating a wide variety of metal NCs. To further develop this research field, the following points should be investigated in the future:

- (1) **Establishment of clear synthesis design guidelines.** For the synthesis of Ag NCs with relatively simple geometric structures, such as $X@Ag_8$ NCs, some reports have described synthetic design guidelines based on stoichiometry [133]. However, the syntheses of most anion-templated Ag NCs appear to be a matter of coincidence. Future research is expected to be conducted on the formation mechanism so that anion-templated Ag NCs with the desired chemical compositions and geometric structures can be synthesized.
- (2) **Development of applied research.** Although it was not addressed in this review, it is possible to add new functions to anion-templated Ag NCs using functional anions. However, there is currently little research on the application of anion-templated Ag NCs. This may be because of the low stability of anion-templated Ag NCs. As discussed in previous studies on SR-protected metal NCs, the stability of metal NCs can be overcome to some extent by selecting the ligand functional group [248–250]. Future studies are expected to establish methods of improving the stability of anion-templated Ag NCs and provide insights into their practical application.
- (3) **Utilization of other metal elements.** This review describes the current status in the field of anion-templated Ag NCs, but more research is expected to be conducted on anion-templated NCs with metal elements other than Ag. Because there have been reports of anion-templated Cu NCs [251–254] and anion-templated lanthanide NCs [255–258,260], it is likely that the anion-template method can be used for the synthesis of other metal NCs. Considering the bonding between the anion species and the cage metal, the use of Ag facilitates the synthesis [259], but more active use of other metal elements is necessary to increase the diversity of their functions and applications.

Disclosure statement

No potential conflict of interest was reported by the author(s).

Funding

This work was supported by the Japan Society for the Promotion of Science KAKENHI [grant numbers 20H02698 and 20H02552] and Scientific Research on Innovative Areas “Aquatic Functional Materials” [grant

numbers and 22H04562]. Funding provided by the Yazaki Memorial Foundation for Science and Technology and the Ogasawara Foundation for the Promotion of Science and Engineering is also gratefully acknowledged.

Notes on contributors



Yusuke Horita is a master's course student in the Negishi group at the Tokyo University of Science (TUS). He received a B.Sc. (2021) in Chemistry from TUS. His research interests include the creation of new atomically precise, anion-templated silver nanoclusters.



Mai Ishimi is a master's course student in the Negishi group at TUS. She received a B.Sc. (2022) in Chemistry from TUS. Her research interests include the creation of new atomically precise, anion-templated silver nanoclusters.



Yuichi Negishi is a Professor at the Department of Applied Chemistry at TUS. He received a Ph.D. degree in Chemistry (2001) from Keio University under the supervision of Prof. Atsushi Nakajima. Before joining TUS in 2008, he was employed as an Assistant Professor at Keio University and the Institute for Molecular Science. His current research interests include the precise synthesis of stable and functionalized metal nanoclusters, metal nanocluster-connected structures, and covalent organic frameworks.

ORCID

Yuichi Negishi  <http://orcid.org/0000-0003-3965-1399>

References

- [1] Chakraborty I, Pradeep T. Atomically precise clusters of noble metals: emerging link between atoms and nanoparticles. *Chem Rev.* 2017;117:8208–8271.
- [2] Jin R, Zeng C, Zhou M, et al. Atomically precise colloidal metal nanoclusters and nanoparticles: fundamentals and opportunities. *Chem Rev.* 2016;116:10346–10413.
- [3] Dass A, Theivendran S, Nimmala PR, et al. $Au_{133}(SPh-tBu)_{52}$ nanomolecules: X-ray crystallography, optical, electrochemical, and theoretical analysis. *J Am Chem Soc.* 2015;137:4610–4613.
- [4] Luo Z, Yuan X, Yu Y, et al. From aggregation-induced emission of Au(I)–thiolate complexes to ultrabright Au(0)@Au(I)–thiolate core–shell nanoclusters. *J Am Chem Soc.* 2012;134:16662–16670.
- [5] Yu Y, Luo Z, Chevrier DM, et al. Identification of a highly luminescent $Au_{22}(SG)_{18}$ nanocluster. *J Am Chem Soc.* 2014;136:1246–1249.

- [6] Du Y, Sheng H, Astruc D, et al. Atomically precise noble metal nanoclusters as efficient catalysts: a bridge between structure and properties. *Chem Rev.* **2020**;120:526–622.
- [7] Häkkinen H. The gold–sulfur interface at the nanoscale. *Nat Chem.* **2012**;4:443–455.
- [8] Negishi Y, Nobusada K, Tsukuda T. Glutathione-protected gold clusters revisited: bridging the gap between gold(I)–thiolate complexes and thiolate-protected gold nanocrystals. *J Am Chem Soc.* **2005**;127:5261–5270.
- [9] Barrabés N, Zhang B, Bürgi T. Racemization of chiral $\text{Pd}_2\text{Au}_{36}(\text{SC}_2\text{H}_4\text{Ph})_{24}$: doping increases the flexibility of the cluster surface. *J Am Chem Soc.* **2014**;136:14361–14364.
- [10] Gautier C, Bürgi T. Chiral gold nanoparticles. *Chemphyschem.* **2009**;10:483–492.
- [11] AbdulHalim LG, Bootharaju MS, Tang Q, et al. $\text{Ag}_{29}(\text{BDT})_{12}(\text{TPP})_4$: a tetravalent nanocluster. *J Am Chem Soc.* **2015**;137:11970–11975.
- [12] Chen G, Zhao Y, Fu G, et al. Interfacial effects in iron–nickel hydroxide–platinum nanoparticles enhance catalytic oxidation. *Science.* **2014**;344:495–499.
- [13] Hossain S, Hirayama D, Ikeda A, et al. Atomically precise thiolate-protected gold nanoclusters: current status of designability of the structure and physico-chemical properties. *Aggregate.* **2022**;e255.
- [14] Pradeep T. *NANO: the essentials: understanding nanoscience and nanotechnology*. 1st ed. New York (NY): MHHE; **2007**.
- [15] Kang X, Li Y, Zhu M, et al. Atomically precise alloy nanoclusters: syntheses, structures, and properties. *Chem Soc Rev.* **2020**;49:6443–6514.
- [16] Schmid G. Large clusters and colloids. Metals in the embryonic state. *Chem Rev.* **1992**;92:1709–1727.
- [17] Tsukuda T, Häkkinen H. Protected metal clusters: from fundamentals to applications. Amsterdam (Netherlands): Elsevier; **2015**.
- [18] Kawawaki T, Kataoka Y, Hirata M, et al. Toward the creation of high-performance heterogeneous catalysts by controlled ligand desorption from atomically precise metal nanoclusters. *Nanoscale Horiz.* **2021**;6:409–448.
- [19] Negishi Y, Hashimoto S, Ebina A, et al. Atomic-level separation of thiolate-protected metal clusters. *Nanoscale.* **2020**;12:8017–8039.
- [20] Kawawaki T, Negishi Y, Kawasaki H. Photo/Electrocatalysis and photosensitization using metal nanoclusters for green energy and medical applications. *Nanoscale Adv.* **2020**;2:17–36.
- [21] Takano S, Tsukuda T. Chemically modified gold/silver superatoms as artificial elements at nanoscale: design principles and synthesis challenges. *J Am Chem Soc.* **2021**;143:1683–1698.
- [22] Omoda T, Takano S, Tsukuda T. Toward controlling the electronic structures of chemically modified superatoms of gold and silver. *Small.* **2021**;17:2001439.
- [23] Negishi Y, Kurashige W, Niihori Y, et al. Isolation, structure, and stability of a dodecanethiolate-protected $\text{Pd}_1\text{Au}_{24}$ cluster. *Phys Chem Chem Phys.* **2010**;12:6219–6225.
- [24] Negishi Y, Iwai T, Ide M. Continuous modulation of electronic structure of stable thiolate-protected Au_{25} cluster by Ag doping. *ChemComm.* **2010**;46:4713–4715.
- [25] Negishi Y, Igarashi K, Munakata K, et al. Palladium doping of magic gold cluster $\text{Au}_{38}(\text{SC}_2\text{H}_4\text{Ph})_{24}$: formation of $\text{Pd}_2\text{Au}_{36}(\text{SC}_2\text{H}_4\text{Ph})_{24}$ with higher stability than $\text{Au}_{38}(\text{SC}_2\text{H}_4\text{Ph})_{24}$. *ChemComm.* **2012**;48:660–662.
- [26] Negishi Y, Munakata K, Ohgake W, et al. Effect of copper doping on electronic structure, geometric structure, and stability of thiolate-protected Au_{25} nanoclusters. *J Phys Chem Lett.* **2012**;3:2209–2214.
- [27] Kurashige W, Munakata K, Nobusada K, et al. Synthesis of stable $\text{Cu}_n\text{Au}_{25-n}$ nanoclusters ($n = 1-9$) using selenolate ligands. *ChemComm.* **2013**;49:5447–5449.
- [28] Niihori Y, Yoshida K, Hossain S, et al. Deepening the understanding of thiolate-protected metal clusters using high-performance liquid chromatography. *Bull Chem Soc Jpn.* **2018**;92:664–695.
- [29] Niihori Y, Koyama Y, Watanabe S, et al. Atomic and isomeric separation of thiolate-protected alloy clusters. *J Phys Chem Lett.* **2018**;9:4930–4934.
- [30] Hossain S, Imai Y, Suzuki D, et al. Elucidating ligand effects in thiolate-protected metal clusters using $\text{Au}_{24}\text{Pt}(\text{TBBT})_{18}$ as a model cluster. *Nanoscale.* **2019**;11:22089–22098.
- [31] Kumara C, Aikens CM, Dass A. X-ray crystal structure and theoretical analysis of $\text{Au}_{25-x}\text{Ag}_x(\text{SCH}_2\text{CH}_2\text{Ph})_{18}^-$ alloy. *J Phys Chem Lett.* **2014**;5:461–466.
- [32] Tian S, Liao L, Yuan J, et al. Structures and magnetism of mono-palladium and mono-platinum doped $\text{Au}_{25}(\text{PET})_{18}$ nanoclusters. *ChemComm.* **2016**;52:9873–9876.
- [33] Knoppe S, Bürgi T. Chirality in thiolate-protected gold clusters. *Acc Chem Res.* **2014**;47:1318–1326.
- [34] Dolamic I, Knoppe S, Dass A, et al. First enantioseparation and circular dichroism spectra of Au_{38} clusters protected by achiral ligands. *Nat Commun.* **2012**;3:798.
- [35] Knoppe S, Wong OA, Malola S, et al. Chiral phase transfer and enantioenrichment of thiolate-protected Au_{102} clusters. *J Am Chem Soc.* **2014**;136:4129–4132.
- [36] Niihori Y, Matsuzaki M, Pradeep T, et al. Separation of precise compositions of noble metal clusters protected with mixed ligands. *J Am Chem Soc.* **2013**;135:4946–4949.
- [37] Niihori Y, Matsuzaki M, Uchida C, et al. Advanced use of high-performance liquid chromatography for synthesis of controlled metal clusters. *Nanoscale.* **2014**;6:7889–7896.
- [38] Niihori Y, Uchida C, Kurashige W, et al. High-resolution separation of thiolate-protected gold clusters by reversed-phase high-performance liquid chromatography. *Phys Chem Chem Phys.* **2016**;18:4251–4265.
- [39] Zeng C, Qian H, Li T, et al. Total structure and electronic properties of the gold nanocrystal $\text{Au}_{36}(\text{SR})_{24}$. *Angew Chem Int Ed.* **2012**;51:13114–13118.
- [40] Sakthivel NA, Theivendran S, Ganeshraj V, et al. Crystal structure of faradaurate-279: $\text{Au}_{279}(\text{SPh-tBu})_{84}$ plasmonic nanocrystal molecules. *J Am Chem Soc.* **2017**;139:15450–15459.
- [41] Kang X, Zhu M. Transformation of atomically precise nanoclusters by ligand-exchange. *Chem Mater.* **2019**;31:9939–9969.
- [42] Jin R, Qian H, Wu Z, et al. Size focusing: a methodology for synthesizing atomically precise gold nanoclusters. *J Phys Chem Lett.* **2010**;1:2903–2910.
- [43] Krishnadas KR, Bakshi A, Ghosh A, et al. Structure-conserving spontaneous transformations between nanoparticles. *Nat Commun.* **2016**;7:13447.

- [44] Takano S, Ito S, Tsukuda T. Efficient and selective conversion of phosphine-protected (MAu_8)²⁺ (M = Pd, Pt) superatoms to thiolate-protected (MAu_{12})⁶⁺ or alkynyl-protected (MAu_{12})⁴⁺ superatoms via hydride doping. *J Am Chem Soc.* **2019**;141:15994–16002.
- [45] Chen T, Fung V, Yao Q, et al. Synthesis of water-soluble $[\text{Au}_{25}(\text{SR})_{18}]^-$ using a stoichiometric amount of NaBH_4 . *J Am Chem Soc.* **2018**;140:11370–11377.
- [46] Yao Q, Chen T, Yuan X, et al. Toward total synthesis of thiolate-protected metal nanoclusters. *Acc Chem Res.* **2018**;51:1338–1348.
- [47] Li Y, Zaluzhna O, Xu B, et al. Mechanistic insights into the Brust–Schiffrin two-phase synthesis of organo-chalcogenate-protected metal nanoparticles. *J Am Chem Soc.* **2011**;133:2092–2095.
- [48] Zeng C, Liu C, Pei Y, et al. Thiol ligand-induced transformation of $\text{Au}_{38}(\text{SC}_2\text{H}_4\text{Ph})_{24}$ to $\text{Au}_{36}(\text{SPh-}t\text{-Bu})_{24}$. *ACS Nano.* **2013**;7:6138–6145.
- [49] Wang Y, Bürgi T. Evidence for stereoelectronic effects in ligand exchange reactions on Au_{25} nanoclusters. *Nanoscale.* **2022**;14:2456–2464.
- [50] Negishi Y, Horihata H, Ebina A, et al. Selective formation of $[\text{Au}_{23}(\text{SPh}^t\text{Bu})_{17}]^0$, $[\text{Au}_{26}\text{Pd}(\text{SPh}^t\text{Bu})_{20}]^0$ and $[\text{Au}_{24}\text{Pt}(\text{SC}_2\text{H}_4\text{Ph})_7(\text{SPh}^t\text{Bu})_{11}]^0$ by controlling ligand-exchange reaction. *Chem Sci.* **2022**;13:5546–5556.
- [51] Mukherjee S, Jayakumar D, Mandal S. Insight into the size evolution transformation process of the fcc-based $\text{Au}_{28}(\text{SR})_{20}$ nanocluster. *J Phys Chem C.* **2021**;125:12149–12154.
- [52] Niihori Y, Hossain S, Kumar B, et al. Perspective: exchange reactions in thiolate-protected metal clusters. *APL Mater.* **2017**;5:053201.
- [53] Niihori Y, Hossain S, Sharma S, et al. Understanding and practical use of ligand and metal exchange reactions in thiolate-protected metal clusters to synthesize controlled metal clusters. *Chem Rec.* **2017**;17:473–484.
- [54] Niihori Y, Hashimoto S, Koyama Y, et al. Dynamic behavior of thiolate-protected gold–Silver 38-atom alloy clusters in solution. *J Phys Chem C.* **2019**;123:13324–13329.
- [55] Niihori Y, Kikuchi Y, Kato A, et al. Understanding ligand-exchange reactions on thiolate-protected gold clusters by probing isomer distributions using reversed-phase high-performance liquid chromatography. *ACS Nano.* **2015**;9:9347–9356.
- [56] Hossain S, Kurashige W, Wakayama S, et al. Ligand exchange reactions in thiolate-protected Au_{25} nanoclusters with selenolates or tellurolates: preferential exchange sites and effects on electronic structure. *J Phys Chem C.* **2016**;120:25861–25869.
- [57] Niihori Y, Eguro M, Kato A, et al. Improvements in the ligand-exchange reactivity of phenylethanethiolate-protected Au_{25} nanocluster by Ag or Cu incorporation. *J Phys Chem C.* **2016**;120:14301–14309.
- [58] Malola S, Lehtovaara L, Enkovaara J, et al. Birth of the localized surface plasmon resonance in monolayer-protected gold nanoclusters. *ACS Nano.* **2013**;7:10263–10270.
- [59] Aikens CM. Geometric and electronic structure of $\text{Au}_{25}(\text{SPhX})_{18}^-$ (X = H, F, Cl, Br, CH_3 , and OCH_3). *J Phys Chem Lett.* **2010**;1:2594–2599.
- [60] Jiang D-E, Kühn M, Tang Q, et al. Superatomic orbitals under spin–orbit coupling. *J Phys Chem Lett.* **2014**;5:3286–3289.
- [61] Taylor MG, Mpourmpakis G. Rethinking heterometal doping in ligand-protected metal nanoclusters. *J Phys Chem Lett.* **2018**;9:6773–6778.
- [62] Sakthivel NA, Shabaninezhad M, Sementa L, et al. The missing link: $\text{Au}_{191}(\text{SPh-}t\text{Bu})_{66}$ janus nanoparticle with molecular and bulk-metal-like properties. *J Am Chem Soc.* **2020**;142:15799–15814.
- [63] Xu WW, Li Y, Gao Y, et al. Unraveling a generic growth pattern in structure evolution of thiolate-protected gold nanoclusters. *Nanoscale.* **2016**;8:7396–7401.
- [64] Weerawardene KLDM, Aikens CM. Theoretical insights into the origin of photoluminescence of $\text{Au}_{25}(\text{SR})_{18}^-$ nanoparticles. *J Am Chem Soc.* **2016**;138:11202–11210.
- [65] Havenridge S, Aikens CM. Deciphering the dual emission in the photoluminescence of $\text{Au}_{14}\text{Cd}(\text{SR})_{12}$: a theoretical study using TDDFT and TDDFT + TB. *J Chem Phys.* **2021**;155:074302.
- [66] Jadzinsky PD, Calero G, Ackerson CJ, et al. Structure of a thiol monolayer-protected gold nanoparticle at 1.1 Å resolution. *Science.* **2007**;318:430–433.
- [67] Heaven MW, Dass A, White PS, et al. Crystal structure of the gold nanoparticle $[\text{N}(\text{C}_8\text{H}_{17})_4][\text{Au}_{25}(\text{SCH}_2\text{CH}_2\text{Ph})_{18}]$. *J Am Chem Soc.* **2008**;130:3754–3755.
- [68] Zhu M, Aikens CM, Hollander FJ, et al. Correlating the crystal structure of a thiol-protected Au_{25} cluster and optical properties. *J Am Chem Soc.* **2008**;130:5883–5885.
- [69] Lopez-Acevedo O, Akola J, Whetten RL, et al. Structure and bonding in the ubiquitous icosahedral metallic gold cluster $\text{Au}_{144}(\text{SR})_{60}$. *J Phys Chem C.* **2009**;113:5035–5038.
- [70] Qian H, Eckenhoff WT, Zhu Y, et al. Total structure determination of thiolate-protected Au_{38} nanoparticles. *J Am Chem Soc.* **2010**;132:8280–8281.
- [71] Cheng L, Ren C, Zhang X, et al. New insight into the electronic shell of $\text{Au}_{38}(\text{SR})_{24}$: a superatomic molecule. *Nanoscale.* **2013**;5:1475–1478.
- [72] Nishigaki J-I, Koyasu K, Tsukuda T. Chemically modified gold superatoms and superatomic molecules. *Chem Rec.* **2014**;14:897–909.
- [73] Nishigaki J-I, Yamazoe S, Kohara S, et al. A twisted bi-icosahedral Au_{25} cluster enclosed by bulky arenethiolates. *ChemComm.* **2014**;50:839–841.
- [74] Shichibu Y, Negishi Y, Watanabe T, et al. Biicosahedral gold clusters $[\text{Au}_{25}(\text{PPh}_3)_{10}(\text{SC}_n\text{H}_{2n+1})_5\text{Cl}_2]^{2+}$ ($n = 2–18$): a stepping stone to cluster-assembled materials. *J Phys Chem C.* **2007**;111:7845–7847.
- [75] Jin R, Liu C, Zhao S, et al. Tri-icosahedral gold nanocluster $[\text{Au}_{37}(\text{PPh}_3)_{10}(\text{SC}_2\text{H}_4\text{Ph})_{10}\text{X}_2]^+$: linear assembly of icosahedral building blocks. *ACS Nano.* **2015**;9:8530–8536.
- [76] Takano S, Yamazoe S, Koyasu K, et al. Slow-reduction synthesis of a thiolate-protected one-dimensional gold cluster showing an intense near-infrared absorption. *J Am Chem Soc.* **2015**;137:7027–7030.
- [77] Zhang H-F, Stender M, Zhang R, et al. Toward the solution synthesis of the tetrahedral Au_{20} cluster. *J Phys Chem B.* **2004**;108:12259–12263.
- [78] Shichibu Y, Konishi K. HCl-induced nuclearity convergence in diphosphine-protected ultrasmall gold clusters: a novel synthetic route to “magic-number” Au_{13} clusters. *Small.* **2010**;6:1216–1220.
- [79] McKenzie LC, Zaikova TO, Hutchison JE. Structurally similar triphenylphosphine-stabilized

- undecagolds, $\text{Au}_{11}(\text{PPh}_3)_7\text{Cl}_3$ and $[\text{Au}_{11}(\text{PPh}_3)_8\text{Cl}_2]\text{Cl}$, exhibit distinct ligand exchange pathways with glutathione. *J Am Chem Soc.* **2014**;136:13426–13435.
- [80] Gutrath BS, Englert U, Wang Y, et al. A missing link in undecagold cluster chemistry: single-crystal X-ray analysis of $[\text{Au}_{11}(\text{PPh}_3)_7\text{Cl}_3]$. *Eur J Inorg Chem.* **2013**;2013:2002–2006.
- [81] Maity P, Tsunoyama H, Yamauchi M, et al. Organogold clusters protected by phenylacetylene. *J Am Chem Soc.* **2011**;133:20123–20125.
- [82] Maity P, Wakabayashi T, Ichikuni N, et al. Selective synthesis of organogold magic clusters $\text{Au}_{54}(\text{C}\equiv\text{CPh})_{26}$. *ChemComm.* **2012**;48:6085–6087.
- [83] Maity P, Takano S, Yamazoe S, et al. Binding motif of terminal alkynes on gold clusters. *J Am Chem Soc.* **2013**;135:9450–9457.
- [84] Tang Q, Jiang D-E. Insights into the $\text{PhC}\equiv\text{C}/\text{Au}$ interface. *J Phys Chem C.* **2015**;119:10804–10810.
- [85] Wan X-K, Tang Q, Yuan S-F, et al. Au_{19} nanocluster featuring a v-shaped alkynyl-gold motif. *J Am Chem Soc.* **2015**;137:652–655.
- [86] Branham MR, Douglas AD, Mills AJ, et al. Arylthiolate-protected silver quantum dots. *Langmuir.* **2006**;22:11376–11383.
- [87] Wu Z, Lanni E, Chen W, et al. High yield, large scale synthesis of thiolate-protected Ag_7 clusters. *J Am Chem Soc.* **2009**;131:16672–16674.
- [88] Udayabhaskararao T, Pradeep T. Luminescent Ag_7 and Ag_8 clusters by interfacial synthesis. *Angew Chem Int Ed.* **2010**;49:3925–3929.
- [89] Udayabhaskararao T, Nataraju B, Pradeep T. Ag_9 quantum cluster through a solid-state route. *J Am Chem Soc.* **2010**;132:16304–16307.
- [90] Udayabhaskararao T, Bootharaju MS, Pradeep T. Thiolate-protected Ag_{32} clusters: mass spectral studies of composition and insights into the Ag-thiolate structure from NMR. *Nanoscale.* **2013**;5:9404–9411.
- [91] Chakraborty I, Govindarajan A, Erusappan J, et al. The superstable 25 kDa monolayer protected silver nanoparticle: measurements and interpretation as an icosahedral $\text{Ag}_{152}(\text{SCH}_2\text{CH}_2\text{Ph})_{60}$ cluster. *Nano Lett.* **2012**;12:5861–5866.
- [92] Bakr OM, Amendola V, Aikens CM, et al. Silver nanoparticles with broad multiband linear optical absorption. *Angew Chem Int Ed.* **2009**;48:5921–5926.
- [93] Harkness KM, Tang Y, Dass A, et al. $\text{Ag}_{44}(\text{SR})_{30}^{4-}$: a silver-thiolate superatom complex. *Nanoscale.* **2012**;4:4269–4274.
- [94] Guo J, Kumar S, Bolan M, et al. Mass spectrometric identification of silver nanoparticles: the case of $\text{Ag}_{32}(\text{SG})_{19}$. *Anal Chem.* **2012**;84:5304–5308.
- [95] Chakraborty I, Udayabhaskararao T, Pradeep T. High temperature nucleation and growth of glutathione protected $\sim\text{Ag}_{75}$ clusters. *ChemComm.* **2012**;48:6788–6790.
- [96] Joshi CP, Bootharaju MS, Alhilaly MJ, et al. $[\text{Ag}_{25}(\text{SR})_{18}]^-$: the “Golden” silver nanoparticle. *J Am Chem Soc.* **2015**;137:11578–11581.
- [97] Bootharaju MS, Lee S, Deng G, et al. $\text{Ag}_{44}(\text{EBT})_{26}(\text{TPP})_4$ nanoclusters with tailored molecular and electronic structure. *Angew Chem Int Ed.* **2021**;60:9038–9044.
- [98] Deng G, Malola S, Yuan P, et al. Enhanced surface ligands reactivity of metal clusters by bulky ligands for controlling optical and chiral properties. *Angew Chem Int Ed.* **2021**;60:12897–12903.
- [99] Bodiuzzaman M, Dar WA, Pradeep T. Cocrystals of atomically precise noble metal nanoclusters. *Small.* **2021**;17:2003981.
- [100] Alamer BJ, Bootharaju MS, Kozlov SM, et al. $[\text{Ag}_9(1,2\text{-BDT})_6]^{3-}$: how square-pyramidal building blocks self-assemble into the smallest silver nanocluster. *Inorg Chem.* **2021**;60:4306–4312.
- [101] Yang J, Pang R, Song D, et al. Tailoring silver nanoclusters *via* doping: advances and opportunities. *Nanoscale Adv.* **2021**;3:2411–2422.
- [102] Xu C, Yuan Q, Wei X, et al. Surface environment complication makes Ag_{29} nanoclusters more robust and leads to their unique packing in the supracrystal lattice. *Chem Sci.* **2022**;13:1382–1389.
- [103] Kim M, Weerawardene KLD, Choi W, et al. Insights into the metal-exchange synthesis of $\text{MAg}_{24}(\text{SR})_{18}$ ($\text{M} = \text{Ni}, \text{Pd}, \text{Pt}$) nanoclusters. *Chem Mater.* **2020**;32:10216–10226.
- [104] Sagadevan A, Ghosh A, Maity P, et al. Visible-light copper nanocluster catalysis for the C–N coupling of aryl chlorides at room temperature. *J Am Chem Soc.* **2022**;144:12052–12061.
- [105] Lee S, Bootharaju MS, Deng G, et al. $[\text{Pt}_2\text{Cu}_{34}(\text{PET})_{22}\text{Cl}_4]^{2-}$: an atomically precise, 10-electron PtCu bimetal nanocluster with a direct Pt–Pt bond. *J Am Chem Soc.* **2021**;143:12100–12107.
- [106] Nematulloev S, Huang R-W, Yin J, et al. $[\text{Cu}_{15}(\text{PPh}_3)_6(\text{PET})_{13}]^{2+}$: a copper nanocluster with crystallization enhanced photoluminescence. *Small.* **2021**;17:2006839.
- [107] Lee S, Bootharaju MS, Deng G, et al. $[\text{Cu}_{32}(\text{PET})_{24}\text{H}_8\text{Cl}_2](\text{PPh}_4)_2$: a copper hydride nanocluster with a bisquare antiprismatic core. *J Am Chem Soc.* **2020**;142:13974–13981.
- [108] Han Z, Dong X-Y, Luo P, et al. Ultrastable atomically precise chiral silver clusters with more than 95% quantum efficiency. *Sci Adv.* **2020**;6:eay0107.
- [109] Yamamoto M, Yoshida T, Yamamoto N, et al. Photocatalytic reduction of CO_2 with water promoted by Ag clusters in $\text{Ag}/\text{Ga}_2\text{O}_3$ photocatalysts. *J Mater Chem A.* **2015**;3:16810–16816.
- [110] Dhayal RS, Liao J-H, Liu Y-C, et al. $\text{Ag}_{21}\{\text{S}_2\text{P}(\text{O}i\text{Pr})_2\}_{12}^+$: an eight-electron superatom. *Angew Chem Int Ed.* **2015**;54:3702–3706.
- [111] Chang W-T, Lee P-Y, Liao J-H, et al. Eight-electron silver and mixed gold/silver nanoclusters stabilized by selenium donor ligands. *Angew Chem Int Ed.* **2017**;56:10178–10182.
- [112] Ren L, Yuan P, Su H, et al. Bulky surface ligands promote surface reactivities of $[\text{Ag}_{141}\text{X}_{12}(\text{S-Adm})_{40}]^{3+}$ ($\text{X} = \text{Cl}, \text{Br}, \text{I}$) nanoclusters: models for multiple-twinned nanoparticles. *J Am Chem Soc.* **2017**;139:13288–13291.
- [113] Khatun E, Ghosh A, Ghosh D, et al. $[\text{Ag}_{59}(2,5\text{-DCBT})_{32}]^{3-}$: a new cluster and a precursor for three well-known clusters. *Nanoscale.* **2017**;9:8240–8248.
- [114] Song Y, Lambright K, Zhou M, et al. Large-scale synthesis, crystal structure, and optical properties of the $\text{Ag}_{146}\text{Br}_2(\text{SR})_{80}$ nanocluster. *ACS Nano.* **2018**;12:9318–9325.
- [115] Liu X, Chen J, Yuan J, et al. A silver nanocluster containing interstitial sulfur and unprecedented chemical bonds. *Angew Chem Int Ed.* **2018**;57:11273–11277.
- [116] Bootharaju MS, Kozlov SM, Cao Z, et al. Doping-induced anisotropic self-assembly of silver icosahedra

- in $[\text{Pt}_2\text{Ag}_{23}\text{Cl}_7(\text{PPh}_3)_{10}]$ nanoclusters. *J Am Chem Soc.* **2017**;139:1053–1056.
- [117] Yang S, Chai J, Lv Y, et al. Cyclic $\text{Pt}_3\text{Ag}_{33}$ and $\text{Pt}_3\text{Au}_{12}\text{Ag}_{21}$ nanoclusters with M_{13} icosahedra as building-blocks. *ChemComm.* **2018**;54:12077–12080.
- [118] Matsuyama T, Kikkawa S, Fujiki Y, et al. Thermal stability of crown-motif $[\text{Au}_9(\text{PPh}_3)_8]^{3+}$ and $[\text{MAu}_8(\text{PPh}_3)_8]^{2+}$ ($\text{M} = \text{Pd}, \text{Pt}$) clusters: effects of gas composition, single-atom doping, and counter anions. *J Chem Phys.* **2021**;155:044307.
- [119] Qu M, Li H, Xie L-H, et al. Bidentate phosphine-assisted synthesis of an all-alkynyl-protected Ag_{74} nanocluster. *J Am Chem Soc.* **2017**;139:12346–12349.
- [120] Duan G-X, Tian L, Wen J-B, et al. An atomically precise all-*tert*-butylethyne-protected Ag_{51} superatom nanocluster with color tunability. *Nanoscale.* **2018**;10:18915–18919.
- [121] Birker PJMWL, Freeman HC. Metal-binding in chelation therapy: X-ray crystal structure of a copper(I)–Copper(II) complex of D-penicillamine. *J Chem Soc Chem Commun.* **1976**;312–313.
- [122] Schugar HJ, Ou C, Thich JA, et al. Molecular structure and copper(II)–mercaptide charge-transfer spectra of a novel $\text{Cu}_{14}[\text{SC}(\text{CH}_3)_2\text{CH}_2\text{NH}_2]_{12}\text{Cl}$ cluster. *J Am Chem Soc.* **1976**;98:3047–3048.
- [123] Tang K, Xia T, Jin X, et al. Formation and X-ray structure of a novel tetradecanuclear copper(I) cluster complex $\text{Cu}_{14}(\mu_2\text{-S})(\text{SPh})_{12}(\text{PPh}_3)_6$. *Polyhedron.* **1993**;12:2895–2898.
- [124] Jin X, Tang K, Liu W, et al. Formation and X-Ray structure of a novel tetradecanuclear silver cluster complex, $\text{Ag}_{14}(\mu_6\text{-S})(\text{SPh})_{12}(\text{PPh}_3)_8\cdot 4\text{CH}_3\text{OH}\cdot 13\text{H}_2\text{O}$. *Polyhedron.* **1996**;15:1207–1211.
- [125] Bian S-D, Jia J-H, Wang Q-M. High-nuclearity silver clusters templated by carbonates generated from atmospheric carbon dioxide fixation. *J Am Chem Soc.* **2009**;131:3422–3423.
- [126] Wang Z, Gupta RK, Luo G-G, et al. Recent progress in inorganic anions templated silver nanoclusters: synthesis, structures and properties. *Chem Rec.* **2020**;20:389–402.
- [127] Ge R, Li X-X, Zheng S-T. Recent advances in polyoxometalate-templated high-nuclear silver clusters. *Coord Chem Rev.* **2021**;435:213787.
- [128] Xie Y-P, Jin J-L, Duan G-X, et al. High-nuclearity silver(I) chalcogenide clusters: a novel class of supramolecular assembly. *Coord Chem Rev.* **2017**;331:54–72.
- [129] Hu H, Lan L, Zhang T, et al. Recent advances in polyoxometalate-based metal-alkynyl clusters. *Cryst Eng Comm.* **2022**;24:3317–3331.
- [130] Wang Q-M, Lin Y-M, Liu K-G. Role of anions associated with the formation and properties of silver clusters. *Acc Chem Res.* **2015**;48:1570–1579.
- [131] Liu CW, Haia H-C, Hung C-M, et al. New halide-centered discrete Ag_8^1 cubic clusters containing diselenophosphate ligands, $\{\text{Ag}_8(\text{X})[\text{Se}_2\text{P}(\text{OR})_2]_6\}(\text{PF}_6)$ ($\text{X} = \text{Cl}, \text{Br}$; $\text{R} = \text{Et}, \text{Pr}, ^i\text{Pr}$): syntheses, structures, and DFT calculations. *Inorg Chem.* **2004**;43:4464–4470.
- [132] Liu CW, Chang H-W, Fang C-S, et al. Anion-templated syntheses of octanuclear silver clusters from a silver dithiophosphate chain. *ChemComm.* **2010**;46:4571–4573.
- [133] Liao J-H, Chang H-W, Li Y-J, et al. Anion templating from a silver(I) dithiophosphate 1D polymer forming discrete cationic and neutral octa- and decanuclear silver(I) clusters. *Dalton Trans.* **2014**;43:12380–12389.
- [134] Chang H-W, Shiu R-Y, Fang C-S, et al. A sulfide (selenide)-centered nonanuclear silver cluster: a distorted and flexible tricapped trigonal prismatic Ag_9 framework. *J Clust Sci.* **2017**;28:679–694.
- [135] Li X-Y, Wang Z, Su H-F, et al. Anion-templated nanosized silver clusters protected by mixed thiolate and diphosphine. *Nanoscale.* **2017**;9:3601–3608.
- [136] Zhang S-S, Su H-F, Wang Z, et al. Anion-templated nanosized silver alkynyl clusters: cluster engineering and solution behavior. *Chem Eur J.* **2017**;23:3432–3437.
- [137] Wang Z, Su H-F, Wang X-P, et al. Johnson solids: anion-templated silver thiolate clusters capped by sulfonate. *Chem Eur J.* **2018**;24:1640–1650.
- [138] Wang Z, Sun Y-M, Qu Q-P, et al. Enclosing classical polyoxometallates in silver nanoclusters. *Nanoscale.* **2019**;11:10927–10931.
- [139] Wang Z, Su H-F, Tung C-H, et al. Deciphering synergistic core-shell transformation from $[\text{Mo}_6\text{O}_{22}@\text{Ag}_{44}]$ to $[\text{Mo}_8\text{O}_{28}@\text{Ag}_{50}]$. *Nat Commun.* **2018**;9:4407.
- [140] Wang Z, Zhuo H-Y, Hu A-Y, et al. Self-assembly of a novel Ag_{48} cluster encapsulating an unprecedented $[\text{Mo}_8\text{O}_{28}]^{8-}$ anion template. *ISR J Chem.* **2019**;59:280–285.
- [141] Yuan S, Deng Y-K, Wang X-P, et al. A temperature-sensitive luminescent Ag_{20} nanocluster templated by carbonate *in situ* generated from atmospheric CO_2 fixation. *New J Chem.* **2013**;37:2973–2977.
- [142] Li J-Z, Bigdeli F, Gao X-M, et al. Trivalent tetrahedral anion template: a 26-nucleus silver alkynyl cluster encapsulating vanadate. *Inorg Chem.* **2019**;58:5397–5400.
- [143] Sun D, Wang H, Lu H-F, et al. Two birds with one stone: anion templated ball-shaped Ag_{56} and disc-like Ag_{20} clusters. *Dalton Trans.* **2013**;42:6281–6284.
- [144] Sun D, Liu F-J, Huang R-B, et al. Anionic heptadecanuclear silver(I) cluster constructed from *in situ* generated 2-mercaptobenzoic acid and a sulfide anion. *Inorg Chem.* **2011**;50:12393–12395.
- [145] Liao J-H, Latouche C, Li B, et al. A twelve-coordinated iodide in a cuboctahedral silver(I) skeleton. *Inorg Chem.* **2014**;53:2260–2267.
- [146] Li B, Liao J-H, Li Y-J, et al. Dihalogen-templated synthesis of dodecanuclear silver dichalcogenophosphate clusters. *Cryst Eng Comm.* **2013**;15:6140–6143.
- [147] Rais D, Yau J, Mingos DMP, et al. Anion-templated syntheses of rhombohedral silver–Alkynyl cage compounds. *Angew Chem Int Ed.* **2001**;40:3464–3467.
- [148] Rais D, Mingos DMP, Vilar R, et al. Directing role of anions in the syntheses of the silver–alkynyl cages $[\text{Ag}_{14}(\text{C}\equiv\text{C}^i\text{Bu})_{12}\text{X}][\text{BF}_4]$ ($\text{X} = \text{F}, \text{Cl}, \text{Br}$) and silver–alkynyl polymers $[\text{Ag}_3(\text{C}\equiv\text{C}^i\text{Bu})_2(\text{X})]_n$ ($\text{X} = \text{tos}, \text{NO}_3$). *J Organomet Chem.* **2002**;652:87–93.
- [149] Shen H, Kubo K, Kume S, et al. Novel chloride-centered Ag_{18} clusters featuring a cuboctahedral Ag_{12} skeleton. *Dalton Trans.* **2017**;46:16199–16204.
- [150] Bian S-D, Wang Q-M. Snowman-like silver alkynyl cluster consolidated by templating chloride and peripheral trifluoroacetates. *ChemComm.* **2008**;5586–5588.
- [151] Zhou K, Wang X-L, Qin C, et al. Serendipitous anion-templated self-assembly of a sandwich-like $\text{Ag}_{20}\text{S}_{10}$ macrocycle-based high-nuclearity luminescent nanocluster. *Dalton Trans.* **2013**;42:1352–1355.

- [152] Xie Y-P, Mak TCW. High-nuclearity silver ethynide clusters assembled with phosphonate and metavanadate precursors. *Angew Chem Int Ed*. **2012**;51:8783–8786.
- [153] Liu X, Yang H, Zheng N, et al. Bromide-induced formation of a highly symmetric silver thiolate cluster containing 36 silver atoms from an infinite polymeric silver thiolate. *Eur J Inorg Chem*. **2010**;2010:2084–2087.
- [154] Zavras A, Mravak A, Bužančić M, et al. Structure of the ligated Ag_{60} nanoparticle $[\{\text{Cl@Ag}_{12}\}@\text{Ag}_{48}(\text{dppm})_{12}]$ (where $\text{dppm}=\text{bis}(\text{diphenylphosphino})\text{methane}$). *Chin J Chem Phys*. **2019**;32:182–186.
- [155] Chen Z-Y, Tam DYS, Mak TCW. Chloride assisted supramolecular assembly of a luminescent gigantic cluster: $[\text{Ag}_{216}\text{S}_{56}\text{Cl}_7(\text{C}\equiv\text{CPh})_{98}(\text{H}_2\text{O})_{12}]^-$ with pseudo- T_h skeleton and five-shell arrangement. *Nanoscale*. **2017**;9:8930–8937.
- [156] MacDonald DG, Eichhöfer A, Campana CF, et al. Ferrocene-based trimethylsilyl chalcogenide reagents for the assembly of functionalized metal–chalcogen architectures. *Chem Eur J*. **2011**;17:5890–5902.
- [157] Li Y-J, Latouche C, Kahlal S, et al. A μ_9 -Iodide in a tricapped trigonal-prismatic geometry. *Inorg Chem*. **2012**;51:7439–7441.
- [158] Duan G-X, Xie Y-P, Jin J-L, et al. High-nuclearity heterometallic *tert*-butylethynide clusters assembled with *tert*-butylphosphonate. *Chem Eur J*. **2018**;24:6762–6768.
- [159] Jin J-L, Shen Y-L, Xie Y-P, et al. Silver ethynide clusters constructed with fluorinated β -diketonate ligands. *Cryst Eng Comm*. **2018**;20:2036–2042.
- [160] Birker PJMWL, Reedijk J, Verschoor GC, et al. Synthesis, structure, and properties of cluster compounds with D -penicillamine containing Cu^{I} , Cu^{II} , Ag^{I} , Ni^{II} , and Pd^{II} . X-ray structure of pentakis (hexaamminecobalt(III)) tris $[\mu_8\text{-chloro-octahydro-hexakis}[\mu_4\text{-[cis-bis}(D\text{-penicillaminato}(2-)-N,S)\text{nickel(II)}]\text{-S,S'}]\text{-cubo-octaargentate(I)}]\text{-}n\text{-water}$, $[\text{Co}(\text{NH}_3)_6]_5[\text{Ag}_8^{\text{I}}\text{Ni}_6^{\text{II}}(\text{SC}(\text{CH}_3)_2\text{CH}(\text{NH}_2)\text{COO})_{12}\text{Cl}]_3\cdot\sim 197\text{H}_2\text{O}$. *Inorg Chem*. **1981**;20:2877–2882.
- [161] Connell TU, Sandanayake S, Khairallah GN, et al. Halide-ion-templated Ag_8Cu_6 rhombic dodecahedrons: synthesis, structure and reactivity of $[\text{Ag}_8\text{Cu}_6(\text{C}\equiv\text{CtBu})_{12}\text{X}]\text{BF}_4$ ($\text{X} = \text{Cl}, \text{Br}$). *Dalton Trans*. **2013**;42:4903–4907.
- [162] Alhilaly MJ, Huang R-W, Naphade R, et al. Assembly of atomically precise silver nanoclusters into nanocluster-based frameworks. *J Am Chem Soc*. **2019**;141:9585–9592.
- [163] Das AK, Biswas S, Manna SS, et al. An atomically precise silver nanocluster for artificial light-harvesting system through supramolecular functionalization. *Chem Sci*. **2022**;13:8355–8364.
- [164] Wang Q-M, Mak TCW. Novel honeycomb-like layered structure: the first isomorphous triple salts of silver acetylide. *J Am Chem Soc*. **2000**;122:7608–7609.
- [165] Crabtree RH, Hlatky GG, Holt EM. Bidodecahedral coordination geometry in a dimolybdenum tetrahydride containing three fluoride bridges: crystal and molecular structure of $[(\text{PMePh}_2)_3\text{H}_2\text{Mo}]_2(\mu\text{-F})_3]\text{BF}_4$. *J Am Chem Soc*. **1983**;105:7302–7306.
- [166] Lozinsek M, Belak Vivod M, Dragomir M. Crystal structure reinvestigation of silver(I) fluoride, AgF . *IUCrData*. **2023**;8:x230018.
- [167] Hull S, Keen DA. Pressure-induced phase transitions in AgCl , AgBr , and AgI . *Phys Rev B*. **1999**;59:750–761.
- [168] Liu CW, Shang I-J, Hung C-M, et al. Novel silver diselenophosphate clusters: structures of $\text{Ag}_{10}(\mu_{10}\text{-Se})[\text{Se}_2\text{P}(\text{OEt})_2]_8$ and $\{\text{Ag}[\text{Se}_2\text{P}(\text{OPr}^i)_2]\}_6$. *J Chem Soc Dalton Trans*. **2002**:1974–1979.
- [169] Zhu Y-B, Lu S-F, Huang X-Y, et al. Synthesis and crystal structure of a decanuclear silver(I)-thiolate compound $\text{Ag}_{10}\text{S}[\text{S}_2\text{P}(\text{OEt})_2]_8$. *Chin J Chem*. **2004**;22:673–677.
- [170] Liu CW, Chang H-W, Liao P-K, et al. Crystal structure, photophysical properties, and theoretical investigation of extremely distorted pentacapped trigonal-prismatic undecasilver clusters. *J Clust Sci*. **2011**;22:381–396.
- [171] Tian F, Chen R. $\text{Ag}_{18}(\mu_8\text{-S})(p\text{-TBBT})_{16}(\text{PPh}_3)_8$: symmetry breaking induced by the core to generate chirality. *ChemComm*. **2020**;56:2719–2722.
- [172] Xie Y-P, Jin J-L, Lu X, et al. High-nuclearity silver thiolate clusters constructed with phosphonates. *Angew Chem Int Ed*. **2015**;54:15176–15180.
- [173] Li G, Lei Z, Wang Q-M. Luminescent molecular Ag–S nanocluster $[\text{Ag}_{62}\text{S}_{13}(\text{SBu}^t)_{32}](\text{BF}_4)_4$. *J Am Chem Soc*. **2010**;132:17678–17679.
- [174] Langer R, Breitung B, Wünsche L, et al. Functionalised silver chalcogenide clusters. *Z Anorg Allg Chem*. **2011**;637:995–1006.
- [175] Nayek HP, Massa W, Dehnen S. Presence or absence of a central Se atom in silver selenide/selenolate clusters with halite topology: syntheses and properties of $[(\text{Ph}_3\text{P})_8\text{Ag}_6(\mu_6\text{-Se})_{1-x/2}(\text{SePh})_{12}]^{x+}$ ($x = 0, 1$). *Inorg Chem*. **2010**;49:144–149.
- [176] Shi W, Ahlrichs R, Anson CE, et al. Reactions of P/S-containing proligands with coinage metal salts: a new route to polynuclear complexes with unusual structural types. *ChemComm*. **2005**:5893–5895.
- [177] Jin J-L, Shen Y-L, Xie Y-P, et al. Anion templated synthesis of silver(I)-ethynide dithiophosphate clusters. *Cryst Growth Des*. **2018**;18:4372–4377.
- [178] Liu CW, Shang I-J, Fu R-J, et al. Selenium-centered, undecanuclear silver cages surrounded by Iodo and dialkyldiselenophosphato ligands. Syntheses, structures, and photophysical properties. *Inorg Chem*. **2006**;45:2335–2340.
- [179] Liu CW, Shang I-J, Wang J-C, et al. Metal dialkyl diselenophosphates: a rare example of co-crystallization with clusters, $\text{Ag}_8(\mu_8\text{-Se})[\text{Se}_2\text{P}(\text{OPr}^i)_2]_6$ and $\text{Ag}_6[\text{Se}_2\text{P}(\text{OPr}^i)_2]_6$, superimposing in a trigonal lattice. *ChemComm*. **1999**:995–996.
- [180] Shen Y-L, Zhao P, Jin J-L, et al. A comparative study of $[\text{Ag}_{11}(\text{PrS})_9(\text{dppb})_3]^{2+}$ and $[\text{Ag}_{15}(\text{S}^t\text{BuS})_{12}(\text{dppb})_3]^+$: templating effect on structure and photoluminescence. *Dalton Trans*. **2021**;50:10561–10566.
- [181] Biswas S, Das AK, Manna SS, et al. Template-assisted alloying of atom-precise silver nanoclusters: a new approach to generate cluster functionality. *Chem Sci*. **2022**;13:11394–11404.
- [182] Biswas S, Das AK, Reber AC, et al. The new Ag–S cluster $[\text{Ag}_{50}\text{S}_{13}(\text{S}^t\text{Bu})_{20}][\text{CF}_3\text{COO}]_4$ with a unique hcp Ag_{14} kernel and Ag_{36} keplerian-shell-based structural architecture and its photoresponsivity. *Nano Lett*. **2022**;22:3721–3727.
- [183] Jenkins HDB, Thakur KP. Reappraisal of thermochemical radii for complex ions. *J Chem Educ*. **1979**;56:576.

- [184] Xie Y-P, Mak TCW. Silver(I)-ethynide clusters constructed with phosphonate-functionized polyoxovanadates. *J Am Chem Soc.* **2011**;133:3760–3763.
- [185] Hau SCK, Cheng P-S, Mak TCW. Ligand-induced assembly of coordination chains and columns containing high-nuclearity silver(I) ethynide cluster units. *Organometallics.* **2014**;33:3231–3234.
- [186] Gao G-G, Cheng P-S, Mak TCW. Acid-induced surface functionalization of polyoxometalate by enclosure in a polyhedral silver-alkynyl cage. *J Am Chem Soc.* **2009**;131:18257–18259.
- [187] Bian S-D, Wu H-B, Wang Q-M. A facile template approach to high-nuclearity silver(I) alkynyl clusters. *Angew Chem Int Ed.* **2009**;48:5363–5365.
- [188] Gruber F, Jansen M. $\{[\text{Ag}_{42}(\text{CO}_3)(\text{C}\equiv\text{CtBu})_{27}(\text{CH}_3\text{CN})_2][\text{CoW}_{12}\text{O}_{40}]_2\}[\text{BF}_4]$: an intercluster sandwich compound. *Angew Chem Int Ed.* **2010**;49:4924–4926.
- [189] Cheng L-P, Wang Z, Wu Q-Y, et al. Small size yet big action: a simple sulfate anion templated a discrete 78-nuclearity silver sulfur nanocluster with a multishell structure. *ChemComm.* **2018**;54:2361–2364.
- [190] Li B, Huang R-W, Qin J-H, et al. Thermochromic luminescent nest-like silver thiolate cluster. *Chem Eur J.* **2014**;20:12416–12420.
- [191] Liao J-H, Chang H-W, You H-C, et al. Tetrahedral-shaped anions as a template in the synthesis of high-nuclearity silver(I) dithiophosphate clusters. *Inorg Chem.* **2011**;50:2070–2072.
- [192] Chang HW, Liao JH, Li B, et al. Trigonal pyramidal oxyanions as structure-directing templates for the synthesis of silver dithiolate clusters. *J Struct Chem.* **2014**;55:1426–1432.
- [193] Liu K-G, Bigdeli F, Li H-J, et al. Hexavalent octahedral template: a neutral high-nucleus silver alkynyl nanocluster emitting infrared light. *Inorg Chem.* **2020**;59:6684–6688.
- [194] Liao J-H, Chang H-W, Fang C-S, et al. T-symmetric 40-nucleus silver clusters assembled by heteroanions. *J Chin Chem Soc.* **2020**;67:2163–2170.
- [195] Li Y-L, Xu Q-Q, Li S, et al. Investigating the influence of a $\text{CrO}_4^{2-}/\text{Cr}_2\text{O}_7^{2-}$ template in the formation of a series of silver-chalcogenide clusters. *New J Chem.* **2019**;43:115–120.
- [196] Wang Z, Li X-Y, Liu L-W, et al. Beyond clusters: supramolecular networks self-assembled from nano-sized silver clusters and inorganic anions. *Chem Eur J.* **2016**;22:6830–6836.
- [197] Zhou K, Qin C, Wang X-L, et al. Unexpected 1D self-assembly of carbonate-templated sandwich-like macrocycle-based $\text{Ag}_{20}\text{S}_{10}$ luminescent nanoclusters. *Cryst Eng Comm.* **2014**;16:7860–7864.
- [198] Xie Y-P, Wang H, Mak TCW. Silver-ethynide clusters with oxovanadate components. *J Clust Sci.* **2012**;23:727–736.
- [199] Tamari S, Ono K, Hashimoto M, et al. Control over the preference for binding sites of polyoxometalates to silver ethynide clusters by surface charge modification. *Dalton Trans.* **2015**;44:19056–19058.
- [200] Liu K-G, Wei X-W, Bigdeli F, et al. Investigation of the effect of a mixed-ligand on the accommodation of a templating molecule into the structure of high-nucleus silver clusters. *Inorg Chem.* **2020**;59:2248–2254.
- [201] Liao J-H, Chen H, You H-J, et al. Oxocarbon anions templated in silver clusters. *Inorg Chem.* **2022**;61:14115–14120.
- [202] Xia Y-H, Xia X-Y, Fang J-J, et al. Anion-templated silver thiolated clusters affected by carboxylate ligands. *Dalton Trans.* **2022**;51:14557–14562.
- [203] Hou L-L, Bigdeli F, Cheng X, et al. Synthesis of two neutral silver alkynyl nanoclusters by a single divalent tetrahedral anion template and a study of their optical features. *Inorg Chem.* **2022**;61:16693–16698.
- [204] Jin J-L, Shen Y-L, Mi L-W, et al. Anion-templated self-assembly for the preparation of silver-*t*-butylthiolate clusters. *Chinese J Struct Chem.* **2022**;41:2203100–2203107.
- [205] Liu K-G, Chen S-K, Lin Y-M, et al. An organic anion template: a 24-nucleus silver cluster encapsulating a squarate dimer. *ChemComm.* **2015**;51:9896–9898.
- [206] Li S, Du X-S, Li B, et al. Atom-precise modification of silver(I) thiolate cluster by shell ligand substitution: a new approach to generation of cluster functionality and chirality. *J Am Chem Soc.* **2018**;140:594–597.
- [207] Li Y, Jin R. Seeing ligands on nanoclusters and in their assemblies by X-ray crystallography: atomically precise nanochemistry and beyond. *J Am Chem Soc.* **2020**;142:13627–13644.
- [208] Pope MT, Müller A. Introduction to polyoxometalate chemistry : from topology via self-assembly to applications. In: Pope M Müller A, editors. *Polyoxometalate chemistry from topology via self-assembly to applications*. Dordrecht: Springer Netherlands; **2001**. p. 1–6.
- [209] Zhou K, Qin C, Li H-B, et al. Assembly of a luminescent core-shell nanocluster featuring a $\text{Ag}_{34}\text{S}_{26}$ shell and a $\text{W}_6\text{O}_{21}^{6-}$ polyoxoanion core. *ChemComm.* **2012**;48:5844–5846.
- [210] Li Y-Y, Gao F, Beves JE, et al. A giant metallo-supramolecular cage encapsulating a single-molecule magnet. *ChemComm.* **2013**;49:3658–3660.
- [211] Qiao J, Shi K, Wang Q-M. A giant silver alkynyl cage with sixty silver(I) ions clustered around polyoxometalate templates. *Angew Chem Int Ed.* **2010**;49:1765–1767.
- [212] Wang J-Y, Liu K-G, Guan Z-J, et al. $[\text{Mn}^{\text{III}}\text{Mn}^{\text{IV}}_2\text{Mo}_{14}\text{O}_{56}]^{17-}$: a mixed-valence meso-polyoxometalate anion encapsulated by a 64-nuclearity silver cluster. *Inorg Chem.* **2016**;55:6833–6835.
- [213] Jiang Z-G, Shi K, Lin Y-M, et al. $[\text{Ag}_{70}(\text{PW}_9\text{O}_{34})_2(\text{tBuC}\equiv\text{C})_{44}(\text{H}_2\text{O})_2]^{8+}$: ionothermal synthesis of a silver cluster encapsulating lacunary polyoxometalate ions. *ChemComm.* **2014**;50:2353–2355.
- [214] Li X-Y, Tan Y-Z, Yu K, et al. Atom-precise Polyoxometalate- Ag_2S core-shell nanoparticles. *Chem Asian J.* **2015**;10:1295–1298.
- [215] Huang R-W, Xu Q-Q, Lu H-L, et al. Self-assembly of an unprecedented polyoxomolybdate anion $[\text{Mo}_{20}\text{O}_{66}]^{12-}$ in a giant peanut-like 62-core silver-thiolate nanocluster. *Nanoscale.* **2015**;7:7151–7154.
- [216] Liu K-G, Liu X-Y, Guan Z-J, et al. The transformation of polyoxometalates in the formation of intercluster compound $[\text{Ag}_{41}(\alpha\text{-SiW}_{10}\text{O}_{37})(\text{tBuC}\equiv\text{C})_{27}(\text{CH}_3\text{CN})_3][\beta\text{-SiW}_{12}\text{O}_{40}]$. *ChemComm.* **2016**;52:3801–3804.
- [217] Zhang S-S, Su H-F, Wang Z, et al. Elimination-fusion self-assembly of a nanometer-scale 72-nucleus silver cluster caging a pair of $[\text{EuW}_{10}\text{O}_{36}]^{9-}$ polyoxometalates. *Chem Eur J.* **2018**;24:1998–2003.
- [218] Liu J-W, Feng L, Su H-F, et al. Anisotropic assembly of Ag_{52} and Ag_{76} nanoclusters. *J Am Chem Soc.* **2018**;140:1600–1603.

- [219] Su Y-M, Liu W, Wang Z, et al. Benzoate-induced high-nuclearity silver thiolate clusters. *Chem Eur J*. **2018**;24:4967–4972.
- [220] Wang Z, Su H-F, Kurmoo M, et al. Trapping an octahedral Ag₆ kernel in a seven-fold symmetric Ag₅₆ nanowheel. *Nat Commun*. **2018**;9:2094.
- [221] Song C-Y, Chai D-F, Zhang R-R, et al. A silver-alkynyl cluster encapsulating a fluorescent polyoxometalate core: enhanced emission and fluorescence modulation. *Dalton Trans*. **2015**;44:3997–4002.
- [222] Kurasawa M, Arisaka F, Ozeki T. Asymmetrically fused polyoxometalate–silver alkynide composite cluster. *Inorg Chem*. **2015**;54:1650–1654.
- [223] Yan B-J, Du X-S, Huang R-W, et al. Self-assembly of a stable silver thiolate nanocluster encapsulating a lacunary kegglin phosphotungstate anion. *Inorg Chem*. **2018**;57:4828–4832.
- [224] Xie Y-P, Mak TCW. A pyrovanadate-templated silver (I)–ethynide cluster circumscribed by macrocyclic polyoxovanadate(V). *ChemComm*. **2012**;48:1123–1125.
- [225] Liu H, Song C-Y, Huang R-W, et al. Acid–base-triggered structural transformation of a polyoxometalate core inside a dodecahedrane-like silver thiolate shell. *Angew Chem Int Ed*. **2016**;55:3699–3703.
- [226] Wang Z, Zheng L-M, Jagodič M, et al. A polyoxochromate templated 56-nuclei silver nanocluster. *Inorg Chem*. **2020**;59:3004–3011.
- [227] Zhang S-S, Chen J-Y, Li K, et al. Janus cluster: asymmetric coverage of a Ag₄₃ cluster on the symmetric preysler P₅W₃₀ polyoxometalate. *Chem Mater*. **2021**;33:9708–9714.
- [228] Li L, Zhu Y, Han B, et al. A classical [V₁₀O₂₈]^{6−} anion templated high-nuclearity silver thiolate cluster. *ChemComm*. **2022**;58:9234–9237.
- [229] Villanneau R, Proust A, Robert F. Synthesis and characterization of [NBu₄]₄[Ag₂{Mo₅O₁₃(OMe)₄(NO)}₂], a novel polyoxomolybdate complex with a short Ag^I...Ag^I distance. *ChemComm*. **1998**;1491–1492.
- [230] Rhule JT, Neiwert WA, Hardcastle KI, et al. Ag₅PV₂Mo₁₀O₄₀, a heterogeneous catalyst for air-based selective oxidation at ambient temperature. *J Am Chem Soc*. **2001**;123:12101–12102.
- [231] Abbas H, Pickering AL, Long D-L, et al. Controllable growth of chains and grids from polyoxomolybdate building blocks linked by silver(I) Dimers. *Chem Eur J*. **2005**;11:1071–1078.
- [232] Abbas H, Streb C, Pickering AL, et al. Molecular growth of polyoxometalate architectures based on [−Ag{Mo₈}Ag−] synthons: toward designed cluster assemblies. *Cryst Growth Des*. **2008**;8:635–642.
- [233] Wilson EF, Abbas H, Duncombe BJ, et al. Probing the self-assembly of inorganic cluster architectures in solution with cryospray mass spectrometry: growth of polyoxomolybdate clusters and polymers mediated by silver(I) Ions. *J Am Chem Soc*. **2008**;130:13876–13884.
- [234] Streb C, Tsunashima R, MacLaren DA, et al. Supramolecular silver polyoxometalate architectures direct the growth of composite semiconducting nanostructures. *Angew Chem Int Ed*. **2009**;48:6490–6493.
- [235] Liu CW, Lin Y-R, Fang C-S, et al. [Ag₇(H){E₂P(OR)₂}]₆ (E = Se, S): precursors for the fabrication of silver nanoparticles. *Inorg Chem*. **2013**;52:2070–2077.
- [236] Liu CW, Chang H-W, Sarkar B, et al. Stable silver(I) hydride complexes supported by diselenophosphate ligands. *Inorg Chem*. **2010**;49:468–475.
- [237] Liu CW, Liao P-K, Fang C-S, et al. An eleven-vertex deltahedron with hexacapped trigonal bipyramidal geometry. *ChemComm*. **2011**;47:5831–5833.
- [238] Liao P-K, Liu K-G, Fang C-S, et al. [Ag₇(H){S₂CC(CN)₂}]₆^{6−}: an anionic heptanuclear silver hydride cluster compound stabilized by dithiolate ligands. *J Clust Sci*. **2019**;30:1185–1193.
- [239] Liao P-K, Liu K-G, Fang C-S, et al. A copper(I) homocubane collapses to a tetracapped tetrahedron upon hydride insertion. *Inorg Chem*. **2011**;50:8410–8417.
- [240] Fukuda Y, Yoshinari N, Konno T. Insertion of a hydride ion into a tetrasilver(I) cluster covered by s-donating rhodium(III) metalloligands. *Inorg Chem*. **2021**;60:468–475.
- [241] Khairallah GN, O’Hair RAJ. Gas-phase synthesis of [Ag₄H]⁺ and its mediation of the C–C coupling of allyl bromide. *Angew Chem Int Ed*. **2005**;44:728–731.
- [242] Yuan X, Sun C, Li X, et al. Combinatorial identification of hydrides in a ligated Ag₄₀ nanocluster with noncompact metal core. *J Am Chem Soc*. **2019**;141:11905–11911.
- [243] Zhu C, Duan T, Li H, et al. Structural determination of a metastable Ag₂₇ nanocluster and its transformations into Ag₈ and Ag₂₉ nanoclusters. *Inorg Chem Front*. **2021**;8:4407.
- [244] Konno T, Okamoto K, Hidaka J. Synthesis and properties of t-cage-type s-bridged Rh^{III}Zn^{II} octanuclear complexes with 2-aminoethanethiolate or L-cysteinate. *Inorg Chem*. **1994**;33:538–544.
- [245] Yamashita U, Yoshinari N, Sodkhomkhum R. Hydrogen-bonded metallosupramolecular helices composed of a nona-protonated spherical Rh^{III}₄Zn^{II}₄ cluster with twelve carboxylate arms. *Cryst Eng Comm*. **2020**;22:2700–2704.
- [246] Yoshinari N, Yamashita S, Fukuda Y, et al. Mobility of hydrated alkali metal ions in metallosupramolecular ionic crystals. *Chem Sci*. **2019**;10:587–593.
- [247] Yoshinari N, Meundaeng N, Tabe H, et al. Single-crystal-to-single-crystal installation of Ln₄(OH)₄ cubanes in an anionic metallosupramolecular framework. *Angew Chem Int Ed*. **2020**;59:18048–18053.
- [248] Jin R. Atomically precise metal nanoclusters: stable sizes and optical properties. *Nanoscale*. **2015**;7:1549–1565.
- [249] Das A, Liu C, Zeng C, et al. Cyclopentanethiolate-protected Au₃₆(SC₅H₉)₂₄ nanocluster: crystal structure and implications for the steric and electronic effects of ligand. *J Phys Chem A*. **2014**;118:8264–8269.
- [250] Zeng C, Chen Y, Li G, et al. Magic size Au₆₄(S-c-C₆H₁₁)₃₂ nanocluster protected by cyclohexanethiolate. *Chem Mater*. **2014**;26:2635–2641.
- [251] Liu F-L, Kozlevčar B, Strauch P, et al. Robust cluster building unit: icosanuclear heteropolyoxocopperate templated by carbonate. *Chem Eur J*. **2015**;21:18847–18854.
- [252] Chen Z, Shen Y, Li L, et al. High-nuclearity heterometallic clusters with both an anion and a cation sandwiched by planar cluster units: synthesis, structure and properties. *Dalton Trans*. **2017**;46:15032–15039.
- [253] Zhang L-M, Mak TCW. Comproportionation synthesis of copper(I) alkynyl complexes encapsulating polyoxomolybdate templates: bowl-shaped Cu₃₃ and peanut-shaped Cu₆₂ nanoclusters. *J Am Chem Soc*. **2016**;138:2909–2912.

- [254] Zhang L-M, Zhou G, Zhou G, et al. Core-dependent properties of copper nanoclusters: valence-pure nanoclusters as NIR TADF emitters and mixed-valence ones as semiconductors. *Chem Sci.* [2019](#);10:10122–10128.
- [255] Zheng X-Y, Kong X-J, Zheng Z, et al. High-nuclearity lanthanide-containing clusters as potential molecular magnetic coolers. *Acc Chem Res.* [2018](#);51:517–525.
- [256] Zheng X-Y, Peng J-B, Kong X-J, et al. Mixed-anion templated cage-like lanthanide clusters: Gd_{27} and Dy_{27} . *Inorg Chem Front.* [2016](#);3:320–325.
- [257] Li X-Y, Su H-F, Q-W L, et al. A giant Dy_{76} cluster: a fused bi-nanopillar structural model for lanthanide clusters. *Angew Chem Int Ed.* [2019](#);58:10184–10188.
- [258] Guo F-S, Chen Y-C, Mao L-L, et al. Anion-templated assembly and magnetocaloric properties of a nanoscale $\{\text{Gd}_{38}\}$ cage versus a $\{\text{Gd}_{48}\}$ barrel. *Chem Eur J.* [2013](#);19:14876–14885.
- [259] Liao P-K, Sarkar B, Chang H-W, et al. Facile entrapment of a hydride inside the tetracapped tetrahedral Cu^{I}_8 cage inscribed in a S_{12} icosahedral framework. *Inorg Chem.* [2009](#);48:4089–4097.
- [260] Zheng X-Y, Xie J, Kong X-J, et al. Recent advances in the assembly of high-nuclearity lanthanide clusters. *Coord Chem Rev.* [2019](#);378:222–236.